THE INHIBITION OF THE VIM-2 AND IMP-1 METALLO-β-LACTAMASES BY CATIONIC PEPTIDES

by

Caitlyn Michelle Rotondo

A thesis submitted in partial fulfillment
of the requirements for the degree of
Master of Science (MSc) in Chemical Sciences

The Faculty of Graduate Studies
Laurentian University
Sudbury, Ontario, Canada

THESIS DEFENCE COMMITTEE/COMITÉ DE SOUTENANCE DE THÈSE
Laurentian Université/Université Laurentienne
Faculty of Graduate Studies/Faculté des études supérieures

Title of Thesis Titre de la thèse	THE INHIBITION OF THE VIM-2 AND IMP-1 METALLO-β-LACTAMASES BY CATIONIC PEPTIDES
Name of Candidate Nom du candidat	Rotondo, Caitlyn
Degree Diplôme	Master of Science
Department/Program Département/Programme	Chemical Sciences
Date of Defence Date de la soutenance	October 24, 2014

APPROVED/APPROUVÉ

Thesis Examiners/Examinateurs de thèse:

Dr. Stefan Siemann
(Supervisor/Directeur(trice) de thèse)

Dr. Eric Gauthier
(Committee member/Membre du comité)

Dr. Gerardo Ulibarri
(Committee member/Membre du comité)

Dr. Guy Guillemette
(External Examiner/Examinateur externe)

Approved for the Faculty of Graduate Studies
Approuvé pour la Faculté des études supérieures
Dr. David Lesbarrères
M. David Lesbarrères
Acting Dean, Faculty of Graduate Studies
Doyen intérimaire, Faculté des études supérieures

ACCESSIBILITY CLAUSE AND PERMISSION TO USE

Abstract

Metallo-β-lactamases (MBLs) are major contributors to bacterial antibiotic resistance due to their ability to cleave most β-lactam antibiotics. At the present time there are no clinically approved inhibitors of MBLs. However, previous preliminary studies have demonstrated that cationic peptides have the ability to inhibit these enzymes.

Herein, more thorough investigations into the structure-activity relationship between two MBLs, VIM-2 and IMP-1, and cationic peptides are described, demonstrating that the inhibitory potency of these peptides increased with the number of arginine residues (IC_{50} of 10 nM for the most potent VIM-2 inhibitor). The degree of inhibition also varied depending on the β-lactam substrate and the MBL employed. Furthermore, steady-state and stopped-flow spectrophotometric studies demonstrated that the inhibition mediated by these peptides followed a complex mode of inhibition. In addition, results from spectroscopic studies (including UV-Vis, tryptophan fluorescence and dynamic light scattering) showed that the inhibition of MBLs by cationic peptides results in partially reversible peptide-influenced MBL aggregation. The better understanding of the relationship between these peptides and MBLs may lead to the development of novel MBL inhibitors suitable for clinical use.

Keywords: Bacteria, Antibiotic Resistance, β-Lactamases, Metallo-β-lactamases, Enzyme mechanism, Inhibitors, Cationic Peptides

Acknowledgements

Though only my name appears on the cover of this Master's thesis, many others have made its production possible. I owe my gratitude to everyone who contributed assistance, support and encouragement during one of the most significant academic challenges that I have ever had to face.

First and foremost, I would like to extend my deepest gratitude to my thesis supervisor Dr. Stefan Siemann for his unwavering support, infinite patience and vast knowledge through every step of this undertaking. Your sound guidance has helped me improve my laboratory skills and grow as a scientific researcher.

I would also like to express my sincere gratitude to Dr. Eric Gauthier and Dr. Gerardo Ulíbarri for serving as my supervisory committee members, and for taxing me to excel and enhance my knowledge base. I would also like to extend a special thank you to Dr. Gary Dmitrienko for his many recommendations and continued support on this project. Finally, I would like extend my utmost gratitude to Dr. Guy Guillemette for taking on the important responsibility of acting as an external reader of this thesis paper. My heartfelt thanks go out to all of you for challenging me to do my best, and for providing me with insightful comments and honest feedback as guiding tools in this process.

In addition, I would like to thank Dr. Sabine Montaut as well as Dr. Zhibin Ye's and Dr. Ulíbarri's laboratory researchers for assisting me in using the equipment required for HPLC, dynamic light scattering and peptide synthesis. I'm also grateful to Dr. Dmitrienko's laboratory group for providing me with the enzymes and the substrates necessary for my research.

Furthermore, I would like to express my gratitude to the Siemann research group members, past and present, for all of their encouragement over the years. Their companionship and support made the laboratory a comfortable and enjoyable research environment. I extend a special thanks to research assistant Suet Lo whose input and insight allowed me to conduct my research more efficiently.

I would also like to thank the Canadian Institutes of Health Research (CIHR) for financial support in the form of a Canada-UK team grant on antibiotic resistance.

A special thanks to family and friends for being a constant source of patience, understanding, support and strength throughout my degree. Words cannot express how grateful I am to my dear parents whose unconditional love and encouragement helped me overcome setbacks and stay focus during my graduate studies. Thank you for believing in me.

Last but not least, I would like to thank God for the wisdom and perseverance that He bestowed upon me in the pursuit of my dreams.

Table of Contents

List of Tables

List of Figures

List of Abbreviations

× *g* ..... Relative centrifugal force
°C ..... Degree Celsius
βAla ..... β-Alanine
µg ..... Microgram
µL ..... Microliter
µM ..... Micromolar
ε ..... Extinction coefficient
ABC ..... ATP-binding cassette
abs ..... Absorbance
Ac ..... Acetyl
Ala ..... Alanine
APS ..... Ammonium persulfate
Arg ..... Arginine
Asp ..... Aspartate
ATP ..... Adenosine 5′-triphosphate
AU ..... Arbitrary unit
BME ..... β-mercaptoethanol
BSA ..... Bovine serum albumin
cm ..... Centimeter
Cys ..... Cysteine
Da ..... Dalton
DCH ..... Aspartate – Cysteine – Histidine
DMSO ..... Dimethyl sulfoxide
DNA ..... Deoxyribonucleic acid
DPA ..... 2,6-pyridinedicarboxylic acid (Dipicolinic acid)
DTNB ..... 5,5′-dithio-bis(2-nitrobenzoic acid)
E ..... Enzyme
eq ..... Molar equivalent
FI ..... Fluorescence intensity
FRET ..... Fluorescence resonance energy transfer
g ..... Gram
GdnHCl ..... Guanidine hydrochloride
Glu ..... Glutamate
Gly ..... Glycine
HEPES ..... N-2-hydroxyethylpiperazine-N′-2-ethanesulfonic acid
HPLC ..... High-performance liquid chromatography
I ..... Inhibitor
k_{cat} ..... Catalytic constant
kDa ..... Kilodalton
K_i ..... Inhibition constant
K_M ..... Michaelis constant
Leu ..... Leucine
Lys ..... Lysine
M ..... Molar

MATE ..... Multi-antimicrobial extrusion protein
MBL ..... Metallo-β-lactamase
MDR ..... Multidrug resistance
MFS ..... Major facilitator superfamily
mg ..... Milligram
min ..... Minute
mL ..... Milliliter
mM ..... Millimolar
MW ..... Molecular weight
MWCO ..... Molecular weight cut-off
NAG ..... *N*-acetylglucosamine
NAM ..... *N*-acetylmuramic acid
NDM ..... New Delhi metallo-β-lactamase
NHS ..... *N*-hydroxysuccinimide
Nle ..... Norleucine
nm ..... Nanometer
nM ..... Nanomolar
NTB 2-nitro-5-thiobenzoate
P ..... Product
PAGE ..... Polyacrylamide gel electrophoresis
PAR ..... 4-(2-pyridylazo)resorcinol
PBP ..... Penicillin binding protein
PBS ..... Phosphate-buffered saline
*p*NA ..... *para*-nitroanilide
Pro ..... Proline
RNA ..... Ribonucleic acid
RND ..... Resistance nodulation division
s ..... Second
S ..... Substrate
s.d. ..... Standard deviation
SMR ..... Small multidrug resistance
S-pNA ..... Anthrax lethal factor protease substrate II
t ..... Time
TB ..... Tuberculosis
TCEP ..... Tris(2-carboxyethyl)phosphine
TCEPO ..... Tris(2-carboxyethyl)phosphine oxide
TLC ..... Thin-layer chromatography
TEMED ..... Tetramethylethylenediamine
Tris 2-amino-2-hydroxymethyl-propane-1,3-diol
tRNA ..... Transfer ribonucleic acid
Tyr ..... Tyrosine
v ..... Velocity
V ..... Volt
v/v ..... Volume/volume
Val ..... Valine
VIM ..... Verona integrin-encoded metallo-β-lactamase

V_{max} .... Maximum velocity
w/v... Weight/volume

Chapter 1: Introduction

1.1 Microorganisms

Microorganisms are found everywhere in the environment from air, water, soil and the human body [1]. Most microorganisms are beneficial, and can promote human health and well-being. These microorganisms are commonly included in various types of food products such as milks, cheeses and yogurts. They encourage the maintenance of a healthy intestinal microbial flora, thereby providing protection against gastrointestinal disorders such as inflammatory bowel disease and colon cancer [2, 3]. The large intestine in the human body is estimated to contain hundreds of different types of bacterial species averaging around 10^{12} bacteria per gram of intestine [2]. Although numerous microorganisms confer many health benefits for the human population, some microorganisms are pathogenic and can cause serious health concerns. Bacterial infections such as meningitis, pneumonia, tetanus and tuberculosis are the most common infectious diseases worldwide causing a high degree of mortality among the human population [4].

1.2 Discovery of Microorganisms and Vaccination

Throughout history, disease-causing bacteria wreaked havoc around the globe as the human population went unaware of their existence due to their small size. Sadly, this did not prevent these microorganisms from causing numerous epidemics around the world such as the Black Death (bubonic plague) which claimed the lives of millions of people in Europe after 1346. This plague was caused by the Gram-negative bacterium *Yersinia pestis* [5, 6]. The awareness of the existence of microorganisms began in 1683 with the innovative microscopy of Anthony Van Leeuwenhoek. Among the animalcules from his teeth, Van Leeuwenhoek first observed bacterial species [5, 7]. However, it would take almost another two centuries for this discovery

to promote any advancement in the detection of some of the most deadly microbes since the existence of these small organisms was regarded as an interesting, yet irrelevant fact. Regardless, the awareness of the existence of these microorganisms would go on to create a pathway for the discovery of preventative measures to combat these pathogenic bacteria and viruses [7].

1.2.1 Edward Jenner and the Smallpox Vaccine

The human population's battle against pathogenic bacteria and viruses would be transformed by the fight against smallpox. Smallpox was a highly virulent, easily transmittable infectious disease caused by two virus variants known as *Variola major* and *Variola minor* [8]. In 18th century Europe, an estimated 400,000 people died each year of smallpox, and those who survived were usually left severely disfigured due to scars. In addition, one third of the smallpox survivors were often left blind due to corneal infections [9]. Interestingly, it was also observed that the survivors of smallpox became immune to the disease. Henceforth, variolation became the first method used to combat this highly contagious and deadly disease. The variolation protection method was introduced in Europe in 1717 by Lady Mary Wortley Montague. The technique involved taking a small amount of smallpox pus, and scratching it into the arms of healthy people. Variolation was intended to produce a more mild form of the disease, but the disease still proved to be fatal in 2% to 3% of variolated people [9, 10]. Furthermore, since smallpox, no matter how mild, was still highly contagious, the variolated individuals were still fully capable of transmitting smallpox to other people, and were often the cause of new outbreaks of the disease [11, 12]. Nevertheless, mortality rates associated with the variolation technique were still 10 times lower than those associated with naturally occurring smallpox which demonstrated a mortality rate of 30% [10, 12].

In 1757, an 8-year-old boy by the name of Edward Jenner living in England was variolated against smallpox [12]. As he grew older, Jenner developed a strong interest in the knowledge that milkmaids who contracted cowpox did not develop smallpox [9, 10]. Jenner concluded that cowpox could be transmitted from one person to another to protect against smallpox [9]. In May 1796, Jenner inoculated his gardener's 8-year-old son, James Phipps, with cowpox obtained from the lesions of a local milkmaid. Afterwards, in July 1796, Jenner inoculated Phipps again, but with smallpox. Fortunately, Phipps demonstrated immunity to smallpox since no smallpox infection occurred, and Jenner concluded that the vaccination was a success. This was the first ever successful vaccination. In 1798, Jenner published his research and received great opposition from the medical community. However, Jenner was not discouraged by the opposition and continued to distribute his smallpox vaccine. By the summer of 1799, numerous members of the medical community had confirmed Jenner's hypothesis as over 1,000 people had been vaccinated against smallpox from Europe to North America to Asia [11]. Therefore, in 1840 in England, variolation was made illegal while vaccination was rendered free upon request [10]. However, vaccination also demonstrated some drawbacks. It was discovered that vaccination did not confer a lifelong immunity against the disease, and subsequent vaccination was necessary to ensure protection against smallpox. The main drawbacks of Jenner's vaccination presented themselves when it came to ensuring the quantity and the quality of the vaccine. Several diseases contracted by cattle resembled cowpox, although they were caused by different viruses. Furthermore, contamination with other microorganisms was also common resulting in vaccinated people developing hepatitis B and syphilis. In addition, the vaccine was susceptible to deactivation by heat during its transportation. This would persist until the 1930s when refrigeration became widely available [11]. By the 1950s, smallpox was eradicated in

many regions of Europe and North America. In 1958, the process of the worldwide eradication of smallpox began since the disease was still demonstrating devastating effects in 63 countries. On May 8th, 1980, close to two hundred years after the first vaccination by Jenner, the World Health Organization finally announced the worldwide eradication of smallpox [9].

1.2.2 Robert Koch

Although vaccination was common after Jenner's discovery, the underlining cause of infectious diseases remained unknown. German physician Robert Koch was the first to actually establish the link between a bacterium and the causative agent of an infectious disease [13]. Anthrax is a highly virulent, highly contagious, potentially fatal infectious disease. This disease not only affects the human population, but also wreaks devastation on animals such as cattle, sheep and horses since it has the capacity to be transmitted to all warm-blooded animals [14]. In 1870, the disease killed 56,000 farm animals and 528 people in Russia [13]. Koch's studies demonstrated that rod-shaped structures were present in the blood of anthrax-infected animals. In addition, the blood of these disease-stricken animals could transmit anthrax to healthy animals through inoculation [13, 14]. As Koch observed these rod-shaped structures through a microscope, he concluded that they were actually living bacteria [13, 15]. Koch later identified these bacteria as the Gram-positive bacterium *Bacillus anthracis* which was originally discovered in 1850 by French physician Casimir Davaine and German physician Aloys Pollender [15]. In 1876, Koch concluded that *B. anthracis* was the cause of anthrax, and that the presence of these bacteria was required for the transmission of anthrax among animals [13, 15].

Following his research on anthrax, Koch decided to study tuberculosis. Tuberculosis (also known as TB, which is short for *tubercle bacillus*) is one of the oldest and deadliest infectious diseases. TB typically attacks the lungs, and is transmitted through the respiratory route (i.e.,

coughs and sneezes) [16, 17]. TB dates back to over 10,000 years ago, and continues to be fatal for approximately two million people each year [17–19]. Although tuberculosis existed for thousands of years, the bacillus causing the disease, *Mycobacterium tuberculosis*, was originally identified and described by Koch in 1882 [17, 20].

Following his work with tuberculosis, Koch focused his attention on cholera. Cholera is an infectious disease which is characterized by voluminous amounts of watery diarrhea that results in high mortality rates despite rehydration therapy [21, 22]. Cholera pandemics have been recorded since 1817 [22, 23]. In 1884, Koch identified that Gram-negative, comma-shaped bacilli were responsible for causing cholera. These bacilli, known as *Vibrio cholerae*, were originally discovered by Italian anatomist Filippo Pacini in 1854 [21, 24]. Although, Robert Koch discovered the etiologic agents for three different infectious diseases, his identification of the tuberculosis bacteria still remains his greatest scientific achievement over 100 years later [18, 25].

1.2.3 Louis Pasteur

Louis Pasteur, also known as the father of microbiology, played an essential role in the history of microorganisms and vaccination. In 1879, Pasteur successfully isolated the chicken cholera bacillus, and demonstrated that the disease could be transmitted to healthy chicken through the injection of this bacillus. However, his research was interrupted, and a culture containing the bacilli involved in chicken cholera aged in the laboratory. This culture later failed to induce cholera when injected into healthy chickens upon Pasteur's return. In addition, Pasteur observed resistance to cholera in these healthy chickens even when he tried re-injecting them with a fresh culture of the cholera bacillus [26, 27]. Pasteur understood that the chickens survived since the cholera-causing bacillus was attenuated (i.e., weakened) due to their exposure to air. Pasteur

observed a connection between his observations and that of Edward Jenner's research on vaccination, and therefore named his injections vaccines in honour of Jenner's discovery. Henceforth, Pasteur suggested that an animal could become less susceptible to a bacterial disease as they come into contact with an attenuated form of the etiologic bacteria [26, 28].

In the 1870s, Pasteur studied sheep anthrax since this disease was causing a lot of devastation on livestock. Pasteur was already aware of Robert Koch's discovery that *Bacillus anthracis* was the etiological agent of anthrax [26, 27]. Pasteur had a harder time creating a vaccine for anthrax since the bacillus could be present in its rod form (i.e., sensitive to attenuation) and its spore form (i.e., resistant to attenuation). Pasteur had to find a way to keep the bacteria alive while preventing spore formation. Pasteur finally attenuated the bacteria by storing them in oxygenated containers at 42°C to 43°C [26]. In 1881, Pasteur injected a variety of animals with anthrax bacilli. Some of the animals had been vaccinated with Pasteur's attenuated anthrax bacilli while others remained unvaccinated. The experiment was considered completely successful as only the vaccinated animals survived [14, 26].

Following his work of anthrax, Pasteur went on to study and work on rabies. Rabies is an infectious disease affecting all warm-blooded animals. Although rabies is mostly prevalent among wild animals such as the fox and the dog, it can also be transmitted to humans through exposure to saliva from these rabid animals [29, 30]. This disease dates back to ancient Egypt, and is caused by a virus belonging to the *Lyssavirus* genus [30]. Rabies causes acute inflammation of the brain through the infection of the central nervous system. On average, one person every 15 min dies from rabies while 300 other people are exposed [31]. The rabies vaccine was initially created by a French doctor and a colleague of Pasteur, Émile Roux, who had been working on killing the virus by drying out the spinal cords of rabbits that were infected

with the disease. Pasteur sped up the dehydration process of the spinal cords through the addition of potassium particles [26]. The vaccine was initially tested on 9-year-old Joseph Meister in 1885 after the boy was badly mauled by a rabid dog, and his death appeared inevitable [5, 26]. Although Pasteur's vaccines were not as successful as Jenner's smallpox vaccine (i.e., the smallpox vaccine is still described as the most successful vaccine in history), Pasteur still made significant contributions to the world of microbiology through his effective vaccines created by the attenuation of microorganisms [10, 26]. However, although vaccinations were a great advancement for preventing infectious diseases, there was still a need to create something that could ultimately combat the bacteria causing these diseases once someone was already infected.

1.3 History of Antibiotics

In 1942, the term *antibiotic* was used for the first time by Selman Waksman. This term was originally used to describe small molecules synthesized by microorganisms that hindered the growth of other microorganisms [32]. The first antibiotic discovered was the sulfa drug arsphenamine (initially known as compound 606 or Salvarsan). This antibiotic was originally discovered in 1909 by Paul Ehrlich and Sahachiro Hata, and was used for the treatment of syphilis [33]. In 1932, another sulfa drug was synthesized by two German chemists, Josef Klarer and Fritz Mietzsch. This sulfa drug, Prontosil, whose antimicrobial properties were discovered by German physician Gerhard Domagk, was the first to be commercially available [33, 34]. This breakthrough in the fight against bacterial infections resulted in a mass production of natural and synthetic antibiotics from 1945 to 1955 [32].

Penicillin, an antibiotic derived by the *Penicillium* fungi, was the first antibiotic that demonstrated significant results in combating bacterial infections that were previously fatal for

humans [4, 32, 35]. Penicillin was originally discovered by French medical student Ernest Duchesne. In 1897, Duchesne demonstrated that the fungus *Penicillium glaucum* had the ability to combat infections caused by *Escherichia coli* and *Salmonella typhi* [36]. However, Duchesne never continued his research, and the discovery of penicillin was credited to Scottish bacteriologist Alexander Fleming [36, 37]. In 1928, Fleming accidently discovered the anti-pathogenic properties of mold upon returning from his vacation. Fleming noticed that mold was growing on some discarded Petri dishes containing staphylococci. Upon further observation, Fleming discovered that no staphylococci were growing around the mold. Fleming concluded that the mold released a substance with antibacterial properties. This substance was later termed penicillin. Fleming published his findings in 1929, but stopped studying penicillin in 1931 as he was never able to concentrate or purify the antibiotic. The commercialization of penicillin would begin in 1940 with the successful production and purification of penicillin by Australian pathologist Howard Florey and German-born British biochemist Ernst Chain [37]. With the discovery of these antibiotics, the so-called miracle drugs, it was believed that the fight against infectious diseases had been won [38].

1.4 Antibiotics

Antibiotics are chemical substances that either restrain the growth (bacteriostatic agent) or kill the bacteria (bactericidal agent) causing bacterial infections. However, the mechanism of action of antibiotics is rarely exclusively bactericidal or bacteriostatic [39, 40]. Even antibiotics categorized under bactericidal usually fail to kill every bacterium causing the infectious disease. In addition, certain bacteriostatic antibiotics can kill 90% to 99% of the bacteria causing the infection, but cannot be considered bactericidal as over 1% of bacteria remain [39]. Furthermore, antibiotics can also be classified depending on the range of bacteria that they affect.

Broad-spectrum antibiotics are effective against a wide range of microorganisms including both Gram-positive and Gram-negative bacteria. However, these antibiotics not only target the pathogenic bacteria causing the bacterial infections, but also affect the bacteria residing in the natural intestinal flora of the host. In contrast, narrow-spectrum antibiotics are only active against a narrow range of bacteria, either Gram-positive or Gram-negative. These antibiotics only target the pathogenic bacterial strains causing the bacterial infection, and do not majorly affect the natural intestinal flora of the host [41, 42]. Furthermore, antibiotics can be produced either synthetically or by microorganisms. Therefore, antibiotics are either classified as natural, semi-synthetic or synthetic agents. Natural antibiotics are produced solely by microorganisms. Many of these antibiotics were obtained through secretions by fungi or soil bacteria. Semi-synthetic antibiotics are synthesized through chemical modifications of natural compounds. These chemical modifications are typically performed to improve the efficacy of the natural antibiotic or to reduce side effects associated with its use. Synthetic antibiotics are produced exclusively in the laboratory [43]. Therefore, antibiotics are typically classified, based on their mechanism of action (i.e., bacteriostatic or bactericidal), their chemical structure, or their spectrum of activity. However, antibiotics can also be grouped depending on their bacterial targets [4, 40].

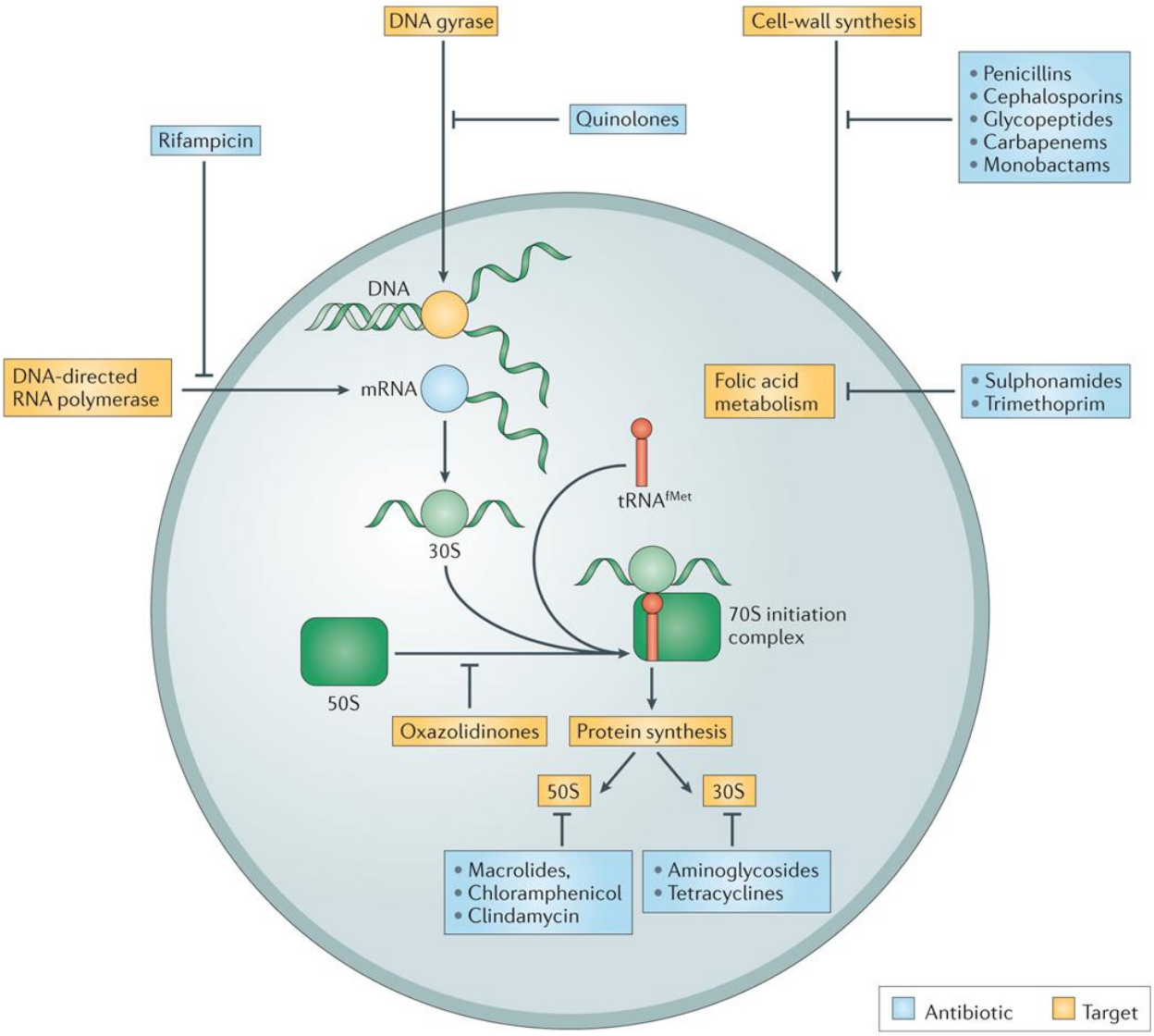

Figure 1.1: Targets of antibiotics. Most antibiotics target only three pathways: the ribosome (30S or 50S subunits), cells wall synthesis, and DNA replication (i.e., DNA gyrase or DNA-directed RNA polymerase). Figure taken, with permission, from reference [44] and Macmillan Publishers Ltd. © 2013 Macmillan Publishers Ltd. All rights reserved.

Antibiotics are effective at slowing down or killing bacteria since they have the capacity to inhibit essential components of microbial processes such as cell wall synthesis, DNA replication and protein synthesis. Antibiotics are separated into several groups depending on the bacterial process that they inhibit [4, 40]. Quinolones are synthetic broad-spectrum antibiotics that inhibit DNA synthesis. More specifically, quinolones inhibit DNA gyrase preventing bacterial DNA from unwinding and consequently, duplicating (see Figure 1.1). The majority of clinically

relevant quinolones are fluoroquinolones (i.e., quinolones that contain a fluorine atom) [40, 45]. The first quinolone discovered in 1962 was nalidixic acid, which was used for the treatment of urinary tract infections [45]. Rifamycins are natural and semi-synthetic bactericidal antibiotics that inhibit RNA synthesis through binding of prokaryotic DNA-directed RNA polymerase (see Figure 1.1) [40, 46]. The first rifamycin, rifampicin, was originally isolated from the Gram-positive bacterium *Amycolatopsis mediterranei* (originally known as *Streptomyces mediterranei*) in 1957 [44, 46]. Antibiotics that inhibit bacterial protein synthesis are among the broadest classes of antibiotics, and they are divided into two subclasses depending on whether they inhibit the 30S or the 50S ribosomal subunit [40, 47]. In addition, protein synthesis also involves transfer RNA (tRNA) molecules that bring the amino acid moieties to the ribosome. The ribosome has three tRNA binding sites: the A (aminoacyl) site, the P (peptidyl) site and the E (exit) site [47]. The 50S subunit inhibitors include macrolides, chloramphenicol, lincosamides and oxazolidinones (see Figure 1.1). These antibiotics function by blocking the initiation of protein translation or by blocking the translocation of tRNAs located in the peptidyl site of the ribosome. Blocking the translocation of peptidyl tRNAs inhibits the reaction that allows for the elongation of the nascent peptide chain. The 30S inhibitors include tetracyclines and aminoglycosides. Tetracyclines block tRNAs from assessing the aminoacyl site of the ribosome [40]. Aminoglycosides bind the 30S ribosomal subunit which interferes with the elongation of the nascent peptide chain. This binding impairs the translational proofreading process resulting in misreading of the messenger RNA and/or premature termination [48]. Glycopeptides (e.g., vancomycin) and β-lactams (e.g., penicillins, cephalosporins, carbapenems and monobactams) are natural and semi-synthetic bactericidal antibiotics that inhibit cell wall synthesis (see Figure 1.1). Glycopeptides are narrow-spectrum antibiotics that inhibit cell wall synthesis by binding

the D-Ala-D-Ala terminus of the peptidoglycan subunits. This binding inhibits the cross-linking of the peptidoglycan subunits by the penicillin-binding proteins (PBPs) [40, 44, 49]. β-Lactam antibiotics, such as benzylpenicillin, are broad-spectrum antibiotics that prevent the cross-linking of the peptidoglycan layer of the cell wall by inhibiting the PBPs themselves [40, 50, 51]. The β-lactam antibiotics were the first antibiotics to demonstrate significant results in combating bacterial infections. To date, they still remain the most commonly prescribed antibiotics for the treatment of bacterial infections [4, 32, 35, 52].

1.5 β-Lactam Antibiotics

The β-lactam antibiotics are a broad class of antibiotics that includes all antibacterial agents containing a β-lactam ring (a four-membered cyclic amide) in their molecular structure [50, 52]. The different subclasses of β-lactam antibiotics derive from modifications of the β-lactam nucleus and side chain(s). The β-lactam nucleus is typically a bicyclic structure containing the β-lactam ring fused to a second ring structure [52]. As shown in Figure 1.2, there are six major subclasses of β-lactam antibiotics: the cephalosporins (cephems), the carbacephems, the penillins (penams), the clavams, the carbapenems and the monobactams.

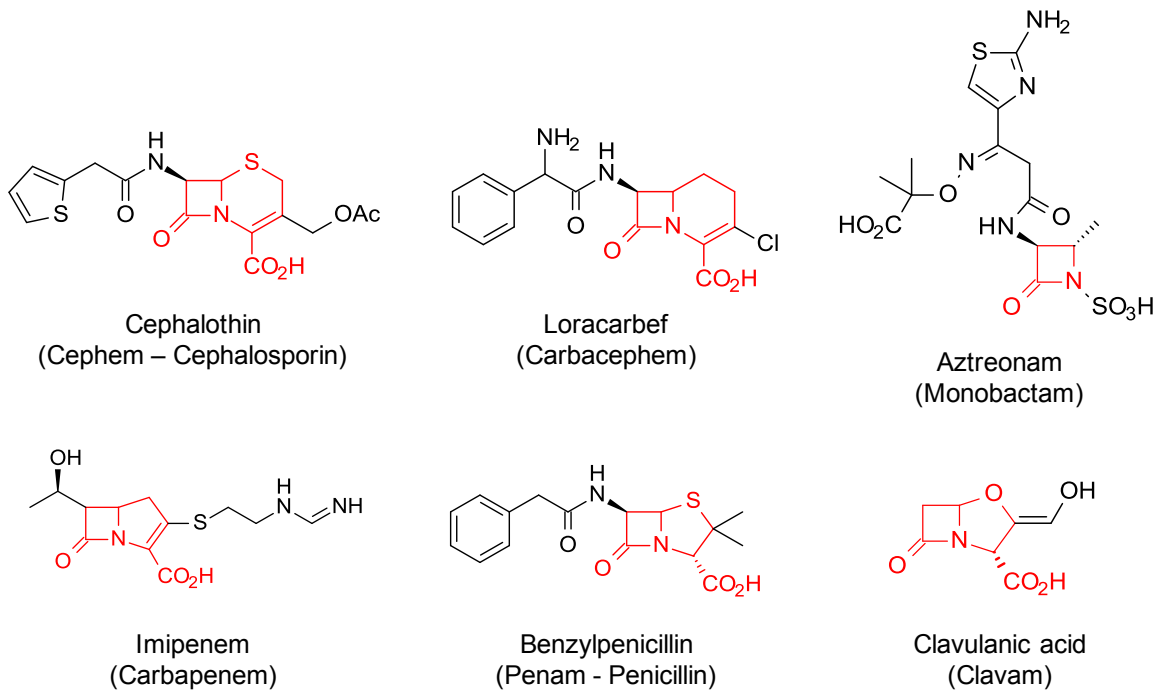

Figure 1.2: Structures of the different types of β-lactam antibiotics. The β-lactam nucleus is highlighted in red. The six major subclasses of β-lactam antibiotics are shown in parentheses. Figure adapted from reference [53].

Cephalosporins, such as cephalothin, are β-lactam antibiotics that contain a β-lactam ring fused to a 6-membered thiazine ring with a sulfur atom (see Figure 1.2). The 6-membered ring of cephalosporins is unsatured [54]. Carbacephams, such as loracarbef, are composed of a β-lactam ring fused to an unsaturated 6-membered pyridine ring (see Figure 1.2). The 6-membered ring of carbacephems, unlike that of cephalosporins, contains no heteroatom other than the nitrogen atom [55]. Penicillins, such as benzylpenicillin, are β-lactam antibiotics that contain a β-lactam ring fused to a 5-membered thiazolidine ring. The 5-membered ring of penicillins is fully saturated [54]. Clavams, such as clavulanic acid, are β-lactamase inhibitors incorporating a β-lactam ring fused to a saturated 5-membered oxazolidine ring (see Figure 1.2) [56]. Carbapenems, such as imipenem, are β-lactam antibiotics containing a saturated 5-membered pyrrolidine ring. The pyrrolidine ring of carbapenems, unlike the thiazolidine ring of penicillins, contains no heteroatom other than the nitrogen atom [57]. Monobactams, such as aztreonam, in

contrast to other subclasses of β-lactam antibiotics, contain only a single β-lactam ring (see Figure 1.2) [58].

The most employed β-lactam antibiotics for the treatment of bacterial infections are the penams (penicillins) whose nucleus arises from the "fusion" of two amino acids, namely cysteine and valine (see Figure 1.3) [52, 54, 59]. The different side chains (R) attached to these rings determines the antibacterial characteristics of the penicillin antibiotics [52].

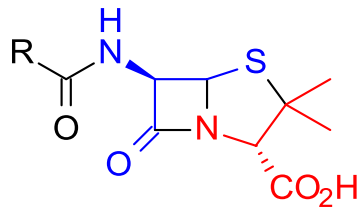

Figure 1.3: Core structure of penicillins. The β-lactam nucleus of penicillins results from the "fusion" of cysteine (blue) and valine (red).

1.6 β-Lactam Antibiotics and Cell Wall Synthesis

The cell wall is critical to bacterial cells as it is the main stress-bearing and shape-maintaining element [60]. Therefore, due to its critical role in bacterial survival, the cell wall and its enzymes are important targets for many antibiotics including β-lactams [61]. More specifically, β-lactam antibiotics inhibit the final stage of bacterial cell wall synthesis by preventing the cross-linking of the subunits forming the peptidoglycan layer of the cell wall. This stage of cell wall synthesis is important since peptidoglycan is a polymer whose cross-linking allows the formation of a strong and elastic structure. This allows the bacterium to maintain the structural integrity of its cell wall, and to uphold osmotic stability within its environment [60, 62].

The basic structure of peptidoglycan is formed by alternating β-1,4-linked *N*-acetylglucosamine (NAG) and *N*-acetylmuramic acid (NAM) subunits (see Figure 1.4) [60, 61]. A specific pentapeptide is also attached to the D-lactyl moiety of each NAM subunit to allow

cross-liking to another strand of alternating NAM and NAG subunits. This allows for the production of a three-dimensional mesh-like structure, and also causes NAM to terminate with two D-alanine residues [61]. The cross-linking of the pentapeptides of different strands of the peptidoglycan layer is mediated by transpeptidases known as penicillin-binding proteins (PBPs) [62]. PBPs assist in the cross-linking of two peptidoglycan strands through the removal of the C-terminal D-Ala residue from one of the pentapeptides [63].

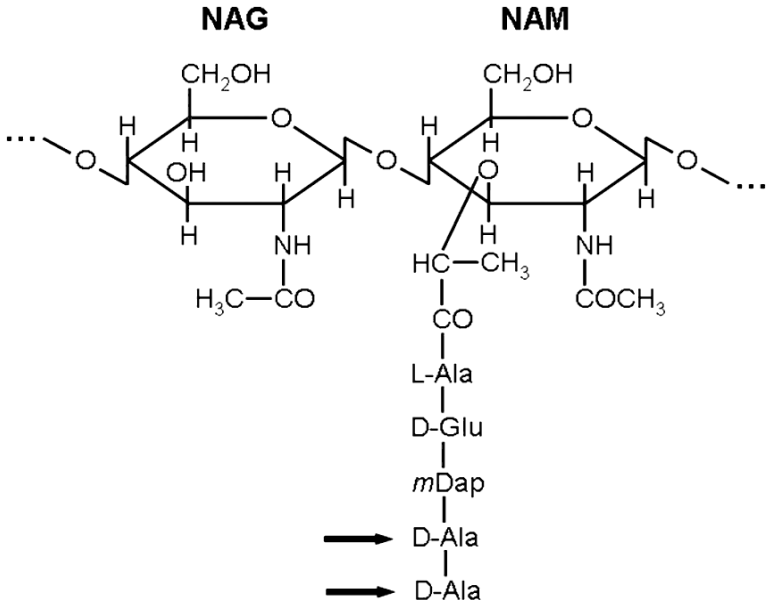

Figure 1.4: Structure of peptidoglycan from the bacterium *Helicobacter pylori*. Peptidoglycan is composed on alternating β-1,4-linked *N*-acetylglucosamine (NAG) and *N*-acetylmuramic acid (NAM) subunits. A pentapeptide is also attached to the NAM subunit for cross-linking of the peptidoglycan layers. In *H. pylori*, the pentapeptide contains a *meso*-diaminopimelate (*m*DAP) residue. The amino acids involved in cross-linking are indicated with arrows. Figure modified from reference [64].

β-Lactam antibiotics prevent peptidoglycan cross-linking since they are analogues of the D-Ala-D-Ala sequence motif of the pentapeptide terminus of the NAM subunits [50, 51]. The structural similarity between the amino acid sequence found in the β-lactam antibiotics and the NAM pentapeptide terminus allows the antibiotics to irreversibly bind the PBPs. Through this irreversible binding to the β-lactam antibiotics, the PBPs are inactivated and consequently, can no longer mediate the cross-linking of the peptidoglycan strands. Therefore, the β-lactam

antibiotics obstruct the final stage of bacterial cell wall synthesis, and cause a diminished integrity of the cell wall [51]. A bacterium unable to maintain the integrity of its cell wall can no longer maintain structural integrity or osmotic stability. Therefore, exposure to β-lactam antibiotics will eventually result in the lysis and the death of the bacterial cell [50]. However, with the commercial (over) usage of β-lactams and other antibiotics in the treatment of bacterial infections, the unavoidable problem of antibiotic resistance emerged [35].

1.7 Bacterial Antibiotic Resistance

The first warning of the potential threat of antibiotic resistance came from Alexander Fleming who warned that the misuse of penicillin and other antibacterial agents could cause the selection of mutant forms of bacterial strains, especially in the case of widespread bacteria such as *Staphylococcus aureus*. However, in the past, antibiotics were seen as miracle drugs and Fleming's warning was ignored [65]. These "miracle" drugs were then used as the treatment for the most minor infections as well as for infections that were non-bacterial in nature [38, 65]. As a result of this misuse, it did not take long to discover the truth behind Fleming's words. For example, *S. aureus* became resistant to antibiotics at record breaking speeds. Within a few years of the usage of penicillin in clinics, this antibiotic became ineffective against 50 % of *S. aureus* strains [65]. Therefore, due the misuse of antibiotics, today's society is in the middle of an emerging antibiotic resistance crisis because of the ever increasing difficulty in treating bacterial infections with traditional antibiotics [4, 35].

1.7.1 Misuse of Antibiotics in Human Medicine

With the discovery of antibiotics, it was believed that the fight against infections had been won. However, since the development of the first antibiotics, bacterial antibiotic resistance has been a threat in combating bacterial infections. The emergence of bacterial resistance to antibiotics has

been aided by the misuse of these miracle drugs. Major causes of antibiotic resistance include inappropriate prescription of antibiotics for flu, colds, coughs, sore throats and runny noses, which are caused by viruses [38]. Furthermore, many people shorten their antibiotic treatment course when symptoms subside, often resulting in re-infection since the shortened treatment only eradicated the most susceptible bacteria, and allowed the most dangerous ones to survive [66]. In addition, poor hand hygiene by healthcare workers has also been associated with bacterial antibiotic resistance due to cross-contaminations of multiple patients by resistant microorganisms [67]. Therefore, the misuse of antibiotics by the human population continues to be an important factor in the emergence of antibiotic resistance.

1.7.2 Transfer of Antibiotic Resistance Genes

Despite the misuse of antibiotics, the selection of resistant bacteria due to improperly employed antibiotics is not the sole cause of the emergence of bacterial antibiotic resistance [68]. In bacteria, antibiotic resistance is mainly caused by the convergence of two main elements. The first element is the presence of an antibiotic with the capacity of killing or inhibiting the growth of the majority of a bacterial colony. The second element is the presence of at least one bacterium within that colony which can express the genes for antibiotic resistance. The consequence of the combination of these two elements is that, upon the usage of an antibiotic, susceptible bacteria will die while resistant bacteria will survive. This causes the selection of resistant bacteria which, consequently, causes the selection of the resistance genes which can then be transferred from one bacterium to another [65, 69]. These resistance genes are typically found in three primary bacterial mobile genetic elements: gene cassettes, transposons and plasmids. These elements can carry the resistance genes for several antibiotics, and they have a very broad host range (i.e., they can be transferred to many different bacterial strains) [70]. Gene

cassettes typically contain a recombination site, and often carry genes for antibiotic resistance [70, 71]. Transposons (also known as transposable elements) are DNA sequences capable of changing positions within the genome through a process known as transposition. Transposons also have the ability to move from one bacterial host to another. Transposons often harbour antibiotic resistance genes. Plasmids are small circular DNA molecules that are separate from chromosomal DNA, and can also replicate independently of the chromosome. Plasmids often carry genes, such as antibiotic resistance genes, which are useful for the survival of their bacterial host [65, 70, 72, 73]. Therefore, the resistance genes located on these bacterial mobile elements are commonly transferred through three primary mechanisms: conjugation, transformation and transduction [65].

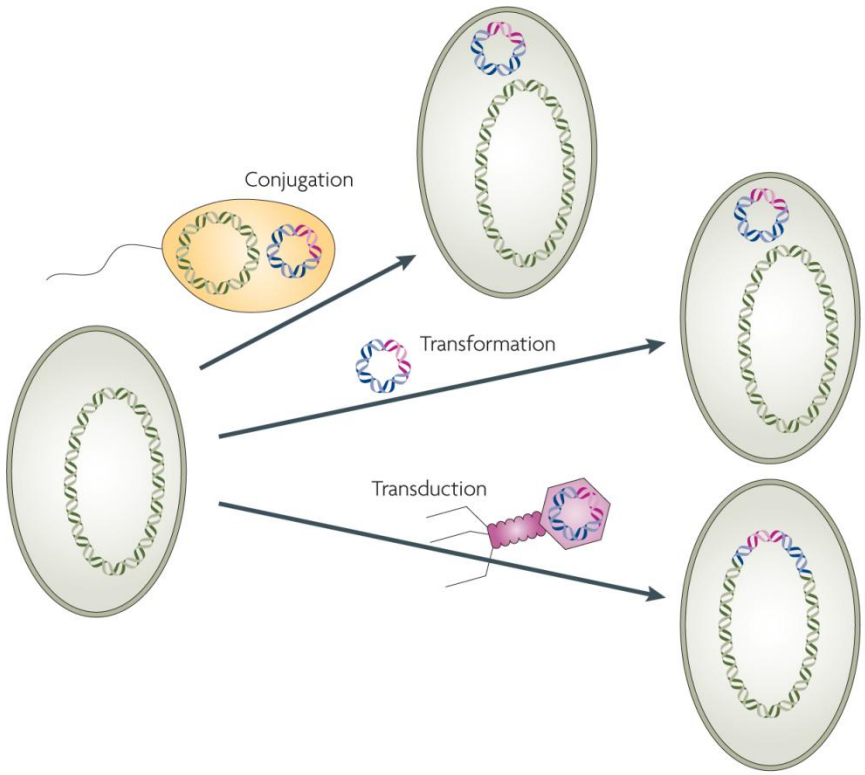

Figure 1.5: Transfer mechanisms of bacterial antibiotic resistance genes. DNA from the donor containing antibiotic resistance genes (pink) can be transferred between bacterial strains by three methods: conjugation, transformation and transduction. Conjugation, transformation and transduction mediate the gene transfer through bacterial cell-to-cell contact, the uptake of free extracellular DNA and bacteriophages, respectively. Figure modified from reference [74].

Conjugation is the most common method for transferring antibiotic resistance genes among bacteria. Conjugation involves the unidirectional transfer of genetic material from a donor to a recipient bacterial cell through direct cell contact (see Figure 1.5). The contact is usually mediated by a conjugative pilus on the donor cell which allows for the temporary transfer of bacterial mobile genetic elements such as plasmids [65, 73]. Another method of resistance gene transfer is transformation. Transformation involves the direct passage of exogenous DNA (also known as free DNA) containing resistance genes from one bacterial cell to another (see Figure 1.5). This free DNA usually originates from resistant bacteria that have died and broken apart in the extracellular environment. The recipient bacteria can simply uptake the exogenous DNA into their cytoplasm and then incorporate this DNA into their own. However, the incorporation of DNA from the extracellular milieu is a complex task requiring the bacteria to be in a state of competence for the transformation. Competence describes the ability of a bacterial cell to uptake DNA from its extracellular environment [65, 75]. Over 40 bacterial species have been identified as being naturally competent and consequently, naturally transformable [75]. The last gene transfer method is known as transduction. Transduction relies on the use of a vector such as a bacteriophage for the transfer (see Figure 1.5). A bacteriophage (or phage) is a virus that can infect bacteria. Therefore, the phage acquires the resistance genes from a previously infected bacterium, and introduces them into the receiving bacterium [65].

1.8 Mechanisms of Bacterial Antibiotic Resistance

Over the years, bacteria themselves have acquired the ability to counteract the effects of antibiotics through four primary mechanisms: altered antibiotic targets, altered outer membrane permeability, efflux pumps and β-lactamases.

1.8.1 Altered Antibiotic Targets

The bacterial cell wall is an essential structure that provides support and protection to bacteria making it the target for many antibiotics including the β-lactam antibiotics [60, 61]. In the case of β-lactam antibiotics, their bacterial targets are the penicillin-binding proteins (PBPs) involved in the cross-linking of the peptidoglycan layer in the final stage of cell wall synthesis. Therefore, resistance to β-lactam antibiotics can emerge though alterations of the PBPs. These modifications result in reduced binding of the β-lactam antibiotics to these transpeptidases [76]. This mechanism of resistance is prevalent in Gram-positive bacteria such as *Staphylococcus aureus* and *Streptococcus pneumoniae*, but is much less commonly used by Gram-negative bacteria. Alterations in the PBPs can occur through mutations of the bacterial chromosomal genes encoding the PBPs or through the acquisition of foreign genes encoding new PBPs [76, 77].

Pneumococci are normally extremely sensitive to β-lactam antibiotics such as penicillin. Non-resistant pneumococci can be killed with concentrations of penicillin $\geq$ 0.1 μg/mL. Resistant strains of pneumococci have the ability to survive up to 8 μg/mL of penicillin [78]. β-Lactam resistance in pneumococci is mainly the result of alterations in the PBPs. Even a single amino acid substitution within the transpeptidase domain of the PBPs can allow for very low-level resistance to penicillin [78]. Mutations occurring in the penicillin-binding motifs of the PBPs result in an increased resistance to penicillin in bacteria such as *S. pneumonia*. These PBPs with decreased affinity for β-lactam antibiotics are known as low-affinity PBPs [78–80]. These low-affinity PBPs can be encoded by the *mecA* gene. The *mecA* gene is found in numerous bacterial strains, but is most commonly found in *S. aureus* strains demonstrating resistance to methicillin [78]. Although the origins of acquisition of the *mecA* gene by *S. aureus* remains

unknown, it is believed that this bacterial strain acquired this gene through gene transfer from an unknown species [79]. The *mecA* gene encodes a low-affinity PBP known as PBP2a (penicillin-binding protein 2a) which does not bind β-lactam antibiotics. This enables the transpeptidase activity of the PBPs even in the presence of β-lactam antibiotics, preventing them from inhibiting bacterial cell wall synthesis [81].

1.8.2 Altered Outer Membrane Permeability

Gram-negative bacteria are generally more resistant to antibiotics than Gram-positive bacteria due to the presence of an outer membrane. The outer membrane is an efficient barrier against certain antibiotics as it contains narrow porin channels which limit the penetration of hydrophilic solutes. Alterations of these porins can limit the number of antibiotics that can cross the outer membrane, and penetrate into the bacterial cell [76, 82, 83]. For example, the Gram-negative bacterium *Pseudomonas aeruginosa* is resistant to imipenem due to the loss of a carbapenem-specific porin [76]. In addition, the outer membrane contains a lipopolysaccharide leaflet which slows down the inward diffusion of solutes such as antibiotics [82, 83]. Therefore, antibiotic resistance in Gram-negative bacteria can be accomplished through the alteration of permeability of the outer membrane. However, even in bacteria such as *P. aeruginosa,* containing an outer membrane of extremely low permeability, the periplasmic concentrations of many antibiotics reach 50% of their external concentrations in 10 s to 20 s [82]. This suggests that the outer membrane alone cannot completely account for the extent of antibiotic resistance in these bacteria. Another mechanism is needed in addition to the membrane barrier in order to obtain these high levels of antibiotic resistance, a mechanism that has been shown to rely on the presence of efflux pumps [79, 82].

1.8.3 Efflux Pumps

Efflux pumps are present in all living organisms. These pumps have the ability to actively export a wide variety of substances from cells including bile, hormones and host defence molecules [84]. Efflux pumps can be specific for one substrate or can transport a range of structurally dissimilar compounds such as antibiotics from different classes. In bacteria, the pumps that transport several antibiotics can be associated with multidrug resistance (MDR) and consequently, they are known as multidrug resistance efflux pumps [79, 82, 84]. In bacteria, there are five families of MDR efflux pumps: the ATP-binding cassette (ABC) superfamily, the major facilitator superfamily (MFS), the multi-antimicrobial extrusion protein (MATE) family, the small multidrug resistance (SMR) family, and the resistance nodulation division (RND) superfamily [85].

The ABC superfamily is one of the largest and oldest families of MDR efflux pumps and includes pumps such as LmrA from the Gram-negative bacterium *Lactococcus lactis* (see Figure 1.6). These transporters are present in all kingdoms of life, and utilize the energy of adenosine triphosphate (ATP) hydrolysis for efflux [85, 86]. The MFS is another large and old family of MDR efflux pumps. These pumps are secondary transporters which are driven by chemiosmotic energy, and include proton/drug antiporters such as QacA from the Gram-positive bacterium *Staphylococcus aureus* (see Figure 1.6) [85]. The MATE family of MDR efflux pumps is the most recently discovered family of MDR efflux pumps. These pumps are found in all kingdoms of life, and they are secondary transporters driven by the movement of sodium ions, and include Na^+/drug antiporters such as NorM from the Gram-negative bacterium *Vibrio parahaemolytic* (see Figure 1.6) [85, 87]. The SMR family is a small family of MDR efflux pumps and includes H^+/drug antiporters such as EmrR from *Escherichia coli* (see Figure 1.6). The proton motive

force (PMF) drives these transporters through the movement of hydrogen ions [85, 88]. The RND superfamily is another smaller family of MDR efflux pumps. These transporters are bacterial-specific and driven by the movement of hydrogen ions. They are commonly found in Gram-negative bacteria and include proton-drug pumps such as the AcrAB-TolC system (efflux pumps comprised of AcrA, AcrB and TolC) from *E. coli* (see Figure 1.6) [82, 85]. Three genes are typically responsible for encoding these pumps. The first gene encodes a membrane fusion protein that is associated with the cytoplasmic membrane such as AcrB. The second gene encodes a transporter which allows for the export of the antibiotic across the inner membrane such as AcrA. The third gene encodes an outer membrane protein that facilitates the passage of the antibiotic across the outer membrane such as TolC. Together, these three proteins form a channel that crosses both the inner and outer membranes of the bacterium. This allows the target antibiotic to be effluxed directly from the cytoplasm to the extracellular environment, a feature distinct from that encountered with the four other families of MDR efflux pumps [84, 89]. Therefore, multidrug resistance in bacteria is due mainly to the presence of efflux pumps which are capable of actively exporting multiple antibiotics [79, 82, 84].

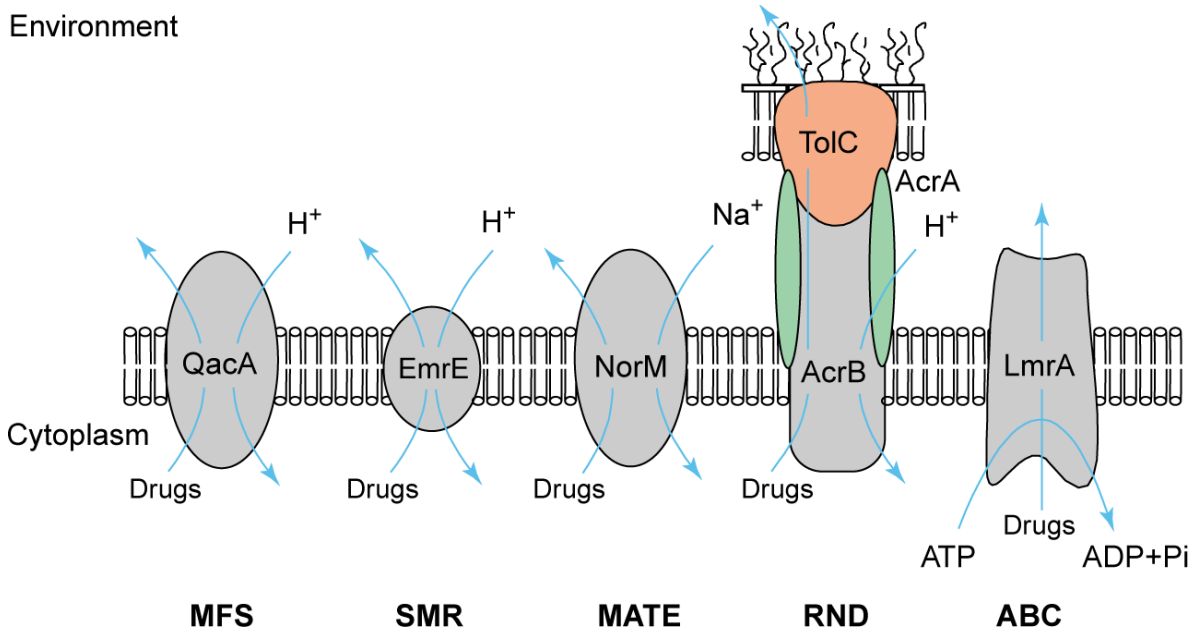

Figure 1.6: Multidrug resistance efflux pumps in bacteria. Bacteria have five families of multidrug resistance efflux pumps: the major facilitator superfamily (MFS), the small multidrug resistance (SMR) family, the multi-antimicrobial extrusion protein (MATE) family, the resistance nodulation division (RND) superfamily, and the ATP-binding cassette (ABC) superfamily. Figure taken from [85].

1.8.4 β-Lactamases

β-Lactam antibiotics are an important threat to the survival of bacteria since they inhibit cell wall synthesis resulting in the lysis and the death of the bacteria [50]. One of the most effective methods employed by bacteria to resist the devastating effects of β-lactam antibiotics is the production of enzymes capable of degrading/modifying β-lactam antibiotics. These enzymes are known as β-lactamases and confer antibiotic resistance to bacteria by rendering β-lactam antibiotics inactive through the hydrolysis of the amide bond of the β-lactam ring [90, 91]. The β-lactamase enzymes are separated into four different classes in accordance with their amino acid sequence, and the nucleophile used in their enzymatic mechanism [90]. Classes A, C and D are serine β-lactamases since they employ a serine residue as the nucleophile (see Figure 1.7A). Class B β-lactamases, also termed metallo-β-lactamases (MBLs), contain zinc ion(s) in their active site (see Figure 1.7B) [92]. However, metal ions such as cobalt, cadmium or manganese

can also be employed by these enzymes *in vitro* [93]. MBLs represent the primary defence mechanism to β-lactam antibiotics in Gram-negative bacteria [94].

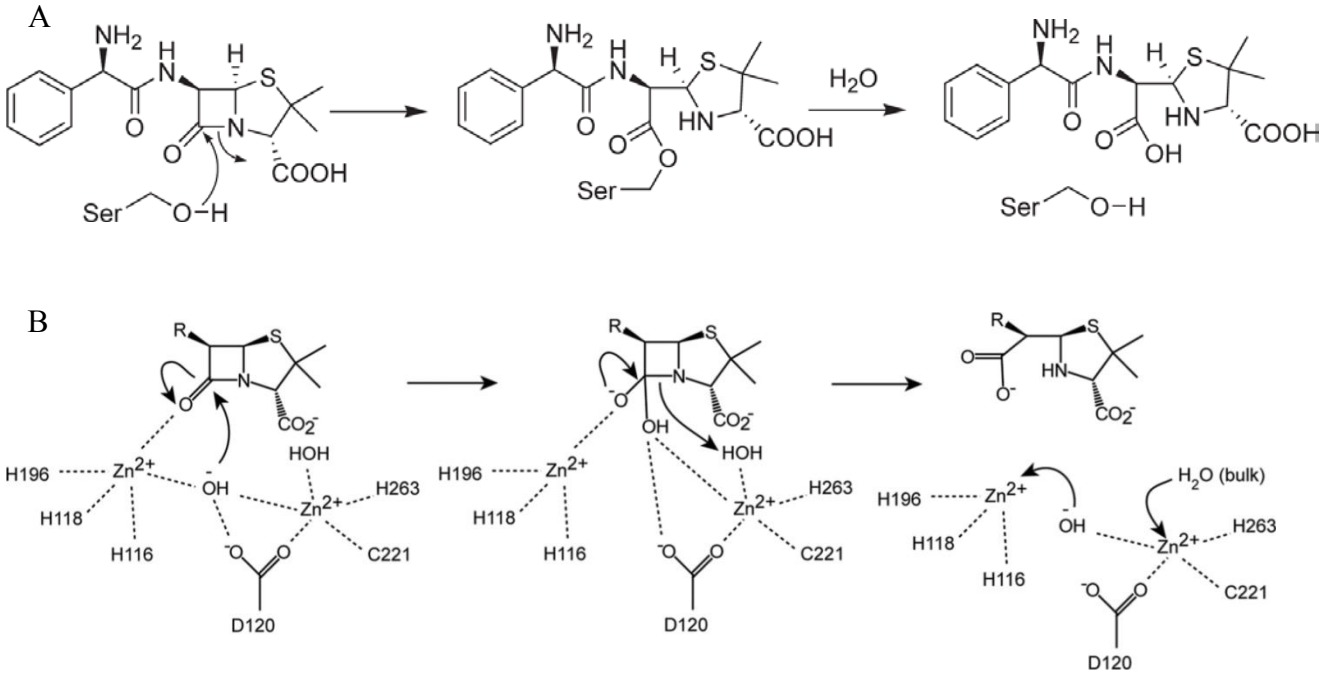

Figure 1.7: Catalytic mechanism of β-lactamases. A) The catalytic mechanism of serine β-lactamases. The hydroxyl group attached to the active site serine residue attacks the amide bond of the β-lactam ring producing an ester intermediate. The hydroxyl group is regenerated following the hydrolysis of the ester. B) The catalytic mechanism of dizinc metallo-β-lactamases. The hydroxide ion bridging both Zn^{2+} ions in the active site attacks the amide bond of the β-lactam ring, forming an oxyanion intermediate, which is stabilized by the Zn^{2+} ions. The oxyanion then attacks the water molecule bound to the second Zn^{2+} ion. The hydroxide and the water molecules are both regenerated following elimination of the product. Figure taken from references [53, 95].

1.9 Metallo-β-Lactamases

MBLs are the most worrisome enzymes capable of conferring bacterial resistance to β-lactam antibiotics [96]. When they were originally discovered, MBLs were only found in a limited number of bacteria. Since then, MBLs are being isolated from numerous Gram-negative bacteria such as *Enterobacteriacea*, *Pseudomonas aeruginosa* and multiple species of *Acinetobacter* [97]. A reason for this rapid spread of MBLs is that over 75% of MBLs are plasmid-encoded, allowing them to be easily transferred from one bacterium to another [91, 97]. In addition, MBLs are

insensitive to a large variety of common serine β-lactamase inhibitors such as clavulanic acid, sulbactam and tazobactam [92]. These β-lactamase inhibitors restore the activity of commonly used β-lactam antibiotics by adapting to the role of mechanism-based (sometimes referred to as suicide) inhibitors. These inhibitors can irreversibly bind, and consequently inactivate serine β-lactamases. Therefore, when supplemented with these inhibitors, β-lactam antibiotics are capable of maintaining their bacteriostatic or bactericidal activity against serine β-lactamase-producing bacteria. However, MBLs are capable of cleaving these inhibitors, thus maintaining their catalytic activity against co-administered β-lactam antibiotics [92]. Furthermore, not only are MBLs capable of resisting β-lactam inhibitors, and inactivating all β-lactam antibiotics (except for monobactams), they are also known for their efficient carbapenemase activity [96]. This is especially worrisome since carbapenems are the β-lactam antibiotics with the broadest spectrum of activity rendering them the last resort for many serious bacterial infections [96, 98]. However, carbapenems are proving to be ineffective in the fight against the over 80 different MBLs that have presently been identified worldwide [91].

MBLs are separated into three subclasses (B1, B2 and B3) based on their zinc coordination and sequence similarities. Most MBLs are between 240 and 310 amino acid residues in length prior to the cleavage of the signal sequence (17 to 30 amino acids residues) to obtain the mature form of these enzymes [53]. The length of these MBLs varies due to insertions and deletions of amino acids. However, the MBLs from all three classes can still be aligned through homologous secondary structure elements (e.g., α-helices and β-sheets) to create a standard numbering scheme for class B β-lactamases known as the BBL numbering scheme [99]. In addition to having similar sequence lengths, the MBLs from all three subclasses are typically monomeric (with few exceptions), and share a common four-layer crystal structure. The four layers consist

of two central β-sheets flanked by two α-helices (see Figure 1.8). This fold is typically called an α-β/β-α sandwich [53, 91, 93]. While this fold was originally discovered in MBLs, it can also be found in a range of other proteins such as glyoxalase II, lactonases, nitric oxide reductase and β-hydroxylase [100–103]. Although the three MBL subclasses share similar fold and sequence length, they differ in their zinc coordination [53, 104]. Divalent zinc (Zn^{2+}) plays an essential role in MBL catalysis since it is an efficient Lewis acid, has a flexible coordination geometry, and fast ligand exchange [53, 104]. MBLs possess two zinc binding site (Zn1 and Zn2), although not all MBLs are functional with two zinc ions (see Figure 1.8). The catalytic activity of the majority of MBLs can be maintained whether the MBLs possess one zinc ion (monozinc form) or two zinc ions (dizinc or binuclear form). In some cases, however, the presence of the second zinc ion has been shown to diminish the catalytic activity of the MBLs [91, 96].

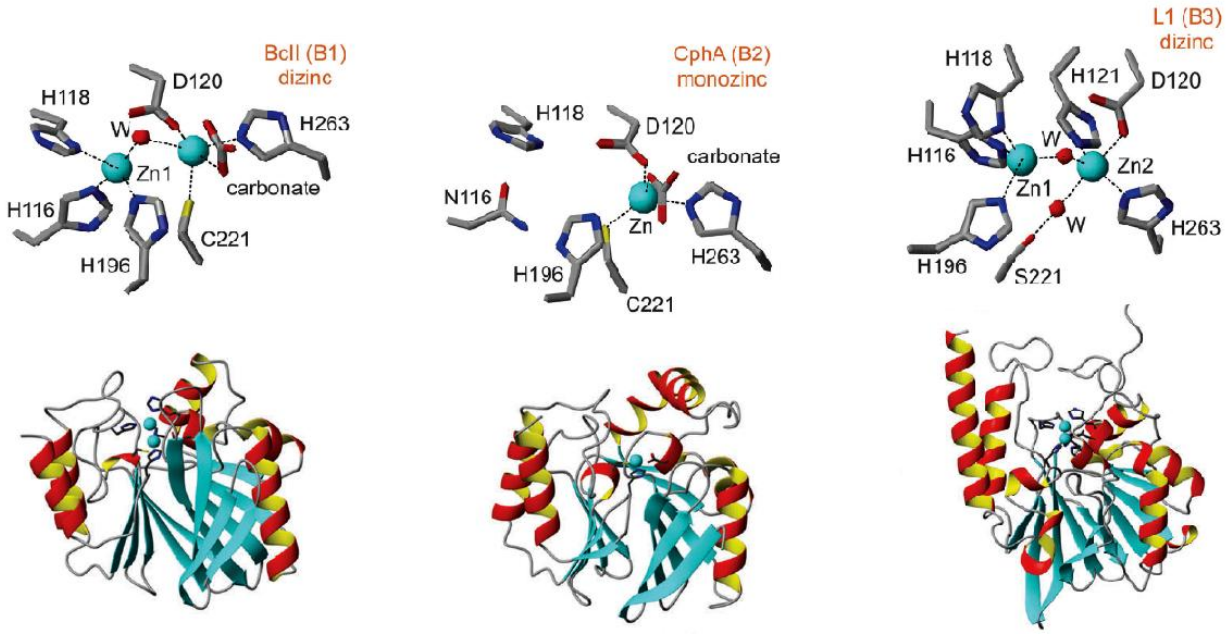

Figure 1.8: Active sites and crystal structures of metallo-β-lactamases. Depicted are the active sites of BcII, CphA and L1 from metallo-β-lactamase subclasses B1, B2 and B3, respectively. Figure modified from reference [53].

1.9.1 Subclass B1

Subclass B1 is the largest MBL subclass and includes well studied MBLs such as BcII from *Bacillus cereus*, CcrA from *Bacteroides fragilis* and NDM-1 from *Klebsiella pneumoniae* as well as SMP-1, IMP-1 and VIM-2 from *Pseudomonas aeruginosa* [93, 105–110]. The MBLs from subclass B1 share a sequence identity of over 23% as well as the broadest substrate specificity. These enzymes have the ability to cleave almost all β-lactam antibiotics including penicillins, cephalosporins and carbapenems. However, subclass B1 enzymes are incapable of hydrolyzing monobactams [53, 96, 104]. Furthermore, all B1 enzymes are monomeric, and their active site is typically located at the edge of the β-sandwich of the α-β/β-α fold. In addition, the zinc-coordinating ligands are highly conserved between the subclass B1 enzymes. In the first zinc site (Zn1), also known as the 3H site, the metal is tetrahedrally coordinated to the side chains of three histidine residues (116, 118 and 196; BBL numbering), and to one water (or hydroxide) molecule (Wat_1). The second zinc site (Zn2), also known as the DCH site, binds zinc trigonal-bipyramidally with aspartate 120, cysteine 221, histidine 263 and one water molecule (or hydroxide) (Wat_1) serving as a ligand (see Figure 1.8). The fifth ligand is usually another water (or a carbonate) molecule which is often referred to as the apical water (Wat_2) [53, 104]. The water (or hydroxide) molecule (Wat_1) bridging both zinc sites acts as the nucleophile which is necessary for the hydrolysis of the β-lactam ring. This nucleophile attacks the carbonyl carbon atom of the β-lactam ring [91, 93]. Although, subclass B1 enzymes have two zinc binding sites, they demonstrate catalytic activity with either one or two zinc ions [53, 104].

1.9.2 Subclass B2

Subclass B2 includes MBLs such as CphA from *Aeromonas hydrophila* and ImiS from *Aeromonas veronii* [111, 112]. As in the case of B1 enzymes, all subclass B2 enzymes are

monomeric, but they only share an 11% sequence identity with subclass B1 enzymes [96]. Unlike subclass B1, the subclass B2 enzymes are strictly carbapenemases, and demonstrate poor activity against penicillins, cephalosporins and monobactams. Although their overall α-β/β-α fold shares the same characteristics as other MBLs, their active site groove is deeper and narrower. This change in the position of the active site is believed to be the cause of the high specificity of these enzymes for carbapenems [53]. Furthermore, the Zn1 site of the B2 enzymes is formed by asparagine 116, histidine 118 and histidine 196. The asparagine residue replaces histidine 116 in comparison to the Zn1 site of the subclass B1 enzymes [53, 104]. However, just as in the case of subclass B1, subclass B2 enzymes demonstrate a conserved Zn2 site which coordinates zinc with aspartate 120, cysteine 221 and histidine 263 (see Figure 1.8) [104]. Although B2 enzymes still possess two zinc binding sites, they are typically active with one zinc ion only since the binding of the second zinc ion has been shown to inhibit the activity of these enzymes [53, 104].

1.9.3 Subclass B3

Subclass B3 includes MBLs such as L1 from *Stenotrophomonas maltophilia* and FEZ-1 from *Legionella gormanii* [113, 114]. Distinct from B1 and B2 subclasses, B3 enzymes can be either monomeric (e.g., FEZ-1) or multimeric (e.g., L1, which is tetrameric) [96, 115]. Subclass B3 proteins only have nine conserved residues when compared to both B1 and B2 enzymes [96]. Similar to subclass B1, the subclass B3 MBLs are capable of cleaving most β-lactam antibiotics (i.e., penicillins and cephalosporins) except for monobactams. However, the B3 enzymes are less efficient in hydrolyzing carbapenems when compared to both other subclasses of MBLs [53]. Nevertheless, like subclass B1 enzymes, the Zn1 site of B3 proteins coordinate zinc using histidine residues 116, 118 and 196 (BBL numbering) and a water molecule [104]. The Zn2 site

coordinates the zinc ion trigonal-bipyramidally with aspartate 120, histidine 121, histidine 263, and two water molecules (histidine 121 replaces cysteine 221 in comparison to the Zn2 site of the subclass B1 enzymes; see Figure 1.8). Although subclass B3 enzymes have two zinc binding sites, they demonstrate significant catalytic activity with one zinc ion [53, 104].

1.10 MBLs of Clinical Importance

1.10.1 NDM-1

In 2008, a previously unknown MBL was isolated from the Gram-negative bacteria *Klebsiella pneumoniae* and *Escherichia coli* [116, 117]. This bacterium was recovered from a Swedish patient of Indian origin who caught a urinary tract infection after receiving treatment in a hospital in New Delhi, India. This unknown MBL was designated the New Delhi metallo-β-lactamase (NDM-1) and was classified as a B1 enzyme [117, 118]. Since its isolation in Sweden, NDM-1 has rapidly spread around the globe being isolated in numerous countries including the United States of America, Canada, the United Kingdom, France, Germany, Japan and China. NDM-1 easily spread worldwide since, like many MBLs, NDM-1 is plasmid-encoded, and can be easily transferred between different bacterial strains [51, 119]. Furthermore, the plasmid harbouring the NDM-1 gene is quite large (180 kb for *K. pneumoniae* and 140 kb for *E. coli*), and contains resistance genes to almost all β-lactam antibiotics making NDM-1 a serious health threat [116]. In 2009, the Health Protection Agency issued a national alert due to the growing concern revolving around the rapid spread of NDM-1 [117].

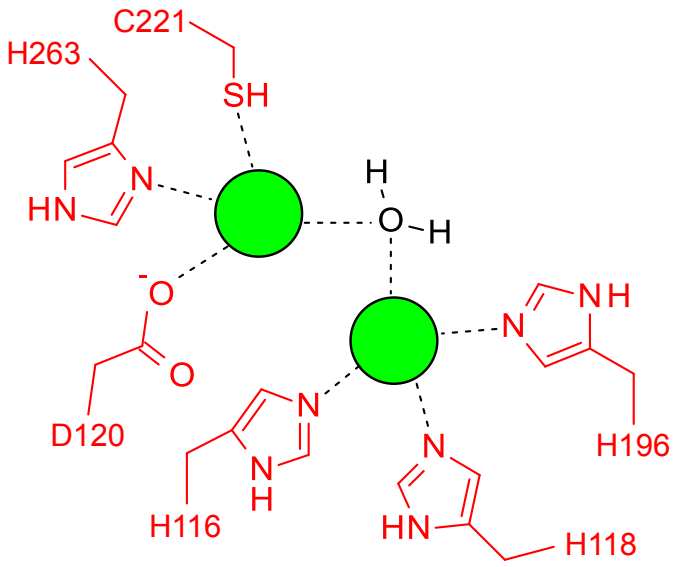

Figure 1.9: Active site of NDM-1. NDM-1 has two zinc ions (green): one in the 3H site and the other in the DCH site. The key amino acid residues for zinc-binding are coloured red.

NDM-1, similar to most MBLs, is a monomer composed of 270 amino acid residues and a signal peptide of 28 amino acid residues. In addition, similar to most MBLs from subclass B1, NDM-1 contains two zinc ions (one in the 3H site and the other in the DCH site; see Figure 1.9) located in an active site at the edge of the two β-sheets of the typical α-β/β-α fold. However, contrary to other MBLs from subclass B1, the structure of NDM-1 presents an open, large and flexible active site. It is thought that this modified active site allows NDM-1 to have the ability to hydrolyze an increased number of β-lactam antibiotics is comparison to other MBLs [51]. Therefore, it is not surprising that NDM-1 possesses a very low sequence identity with other MBLs. The MBLs that demonstrate the highest similarity with NDM-1 are VIM-2 and IMP-1, with 32% sequence identity [91].

1.10.2 VIM-2

MBL subclass B1 contains a variety of enzymes, but none are as prevalent as VIM (Verona integrin-encoded metallo-β-lactamase). VIM, more specifically VIM-1, was originally isolated from *Pseudomonas aeruginosa* in Verona, Italy in 1997 [110, 120]. Since the VIM enzymes are

subclass B1 enzymes, they possess the ability to cleave most β-lactam antibiotics including penicillins, cephalosporins and carbapenems [110, 121]. However, VIM, similar to many other MBLs, is incapable of hydrolyzing monobactams [58, 110]. Currently, 11 different types of VIM enzymes (VIM-1 to VIM-11a and -11b) have been isolated worldwide [120].

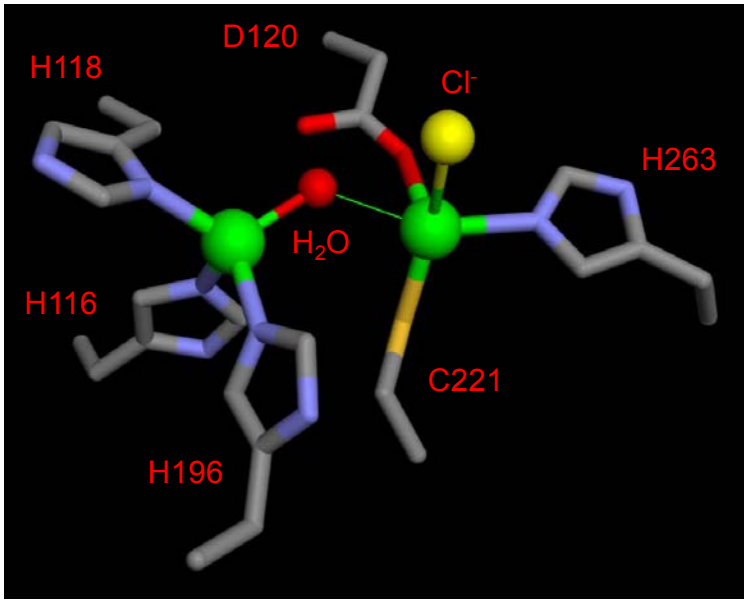

Figure 1.10: Active site of VIM-2. The active site contains two zinc ions (depicted in green) which are coordinated by the 3H and the DCH sites. A water molecule (shown in red) bridges the two zinc ions. A Cl^- ion, bound to the Zn^{2+} ion in the DCH-site (depicted in yellow), is an artifact of the crystallization procedure. Figure adapted from reference [110].

The VIM enzyme that was studied during this research project is VIM-2. VIM-2 shares a 90% amino acid sequence identity with the originally discovered VIM-1 enzyme. VIM-2 was originally isolated in *P. aeruginosa* in France in 1996 [120]. VIM-2 is an MBL with a molecular mass of 25.5 kDa, and contains 240 amino acids in its mature form. In its native, reduced form, VIM-2 possesses two zinc ions in its active site: one in the 3H site and the other in the DCH site. These two zinc ions are bridged by a water molecule (see Figure 1.10) [110]. Furthermore, VIM-2 is currently the most commonly isolated MBL in the clinical environment as well as the most widespread MBL [122], rendering VIM-2 the primary target for this MBL research.

1.10.3 IMP-1

The IMP enzymes (subclass B1) are thought to be the most dangerous MBLs. IMP genes are located on two mobile bacterial genetic elements: plasmids and integron cassettes. Therefore, these two mobile elements allow the IMP enzymes to be easily and rapidly transferred among different bacteria [93, 123]. Currently, 18 different types of IMP enzymes (IMP-1 to IMP-18) have been isolated from numerous bacterial strains [120].

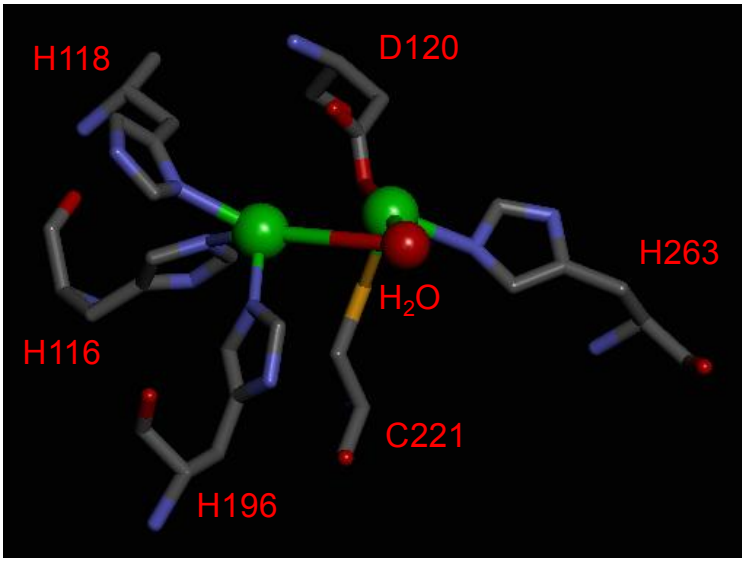

Figure 1.11: Active site of IMP-1. The active site of IMP-1 contains two zinc ions (depicted in green) which are coordinated by the 3H and the DCH sites. A water molecule (shown in red) bridges the two zinc ions. Figure adapted from reference [93].

The IMP enzyme that was the focus of this research project is IMP-1. IMP-1 was originally isolated from *Pseudomonas aeruginosa* in Japan in 1988 [90, 120]. In 1991 and 1993, IMP-1 was once again isolated in Japan, but from the Gram-negative bacterium *Serratia marcescens* [120]. This (rapid) spread of IMP-1 between different bacterial strains is a result of the IMP-1 genes being encoded by both plasmids and integrons. Currently, IMP-1 is being isolated from multiple bacterial species including *Pseudomonas*, *Serratia*, *Acinebacter* and *Klebsiella* [93, 120, 123]. IMP-1 is an MBL with a molecular mass of 25 kDa, and contains 228 amino acid residues

in its mature form. IMP-1 was shown to contain two zinc ions in its active site (see Figure 1.11), and shares a 31% sequence identity with VIM-2 [90, 110].

1.11 Cationic Peptides

To this day, there are still no clinically approved inhibitors for MBLs. The inability to design MBL inhibitors is a direct consequence of the diversity of the active sites that differentiate one MBL from another [90, 91]. However, previous (unpublished) studies have demonstrated that cationic peptides may possibly have the ability to inhibit MBLs. The usage of these cationic peptides as potential inhibitors of MBLs was discovered accidentally by a student of Dr. Siemann's group at Laurentian University (Sudbury, Ontario, Canada). This student noticed that IMP-1 was inhibited by a common substrate of the anthrax lethal factor, a zinc-dependent endopeptidase [124]. The structure of this peptide, the anthrax lethal factor protease substrate (S-*p*NA), is Ac-Gly-Tyr-βAla-$(Arg)_8$-Val-Leu-Arg-*p*NA [125]. Following this discovery, Dr. Dmitrienko's group at the University of Waterloo (Waterloo, Ontario, Canada) discovered that the cationic peptide was also a potent inhibitor of VIM-2.

It is puzzling that a peptide would be able to inhibit these enzymes because of the stereochemistry of the active site. β-Lactams imitate the D-Ala-D-Ala configuration, while the cationic peptides are in the L, L configuration. A better understanding of the molecular basis for the interaction of peptides with MBLs could potentially lead to the development of novel MBL inhibitors.

Chapter 2: Thesis Objectives

With the wide-spread emergence of microbial antibiotic resistance due to the production of MBLs, new inhibitors of these enzymes must be developed as no clinically approved inhibitors currently exist for MBLs. However, preliminary studies on cationic peptides have demonstrated their potential to inhibit MBLs.

Hence, the objective of this study was to determine the structure-activity relationship between subclass B1 metallo-β-lactamases, VIM-2 and IMP-1, and cationic peptides. This relationship was investigated through the assessment of the inhibitory potency of a variety of peptides bearing cationic residues, the examination of the effect of different β-lactam substrates on peptide-mediated inhibition, the evaluation of the inhibition of enzyme function in the presence of salts (which could interfere with inhibition), and the determination of the mechanism of inhibition.

A better understanding of the structure-activity relationship between metallo-β-lactamases and cationic peptides could be exploited for the development of novel MBL inhibitors for potential clinical use.

Chapter 3: Materials and Methods

3.1 Chemicals

Chemicals were obtained as indicated in Table 3.1**,** and were of the highest grade available. All peptides were custom-synthesized by Biomatik Corp. (Cambridge, Ontario, Canada) except for peptides **11** and **17**, which were purchased from EMD Millipore Corp. (Bellerica, Massachusetts, U.S.A.) and Bachem AG (Bubendorf, Switzerland), respectively (see Table 3.2). All other chemical were obtained from Bioshop Canada Inc. (Burlington, Ontario, Canada).

Table 3.1: Chemicals listed according to their suppliers.

Supplier	**Reagent**
AMRESCO LLC. (Solon, Ohio, U.S.A.)	β-mercaptoethanol (BME)
AK Scientific Inc. (Mountain View, California, U.S.A.)	Ceftazidime
BDH Inc. (Toronto, Ontario, Canada)	Sodium sulfate (Na_2SO_4)
Brenntag Canada Inc. (Toronto, Ontario, Canada)	Hydrochloric acid (HCl)
Caledon Laboratories Ltd. (Georgetown, Ontario, Canada)	Dimethyl sulfoxide (DMSO)
Dr. Gary Dmitrienko (Department of Chemistry, University of Waterloo, Waterloo, Ontario, Canada)	Metallo-β-lactamases (IMP-1 and VIM-2) UW substrates (UW-57 and UW-58)
EMD Millipore Corp. (Bellerica, Massachusetts, U.S.A.)	Milli-Q ultrapure water (≥ 18.2 MΩ cm resistivity)
Life Technologies Inc. (Burlington, Ontario, Canada)	Alexa Fluor 488 C_5-maleimide Alexa Fluor 546 C_5-maleimide
Macherey-Nagel GmbH & Co. KG (Düren, Germany)	POLYGRAM CEL 300 AC-10% (Fibrous cellulose with 10% acetylated cellulose on polyester sheet for TLC)
Merck Research Laboratories (Rahway, New Jersey, U.S.A.)	Imipenem
Oxoid Ltd. (Basingstoke, Hampshire, England)	Nitrocefin

Sigma-Aldrich Co. (St-Louis, Missouri, U.S.A.)	2,6-pyridinedicarboxylic acid (Dipicolinic acid) 4-(2-pyridylazo)resorcinol (PAR) 5,5′-dithio-bis(2-nitrobenzoic acid) (DTNB) Benzylpenicillin Bovine Serum Albumin, further purified fraction V (BSA) Calcium chloride ($CaCl_2$) Cefoxitin Cephaloridine Cephalosporin C Cephalothin Chelex 100 sodium Cystamine dihydrochloride Triton X-100
Thermo Fisher Scientific Inc. (Waltham, Massachusetts, U.S.A.)	Bromophenol Blue Magnesium sulfate ($MgSO_4$) Pierce NHS-Activated agarose resin Pierce 660 nm Protein Assay reagent Sodium bromide (NaBr) Tris(2-carboxyethyl)phosphine (TCEP) Zinc Sulfate ($ZnSO_4$)

Table 3.2: Peptides employed as MBL inhibitors. The concentrations of the peptides containing a *para*-nitroanilide (*p*NA) group were determined by measuring their absorbance at 342 nm (ε_{342} = 8,270 M^{-1} cm^{-1}) [125]. The concentrations of peptides containing either tyrosine or cystine residues (ε_{280} = 1,490 M^{-1} cm^{-1} and 125 M^{-1} cm^{-1}, respectively) were determined by measuring their absorbance at 280 nm.

	Peptide	MW (g/mol)	ε (M^{-1} cm^{-1})
1	Ac-Gly-Tyr-βAla-$(Arg)_8$-Val-Leu-Arg-*p*NA	2,089.30	8,270
2	Ac-Gly-Tyr-βAla-$(Arg)_8$-Val-Leu-Pro-*p*NA	2,030.28	8,270
3	Ac-Gly-Tyr-βAla-$(Arg)_8$-Val-Leu-Arg-NHOH	1,984.40	1,490
4	Ac-Gly-Tyr-βAla-$(Arg)_8$-Val-Leu-Arg-OH	1,969.36	1,490
5	Ac-Gly-Tyr-βAla-$(Arg)_7$-Val-Leu-Arg-OH	1,813.17	1,490
6	Ac-Gly-Tyr-βAla-$(Arg)_6$-Val-Leu-Arg-OH	1,656.98	1,490
7	Ac-Gly-Tyr-βAla-$(Arg)_5$-Val-Leu-Arg-OH	1,500.79	1,490
8	Ac-Gly-Tyr-βAla-$(Arg)_4$-Val-Leu-Arg-OH	1,344.60	1,490
9	Ac-Nle-$(Lys)_4$-Val-Leu-Pro-*p*NA	1,115.42	8,270
10	Ac-Nle-$(Arg)_4$-Val-Leu-Arg-OH	1,166.45	—
11	Poly-arginine	10,000.00	—
12	Ac-Cys-Tyr-βAla-$(Arg)_4$-Val-Leu-Arg-OH	1,390.68	1,490
13	Ac-Cys-Tyr-βAla-$(Arg)_4$-Val-Leu-Arg-OH | Ac-Cys-Tyr-βAla-$(Arg)_4$-Val-Leu-Arg-OH	2,779.36	3,105
14	Ac-Cys-Tyr-βAla-$(Arg)_8$-Val-Leu-Arg-OH	2,014.44	1,490
15	Ac-Cys-Tyr-βAla-$(Arg)_8$-Val-Leu-Arg-OH | Ac-Cys-Tyr-βAla-$(Arg)_8$-Val-Leu-Arg-OH	4,026.88	3,105
16	Ac-Cys-Tyr-βAla-$(Arg)_8$-Val-Leu-Cys-OH	1,962.39	1,490
17	Ala-Pro-*p*NA	342.78	8,270

3.2 Preparation of Solutions

3.2.1 Preparation of Buffers and Salt Solutions

HEPES buffers were prepared by adding 0.477 g, 1.192 g and 2.383 g of HEPES (acid form) to 100 mL of Milli-Q water to yield final concentrations of 20 mM, 50 mM and 100 mM, respectively. The pH of the buffers was adjusted to 7.0, 7.2 or 7.4 with the aid of NaOH (5 M).

Tris buffers at concentrations of 0.5 M and 1.5 M were obtained by dissolving 6.057 g and 18.171 g of Tris (base) in 100 mL of Milli-Q water, respectively. The pH was decreased to 6.8 or 8.9 using HCl (5 M).

Phosphate-buffered saline (PBS) at a concentration of 0.1 M was prepared by combining 0.1 M of Na_2HPO_4 and 0.1 M of NaH_2PO_4 in a ratio that permitted the buffer to achieve a final pH of 7.2.

Salts were typically prepared as 100 mM stock solutions in 10 mL of HEPES buffer (50 mM, pH 7.0) except for guanidine hydrochloride (GdnHCl). GdnHCl was prepared as an 8 M stock solution by combining 76.424 g of GdnHCl, 42.856 g of Milli-Q water and 1.192 g of HEPES (acid form). The pH of the GdnHCl stock solution was adjusted to 7.4 with the aid of NaOH (5 M).

3.2.2 Preparation of Substrates

The UW substrates were prepared as 2 mM stock solutions by initially dissolving 4.3 mg and 4.5 mg of UW-57 and UW-58, respectively, in 250 μL of DMSO. A 2 mM stock solution of nitrocefin was obtained by dissolving 5.2 mg of nitrocefin in 250 μL of DMSO. A volume of 4.75 mL of HEPES buffer (50 mM, pH 7.0) was added to each substrate stock solution while being vortexed (to prevent the precipitation of the substrate). The substrate stock solutions were then separated into 1 mL aliquots. Since these substrates are light sensitive, all containers were

wrapped in aluminium foil to protect the aliquots from light. Finally, the aliquots were stored at -20 °C until use.

All other substrates were typically prepared as 2 mM stock solutions in 10 mL of HEPES buffer (50 mM, pH 7.0), and kept at -20 °C until use.

3.2.3 Preparation of Peptides

The peptides listed in Table 3.2 were typically prepared by dissolving 1 mg of peptide in 1 mL of HEPES buffer (50 mM, 7.0) except for Ala-Pro-*p*NA (peptide **17**) and poly-arginine (peptide **11**). A 50 mM stock of Ala-Pro-*p*NA was obtained by dissolving 19.6 mg (taking into account the 14.3% salt content) of the peptide in 1 mL of 95% (v/v) ethanol. Poly-arginine was prepared as a 1 mM stock solution by dissolving 5.0 mg of the peptide in 500 µL of HEPES buffer (50 mM, pH 7.0).

The concentrations of the peptides were determined with a Biochrom Ultrospec 2100 pro UV/Visible Spectrophotometer (Biochrom Ltd., Cambridge, United Kingdom) or a Cary-60 Spectrophotometer (Agilent Technologies Canada Inc., Mississauga, Ontario, Canada) at a wavelength of 280 nm except for the peptides containing a *para*-nitroanilide (*p*NA) group where a wavelength of 342 nm was used. The extinction coefficients of the peptides were used to calculate their concentrations (see Table 3.2).

The disulfide-containing peptides were prepared by leaving the cysteine-containing peptide stock solution in an open 1.5 mL centrifuge tube for three days at room temperature. After three days, a two-fold excess of 5,5'-dithio-bis(2-nitrobenzoic acid) (DTNB) was added to an aliquot of the reaction mixture to verify that the peptides were oxidized. DTNB has the ability to react with free thiol groups (see section 3.8). Thus, when the peptides were oxidized, no free thiol groups remained in the solution.

3.2.4 Preparation of the Alexa Fluor Dyes

Alexa Fluor fluorescent dyes were used for the labeling of VIM-2 and the cysteine-containing $(Arg)_8$ core peptide [Ac-Cys-Tyr-βAla-$(Arg)_8$-Val-Leu-Arg-OH; peptide **14** in Table 3.2]. Two different dyes were employed for the labeling: Alexa Fluor 488 and Alexa Fluor 546. Prior to their usage, 1 mg of the Alexa Fluor dyes was dissolved in 100 μL of DMSO. Since the Alexa Fluor dyes are extremely sensitive to light, all tubes were wrapped in aluminium foil to protect the solutions from light. The concentrations of the Alexa Fluor stock solutions (25.8 mM for Alexa Fluor 488, and 18.1 mM for Alexa Fluor 546) were determined spectrophotometrically at λ_{max} (492 nm for Alexa Fluor 488, and 553 nm for Alexa Fluor 546) using the appropriate extinction coefficients. The extinction coefficient of Alexa Fluor 488 is 73,000 M^{-1} cm^{-1} at 492 nm while that of Alexa Fluor 546 is 120,000 M^{-1} cm^{-1} at 553 nm. All stock solutions were kept at -20 °C prior to use.

3.2.5 Preparation of Enzyme Stock Solutions

Two VIM-2 enzyme stock solutions were obtained from Dr. Dmitrienko's laboratory: one stock had a concentration of 35 μM while the other stock had a concentration of 93 μM. The concentrations of the VIM-2 stock solutions were determined spectrophotometrically at 280 nm using an extinction coefficient (ε_{280}) of 28,500 M^{-1} cm^{-1} [126].

For activity assays, an intermediate VIM-2 stock solution was prepared in a final volume of 200 μL. A volume of 0.7 μL of VIM-2 (35 μM) was diluted in HEPES buffer (50 mM, pH 7.0) to obtain a final VIM-2 concentration of 120 nM. This intermediate VIM-2 stock solution was also supplemented with 20 μM $ZnSO_4$ to ensure maximum enzyme activity.

The IMP-1 enzyme stock solution (626 μM) was supplied by Dr. Dmitrienko (University of Waterloo). The concentration of the IMP-1 stock solution was determined spectrophotometrically at 280 nm using an extinction coefficient (ε_{280}) of 44,380 M^{-1} cm^{-1} [127].

After determining its concentration, the entire IMP-1 enzyme stock solution was diluted with 390 μL of glycerol and 382.5 μL of HEPES buffer (100 mM, pH 7.2), yielding an 8 μM stock solution in 50% glycerol (v/v). The stock solution was then separated into 200 μL aliquots, and kept at -20 °C until use.

For activity assays, an intermediate IMP-1 stock solution was prepared in a final volume of 100 μL. A volume of 0.5 μL of IMP-1 (8 μM) was diluted in HEPES buffer (50 mM, pH 7.2) to obtain a final IMP-1 concentration of 40 nM. This intermediate IMP-1 stock solution was supplemented with 1 mM $ZnSO_4$ to ensure maximum enzyme activity, and with 1 mg/mL BSA as well as 0.01% (w/v) Triton X-100 to prevent enzyme aggregation/denaturation.

3.3 MBL Activity Assays

Typical MBL activity assays were performed in a final assay volume of 100 μL using nitrocefin as the substrate. Prior to initiation of the assays, the enzyme was pre-incubated at room temperature in 50 mM HEPES buffer (pH 7.0 for VIM-2 and pH 7.2 for IMP-1) for 1 min. Typically, 5 μL of an intermediate enzyme stock solution (120 nM for VIM-2 and 40 nM for IMP-1) was added to 90 μL of HEPES buffer. Following incubation, 5 μL of nitrocefin (2 mM) was added to the solution to achieve a final nitrocefin concentration of 100 μM. The progress of the reaction was measured at a wavelength of 482 nm using a Biochrom or a Cary-60 spectrophotometer. Kinetic parameters were obtained by determining the slopes of the initial linear portions of the progress curves (typically, the first 20 s to 30 s).

Assays performed with substrates other than nitrocefin followed the general assay protocol described above. Similar to nitrocefin, these substrates were employed at a final concentration of 100 μM in the assay except for benzylpenicillin and imipenem which were used at concentrations of 350 μM and 45 μM, respectively. Substrates were employed at these concentrations since the concentrations were approximately five-fold higher than the Michaelis constant of the substrates. Furthermore, for nitrocefin-like substrates, such as UW-57 and UW-58, the procedure remained identical with the absorbance being measured at 482 nm. For substrates such as cephaloridine, cephalothin, ceftazidime, cephalosporin C and cefoxitin, the absorbance was measured at a wavelength of 260 nm. In the case of benzylpenicillin and imipenem, the absorbance was measured at a wavelength of 235 nm and 300 nm, respectively.

Assays in the presence of inhibitors were performed as outlined above except that the inhibitor was mixed with the HEPES buffer prior to the addition of the enzyme. By varying the inhibitor concentrations throughout the assays, the concentration of inhibitor required to inhibit 50 % of enzyme (IC_{50} value) was determined.

For assays used in the determination of the inhibition constant and the mode of inhibition, the same general assay as described above was employed. However, both the substrate and inhibitor concentrations were varied. The final substrate concentrations in the assays were 12 μM, 20 μM, 25 μM, 33 μM, 50 μM and 100 μM. Using the data analysis software GraFit4 (Erithacus Software Ltd., Surrey, United Kingdom), the kinetic parameters were determined by fitting the velocity data obtained from the assays to either equations 3.1 or 3.3,

$$v = \frac{V_{max}[S]}{K_M\left(1 + \frac{[I]}{K_i}\right) + [S]\left(1 + \frac{[I]}{K_i{}'_{app}}\right)} \qquad \text{(Equation 3.1)}$$

$$\frac{1}{v} = \frac{K_M\left(1 + \frac{[I]}{K_i}\right)}{V_{max}\,[S]} + \frac{1 + \frac{[I]}{K_i{}'_{app}}}{V_{max}} \qquad \text{(Equation 3.2)}$$

$$v = \frac{V_{max}[S]}{\alpha K_M\left(\frac{[I] + K_i}{\beta[I] + \alpha K_i}\right) + [S]\left(\frac{[I] + \alpha K_i}{\beta[I] + \alpha K_i}\right)} \qquad \text{(Equation 3.3)}$$

$$\frac{1}{v} = \frac{K_M\left(1 + \frac{[I]}{K_i}\right)}{V_{max}\,[S]} + \frac{1 + \frac{[I]}{\alpha K_i}}{V_{max}} \qquad \text{(Equation 3.4)}$$

where v is the velocity, V_{max} represents the maximum velocity, [S] denotes the concentration of substrate, [I] is the concentration of the inhibitor, K_M represents the Michaelis constant, K_i denotes the inhibition constant and $K_{i\,app}^{'}$ is $(k_3/k_2)K_i^{'}$ (see Figure 4.2). Equations 3.1 and 3.2 represent the velocity equation and the corresponding Lineweaver-Burk expression, respectively, for the mechanism involving the production of an enzyme-product-inhibitor ternary complex [128]. On the other hand, equations 3.3 and 3.4 denote the velocity equation and the corresponding Lineweaver-Burk expression for hyperbolic (partial) mixed-type inhibition [129].

3.4 Stopped-flow Studies

All stopped-flow studies were conducted in 50 mM HEPES buffer (pH 7.0) and at a temperature of 20°C using an OLIS spectrophotometry system equipped with a U.S.A. two-syringe stopped-flow device. For single-turnover experiments, 20 µM of VIM-2 was rapidly mixed with 20 µM of nitrocefin. For double-turnover measurements, only 10 µM of VIM-2 was combined with 20 µM of nitrocefin. Absorbance changes that occurred during the reaction were monitored from 350 nm to 575 nm, and from 475 nm to 700 nm for 1.2 s. The single and double-turnover experiments were repeated using 50 µM and 10 µM of the cationic peptide inhibitor, respectively. Since the OLIS spectrophotometry system only possessed a two-syringe stopped-flow device, the inhibitor needed to be pre-exposed to one of the reagents before taking

measurements. Therefore, the inhibitor was pre-exposed to both the enzyme and the substrate in two separate measurements. The rate constants of the reactions were determined by fitting the stopped-flow data to the appropriate enzyme kinetic model using the kinetic data analysis software OLIS GlobalWorks (OLIS Inc., Bogart, Georgia, U.S.A.).

3.5 MBL UV-Vis Wave Scans

All MBL UV-Vis wave scans were performed in a final volume of 100 μL. Prior to the initiation of the scans, the VIM-2 enzyme (at a final concentration of 1 μM) was pre-incubated in the absence and presence of peptide inhibitors (5 μM) at room temperature in HEPES buffer (50 mM, pH 7.0) for 1 min. Following the incubation, the spectra were measured from 250 nm to 400 nm using a Cary-60 spectrophotometer. Furthermore, 25 mM Na_2SO_4 was occasionally added to the VIM-2/inhibitor mixture to determine the effect of salt on the interaction between the enzyme and the cationic peptides.

3.6 Electrophoresis

3.6.1 Native Polyacrylamide Gel Electrophoresis (PAGE)

Native polyacrylamide gel electrophoresis was utilized to study the interaction between VIM-2 and the cationic peptides. Each gel was composed of a resolving portion containing 15% acrylamide as well as a stacking portion which was poured over the resolving gel once the latter was solidified (see Table 3.3 for composition of gels). After the polymerization of the gel, 10 μL of the samples were loaded into the sample wells at the top of the stacking gel. The samples were prepared by 1:2 dilution of 1 mg/mL BSA or 10 μM VIM-2 in the absence and the presence of 100 μM of the $(Arg)_5$ or $(Arg)_8$ core peptides (peptides **7** and **4**, respectively) in 1X native sample buffer (see Table 3.4 for composition).

Table 3.3: Reagents used in the preparation of the resolving and stacking gels.

Reagent	Resolving Gel	Stacking Gel
30% (w/v) Acrylamide/Bis-acrylamide (37.5:1) 30% solution	5.20 mL	1.00 mL
Tris-HCl (1.5 M, pH 8.9)	2.80 mL	—
Tris-HCl (0.5 M, pH 6.8)	—	2.50 mL
Milli-Q Water	3.42 mL	6.40 mL
10% (w/v) APS	60 µL	100 µL
TEMED	15 µL	10 µL

Table 3.4: Reagents employed in the preparation of the native sample buffer. The volumes indicated allowed for the preparation of 10 mL of a 5X sample buffer.

Reagent	Volume (mL)
Glycerol	4.84
Tris-HCl (0.5 M, pH 6.8)	2.06
Milli-Q Water	2.61
0.1% (w/v) Bromophenol Blue	0.49

Once the samples were loaded, the gel was placed in a Bio-Rad Mini-PROTEAN Tetra Electrophoresis System (Bio-Rad Laboratories Ltd., Mississauga, Ontario, Canada) and the chamber was filled with native running buffer (see Table 3.5 for composition) that was prepared directly before use. The electrophoresis was performed at 100 V for 45 min.

Table 3.5: Reagents used in the preparation of the native running buffer. The pH value of the running buffer was adjusted to 8.9 with NaOH (5 M) before use.

Reagent	Amount
Glycine	66.5 g
Tris	15.1 g
Milli-Q Water	500 mL

Following electrophoresis, the gels were stained with Coomassie Brilliant Blue R-250 in order to visualize the protein bands. The Coomassie Blue solution was prepared with 0.2% (w/v) Coomassie Brilliant Blue R-250 in an aqueous solution containing 45.5% (v/v) methanol and 9.1% (v/v) glacial acetic acid. The gels were submerged in the Coomassie Blue solution for 2 h on a ROCKER II rocking platform mixer (Boekel Scientific, Feasterville, Pennsylvania, U.S.A.).

Following staining, the gels were destained using an aqueous destaining solution consisting of 45.5% (v/v) methanol and 9.1% (v/v) glacial acetic acid. The gels were subjected to three exchanges in the destaining solution. Following the third exchange, the gels were left overnight in the destaining solution at room temperature in order to obtain a more evenly destained background. After the destaining, the gels were stored in a solution of 10% (v/v) glacial acetic acid at 4 °C. Densitometry was conducted to quantify the intensity of the protein bands using the gel imaging software AlphaEase (Alpha Innotech Corp., San Leandro, California, U.S.A.).

3.6.2 Paper Electrophoresis

Paper electrophoresis was conducted to study the interaction between VIM-2 and the cationic peptides. Thin layer chromatography (TLC) sheets were utilized as the supporting medium for the electrophoresis and were cut into strips measuring 5 cm in width and 7 cm in length. Prior to electrophoresis, the TLC paper was equilibrated with 50 mM HEPES buffer (pH 7.0) followed by an equilibration with 20 μM of nitrocefin. Once the TLC paper was completely soaked with nitrocefin, 1 μL of the samples was added to the center of the TLC paper. The samples contained 10 μM of VIM-2 and/or 100 μM of the $(Arg)_8$ core peptide (peptide **4**). Following the addition of the samples to the TLC paper, the negative electrode alligator clip was attached to one side of the TLC paper while the positive electrode alligator clip was attached to the other side. The electrophoresis was performed at 120 V for 6 min using an Owl EC-105 Compact Power Supply (Thermo Fisher Scientific Inc., Waltham, Massachusetts, U.S.A.).

3.7 Peptide Labeling and Purification

3.7.1 Peptide Labeling Procedure

Peptide labeling was usually conducted in a final volume of 400 μL. To commence the labeling process, 40 μM of the $(Arg)_8$Cys core peptide (peptide **14** in Table 3.2) was dissolved in HEPES

buffer (50 mM, pH 7.2) at room temperature. A 10-fold molar excess of tris(2-carboxyethyl)phosphine (TCEP) was subsequently added in order to reduce any disulfide bonds which may have been present in the peptide solution. A sufficient amount of the Alexa Fluor dye was then added dropwise from the stock solution to obtain a 10 to 20-fold molar excess of dye for each mole of peptide (i.e., 400 μM to 800 μM). After addition of the dye, the mixture was incubated for 2 h at room temperature, or overnight at 4 °C. Upon completion of the reaction, the excess dye was removed from the labeled peptide solution as outlined below.

3.7.2 Peptide Purification Procedure

Following peptide labeling, the excess dye needed to be removed from the solution. The most commonly used method for the removal of the dye is HPLC. However, initial attempts to purify the labeled peptide solution failed, presumably in view of the small quantities of peptide and dye employed. Therefore, a new technique was developed to allow for the purification of the solution. This method achieved the purification of the labeled peptide using cystamine and NHS-Activated agarose (Thermo Fisher Scientific, Waltham, Massachusetts, U.S.A.). The NHS-Activated agarose resin contains an *N*-hydroxysuccinimide (NHS) ester functional group which can react with primary amines to form stable amide linkages. Furthermore, cystamine is a small disulfide with two terminal amine functional groups. Therefore, the resin can interact with the amine functional group(s) of cystamine (see Figure 3.1). Once cystamine was coupled to the resin, its disulfide bond was reduced by TCEP to generate a free sulfhydryl group (see Figure 3.1). In the end, the maleimide group of the excess Alexa Fluor dye can covalently bind the free sulfhydryl group on the cysteamine-coupled resin. Consequently, the resin would allow for the removal of excess dye from the labeled peptide solution.

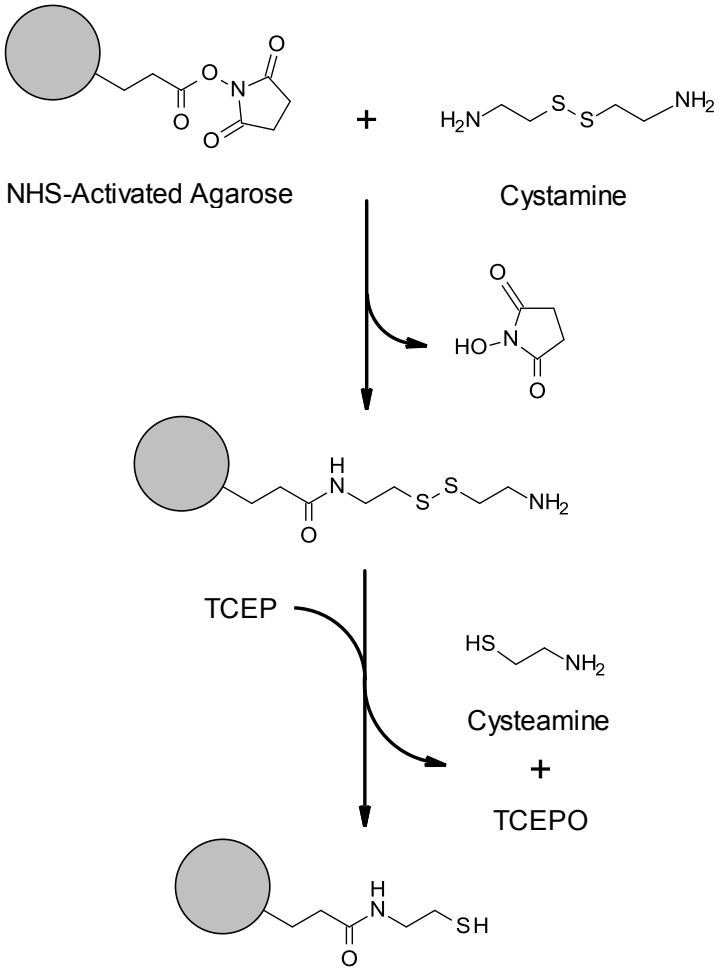

Figure 3.1: Preparation of the cysteamine-coupled agarose resin. In the first step, cystamine reacts with the NHS functional group on the agarose resin forming a stable amide bond. For the second step, TCEP is added to the solution to reduce the disulfide bond generating a free sulfhydryl group. This resin can then be used to scavenge thiol-reactive molecules such as the Alexa Fluor dyes.

Experimentally, for the purification of the labeled peptide solution, 66 mg of the NHS-Activated agarose resin was placed into an empty 800 µL centrifuge column (Thermo Fisher Scientific, Waltham, Massachusetts, U.S.A.). Next, 400 µL of 0.5 M cystamine (pH 7.4) was added to the column. Once cystamine was added, the column was mixed end-over-end using a Roto-Torque fixed speed heavy duty rotator (Cole-Parmer Instrument Co., Chicago, Illinois, U.S.A.) for 1 h to 2 h at room temperature, or overnight at 4 °C. Following incubation, the column was centrifuged at 1,000 × *g* for 1 min. After centrifugation, 400 µL of HEPES buffer

(50 mM, pH 7.0) was added to the column, and subsequently centrifuged at 1,000 × *g* for 1 min. This process (wash step) was repeated twice.

Once cystamine was coupled to the agarose, 400 µL of TCEP (10 mM) was added to the resin. The column was then mixed end-over-end for 10 min using a Roto-Torque rotator. Once the reduction was complete, the column was centrifuged at 1,000 × *g* for 1 min, and the flow-through was saved. The complete removal of TCEP was ascertained by adding DTNB to the filtrate(s) (after 12 spins).

Once TCEP was removed from the column, 400 µL of the Alexa Fluor labeled peptide solution was added to the cysteamine-coupled resin. The column was then mixed end-over-end for one hour using the Roto-Torque rotator. Once the incubation was complete, the column was centrifuged at 1,000 × *g* for 1 min to recover the labeled peptide in the filtrate.

Following purification, the concentration of the labeled peptide was calculated using equation 3.9,

$$c = \frac{A_{280} - (A_{max} - C.F.)}{\varepsilon_P} \times D.F. \qquad \text{(Equation 3.9)}$$

where c is the concentration of the peptide, A_{280} indicates the absorbance of the labeled peptide at 280 nm, A_{max} denotes the maximum absorbance of the labeled peptide at the absorbance maximum of the fluorescent dye (492 nm for Alexa Fluor 488 and 553 nm for Alexa Fluor 546), C.F. represents the correction factor of the dye at 280 nm (0.11 for Alexa Fluor 488 and 0.12 for Alexa Fluor 546), ε_P denotes the extinction coefficient of the peptide, and D.F. is the dilution factor. In the equation, the correction factor accounted for the amount of absorbance caused by the dye at 280 nm while the dilution factor accounted for the extent to which the labeled peptide solution was diluted prior to the absorbance measurement.

3.8 Preparation of Mononuclear VIM-2

The preparation of mononuclear VIM-2 was achieved following the protocols reported by Gardonio and Siemann for the generation of mononuclear IMP-1 [130]. For the generation of mononuclear VIM-2, the first step encompassed the chemical modification of the zinc-bound cysteine residue through the addition of 5,5'-dithio-bis(2-nitrobenzoic acid) (DTNB) in the presence of dipicolinic acid (DPA) (see Figure 3.2). The second step incorporated the release of

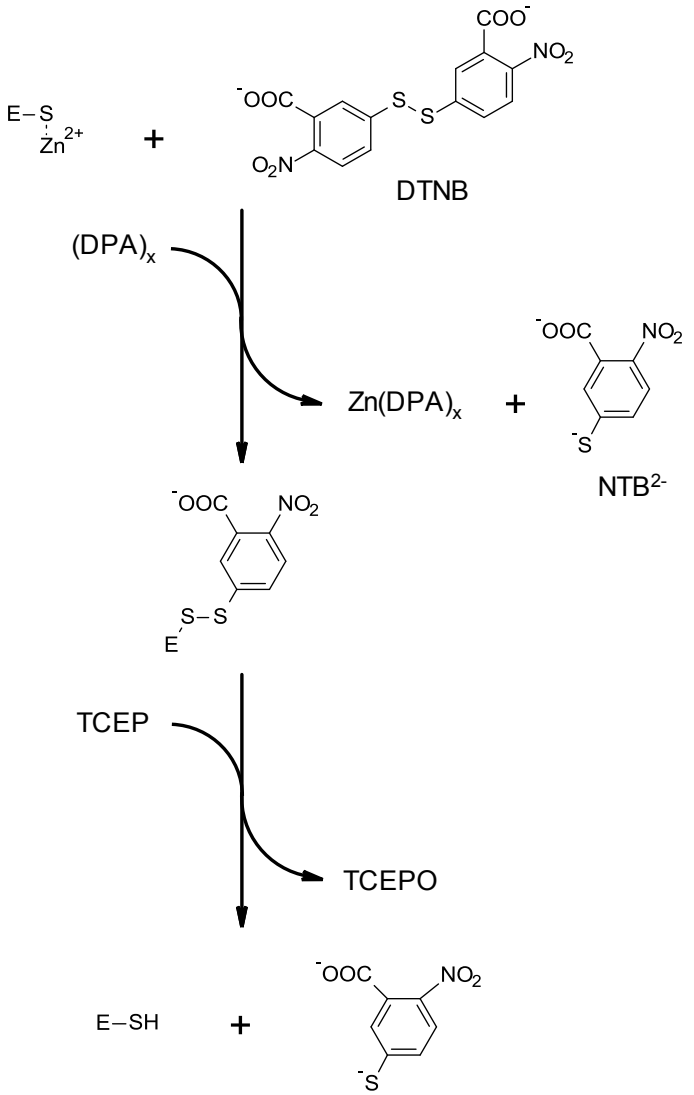

Figure 3.2: Schematic representation of the removal of the cysteine-bound Zn^{2+} from VIM-2. The first step incorporates the modification of the cysteine residue of the enzyme, represented by E-S--Zn^{2+}, in the presence of DPA. The second step involves the release of the modifying group from the cysteine residue through the reduction of the disulfide bond by TCEP. Both reaction steps can be followed spectrophotometrically at 412 nm in view of the release of the NTB^{2-} ion.

the DNTB modifying group from the enzyme through the reduction of its disulfide bond by TCEP (see Figure 3.2). Both steps of the reaction were followed spectrophotometrically at 412 nm as a consequence of the release of the chromophoric 2-nitro-5-thiobenzoate (NTB^{2-}) anion.

The chemical modification of VIM-2 was performed in a volume of 180 µL. Initially, 8 µM of VIM-2 in HEPES buffer (50 mM, pH 7.0) was allowed to equilibrate at 25 °C for 1 min. Furthermore, the HEPES buffer used was treated with 2.5 g/100 mL of Chelex-100 to minimize contamination by trace elements. The reaction was initiated by the addition of 20 µL of DTNB (5 mM in buffer). The reaction was monitored at a wavelength of 412 nm for 5 min. After 5 min, 6.9 µL of DPA (30 mM in buffer) was added to the solution. Following mixing for approximately 30 s, the monitoring of the reaction at 412 nm was resumed. The final concentrations of VIM-2, DTNB and DPA in the assay were 6.97 µM, 483 µM and 1000 µM, respectively. Following the completion of the assay, an Amicon Ultra 0.5 mL centrifugal filter (10 kDa MWCO) (Thermo Fisher Scientific Inc., Waltham, Massachusetts, U.S.A.) was used to remove any excess DTNB and DPA from the solution. The successful removal of DTNB was assessed using TCEP (absence of the NTB^{2-} ion in the filtrate), while the complete removal of DPA was assessed using zinc sulfate and 4-(2-pyridylazo)resorcinol (PAR) at final concentrations of 5 µM and 10 µM, respectively. Following centrifugation, TCEP, at a final concentration of 250 µM, was added to remove the remaining modifying agent from the enzyme. The reaction was allowed to equilibrate for 5 min at room temperature. Once the assay was complete, an Amicon Ultra 0.5 mL centrifugal filter (10 kDa MWCO) was used to remove the excess TCEP and the released NTB^{2-} anion. The absence of TCEP was assessed using DTNB. Following centrifugation, a PAR test was used to assess the zinc content of the enzyme (see section 3.12).

3.9 Labeling of VIM-2 with the Alexa Fluor Dyes

The labeling of VIM-2 with the Alexa Fluor dyes was achieved by following a modified version of the protocols outlined in the previous section. The main modification was that the Alexa Fluor dyes were used as the cysteine-modifying agent instead of DTNB. The labeling of VIM-2 with Alexa Fluor 488 and Alexa Fluor 546 was accomplished in a total volume of 200 μL. VIM-2 (40 μM) and TCEP (400 μM) were allowed to incubate at room temperature for 1 min. Following the incubation, 800 μM of the desired Alexa Fluor dye was added to the solutions to initiate the reaction. A volume of 22.3 μL of DPA (30 mM in buffer) was then added to the solution. The mixture was incubated at room temperature for 2 h. Following incubation, a 10-fold molar excess of β-mercaptoethanol (BME) was added, and the solution was incubated for another 30 min at room temperature. The addition of BME allowed for the quenching of any thiol-reactive dye that was still present in the solution, hence ensuring that no reactive species were remaining during the purification process. For VIM-2 labeled with Alexa Fluor 488, the final concentrations of VIM-2, TCEP, Alexa Fluor 488 and DPA were 35 μM, 350 μM, 720 μM and 3000 μM, respectively. For VIM-2 labeled with Alexa Fluor 546, the final concentrations of VIM-2, TCEP, Alexa Fluor 546 and DPA in the reaction mixture were 35 μM, 340 μM, 720 μM and 3000 μM, respectively. Following the completion of the reaction, an Amicon Ultra 0.5 mL centrifugal filter (10 kDa MWCO) was used to remove any excess DPA, BME and Alexa Fluor dye from the solution. The successful removal of DPA was assessed using PAR/Zn^{2+}. Following centrifugation, a Pierce 660 nm Protein Assay was conducted to determine protein concentration. The zinc content of labeled VIM-2 was also assessed using PAR (see section 3.12).

Protein concentration following the labeling of VIM-2 with the Alexa Fluor dyes was assessed using Thermo Fisher Scientific's Pierce 660 nm Protein Assay. This assay represents a simple and rapid colorimetric method for the determination of protein concentration that is more sensitive than the Coomassie Blue-based Bradford assays. All assays were performed using the 96-well microplate procedure (working range 50 to 2,000 μg/mL). For the assay, BSA standards ranging from 50 μg/mL to 600 μg/mL were prepared using a 2 mg/mL stock solution of BSA dissolved in PBS buffer (0.1 M, pH 7.2). A volume of 10 μL of each standard, sample, and a reagent blank were added to separate wells of the 96-well microplate along with 150 μL of the Pierce 660 nm Protein Assay reagent. The solutions were then mixed with a pipette, incubated for 5 min at room temperature, and the absorbance of the samples was measured at a wavelength of 660 nm using an Epoch Microplate Spectrophotometer (BioTek Instruments Inc., Winooski, Vermont, U.S.A.). A BSA standard curve was prepared to determine the concentrations of the protein samples.

3.10 Fluorescence Spectroscopy

3.10.1 Tryptophan Fluorescence

Typical tryptophan fluorescence studies were performed in a final volume of 800 μL. Prior to the measurements, the enzyme (1 μM) was pre-incubated at room temperature in 50 mM HEPES buffer (pH 7.0 for VIM-2 and pH 7.2 for IMP-1) for 1 min. After incubation, the fluorescence emission spectra were measured from 295 nm to 460 nm. The excitation wavelength was set to 295 nm to selectively excite the tryptophan residues present in the proteins. The spectra were measured using an OLIS RSM 1000 DeSa Rapid-Scanning Monochromator Spectrofluorometer (OLIS Inc., Bogart, Georgia, U.S.A.) equipped with a 150 W xenon arc lamp.

In studies on the interaction of VIM-2 or IMP-1 with inhibitors, spectra were measured analogously using a final inhibitor concentration of 5 µM. Furthermore, 25 µM TCEP was occasionally added to the samples to determine the effect of a reducing agent on the interaction between VIM-2 and oxidized, disulfide-containing cationic peptides.

3.10.2 FRET

Fluorescence resonance energy transfer (FRET) measurements were carried out using two fluorescent dyes: Alexa Fluor 488 and Alexa Fluor 546. For these experiments, Alexa Fluor 488 was used as the donor while Alexa Fluor 546 acted as the acceptor. The measurements were performed at an excitation wavelength of 492 nm as this wavelength coincides with the absorbance maximum of the donor. For the experiments, changes in donor fluorescence emission (fluorescence maximum at 514 nm) and acceptor emission (fluorescence maximum at 568 nm) were recorded. Using the OLIS fluorometer, fluorescence emission spectra were measured from 500 nm to 600 nm to evaluate the fluorescence emission of both the donor and the acceptor. With this procedure, two types of FRET measurements were conducted: protein-protein FRET and peptide-protein FRET.

For the protein-protein FRET, measurements were performed using VIM-2 labeled with Alexa Fluor 488, and VIM-2 labeled with Alexa Fluor 546 in a 1:1 ratio. In the samples, both of the labeled proteins were measured at a final concentration of 200 nM. A concentration of 2 µM of the unlabeled cysteine-containing $(Arg)_8$ peptide (peptide **14**) was used in measurements aimed at assessing the influence of cationic peptides on FRET.

For the protein-peptide FRET, measurements were performed using VIM-2 labeled with Alexa Fluor 488, and the cysteine-containing $(Arg)_8$ peptide (peptide **14**) labeled with Alexa

Fluor 546 in a 1:4 ratio. In the samples, the final concentrations of the labeled protein and the labeled peptide were 100 nM and 400 nM, respectively.

Following FRET measurements, the distance between the labels was calculated using equations 3.5, 3.6, 3.7 and 3.8,

$$R_0 = 0.2108\ [\kappa^2 n^{-4} \Phi_0 J(\lambda)]^{1/6} \qquad \text{(Equation 3.5)}$$

$$J(\lambda) = \int F_D(\lambda)\varepsilon_A(\lambda)\lambda^4 d\lambda \qquad \text{(Equation 3.6)}$$

$$E = R_0^6 / (R_0^6 + r^6) \qquad \text{(Equation 3.7)}$$

$$r = R_0\ [(1/E)-1]^{1/6} \qquad \text{(Equation 3.8)}$$

where R_0 is the Förster distance (i.e, energy transfer is 50% at this distance; expressed in Å), κ^2 denotes the orientation factor (0.476 for rigid donor and acceptor molecules such as the Alexa Fluor dyes), n represents the refraction index (1.4 for HEPES buffer), Φ_0 is the quantum yield of the donor (0.92 for Alexa Fluor 488), $J(\lambda)$ is the spectral overlap integral between the donor emission and the acceptor absorption, F_D represents the normalized donor emission spectra (i.e., the fluorescence intensity at λ_{max} is set to 1), ε_A denotes the extinction coefficient of the acceptor (120,000 $M^{-1}cm^1$ for Alexa Fluor 546 at 553 nm), λ represents the wavelength (in nm), E is the energy transfer efficiency, and r is the distance between the donor and acceptor molecules.

3.11 Dynamic Light Scattering

All dynamic light scattering studies were conducted in a final volume of 1 mL, and at a temperature of 25 °C using a Zetasizer Nano S90 (Malvern Instruments Inc., Westborough, Massachusetts, U.S.A.). The average hydrodynamic size distribution of the particles in the samples was determined using the Zetasizer software (Malvern Instruments Inc., Westborough, Massachusetts, U.S.A.). As controls, at the beginning of each experiment, HEPES buffer (20 mM, pH 7.4), VIM-2 and/or the $(Arg)_8$ core peptide [Ac-Gly-Tyr-βAla-$(Arg)_8$-Val-Leu-Arg-OH;

peptide **7** in Table 3.2] were measured. For the first experiment, 8 μM VIM-2 and 80 μM of the peptide were incubated with 20 mM HEPES buffer (pH 7.4) for 1 min at room temperature. A second experiment was performed to further study the interaction between VIM-2 and the peptide by combining 8 μM VIM-2 with increasing concentrations of the peptide in 20 mM HEPES buffer to obtain a titration curve. The final concentrations of the $(Arg)_8$ core peptide in the assays were 1.6 μM, 4 μM, 8 μM, 16 μM, 40 μM and 80 μM. The initial concentration of VIM-2 (8 μM) slightly decreased upon the addition of the increasing concentrations of the peptide to the sample, but this decrease in concentration was negligible due to the high concentration of the peptide stock solution used for the dilutions.

3.12 Determination of Metal Content

PAR [4-(2-pyridylazo)resorcinol] is a chromogenic chelator frequently used to detect metals present in protein samples [131]. Therefore, a PAR test was used to assess the zinc content of VIM-2. The PAR assay was performed in a 96-well microplate. For a typical assay, 4 M GdnHCl was combined with 2 μM to 5 μM of the protein in 50 mM HEPES buffer (pH 7.4). GdnHCl was used to denature/unfold the protein to release the zinc ion from the protein. Afterwards, 50 μM of PAR was added to the solution to initiate its complexation to the Zn^{2+} ions. The solution was then incubated for 15 min. Following incubation, the absorbance of the samples was measured at 500 nm using the Epoch Microplate Spectrophotometer. Zinc standards were also prepared in the range from 1 μM to 10 μM, and assayed under analogous conditions. A standard curve was prepared to determine the concentration of zinc in the protein samples.

Chapter 4: Results

4.1 Inhibition of VIM-2 by Cationic Peptides

Previous (unpublished) studies have shown that S-*p*NA (peptide **1** in Table 4.1), a peptidic lethal factor substrate, has the ability to inhibit VIM-2. This observation is unusual due to the stereochemistry of β-lactams imitating the D-Ala-D-Ala configuration rather than the L, L configuration found in S-*p*NA. Hence, a more thorough study of the effect of cationic peptides on MBLs was initiated. The interaction between VIM-2 and cationic peptides was studied by monitoring the rate of the enzyme-mediated hydrolysis of nitrocefin as a function of the concentration of the inhibitors. Among the cationic peptides listed in Table 4.1, peptides that differed in their C-terminal moieties were analyzed. The results indicated that the inhibition of VIM-2 was relatively independent of the nature of the C-terminal moiety (*para*-nitroanilide, hydroxamate or a free carboxylic acid; see peptides **1**, **3** and **4** in Table 4.1). Furthermore, Ala-Pro-*p*NA, which contains the C-terminal *p*NA group, but is devoid of cationic residues, was shown to be a very poor inhibitor of VIM-2 with an IC_{50} value of 1155 μM. Replacement of the C-terminal arginine residue of S-*p*NA (peptide **1**) with a proline residue led to only slightly lower inhibitory potency (compare peptides **1** and **2** in Table 4.1).

Table 4.1: IC_{50} values for the inhibition of VIM-2 by various cationic peptides. Inhibition was assessed at room temperature using 6 nM of VIM-2 and 100 μM of nitrocefin. The values represent the mean (± 1 s.d.) of three independent experiments.

Peptide		IC_{50} (μM)
1	Ac-Gly-Tyr-βAla-$(Arg)_8$-Val-Leu-Arg-*p*NA	0.096 ± 0.002
2	Ac-Gly-Tyr-βAla-$(Arg)_8$-Val-Leu-Pro-*p*NA	0.179 ± 0.004
3	Ac-Gly-Tyr-βAla-$(Arg)_8$-Val-Leu-Arg-NHOH	0.329 ± 0.026
4	Ac-Gly-Tyr-βAla-$(Arg)_8$-Val-Leu-Arg-OH	0.174 ± 0.014
5	Ac-Gly-Tyr-βAla-$(Arg)_7$-Val-Leu-Arg-OH	0.317 ± 0.037
6	Ac-Gly-Tyr-βAla-$(Arg)_6$-Val-Leu-Arg-OH	2.484 ± 0.988
7	Ac-Gly-Tyr-βAla-$(Arg)_5$-Val-Leu-Arg-OH	> 500
8	Ac-Gly-Tyr-βAla-$(Arg)_4$-Val-Leu-Arg-OH	> 500
9	Ac-Nle-$(Lys)_4$-Val-Leu-Pro-*p*NA	> 500
10	Ac-Nle-$(Arg)_4$-Val-Leu-Arg-OH	27 ± 4
11	Poly-arginine (5 to 15 kDa)	0.017 ± 0.004
12	Ac-Cys-Tyr-βAla-$(Arg)_4$-Val-Leu-Arg-OH	0.826 ± 0.150
13	Ac-Cys-Tyr-βAla-$(Arg)_4$-Val-Leu-Arg-OH | Ac-Cys-Tyr-βAla-$(Arg)_4$-Val-Leu-Arg-OH	0.534 ± 0.063
14	Ac-Cys-Tyr-βAla-$(Arg)_8$-Val-Leu-Arg-OH	0.118 ± 0.021
15	Ac-Cys-Tyr-βAla-$(Arg)_8$-Val-Leu-Arg-OH | Ac-Cys-Tyr-βAla-$(Arg)_8$-Val-Leu-Arg-OH	0.013 ± 0.001
16	Ac-Cys-Tyr-βAla-$(Arg)_8$-Val-Leu-Cys-OH	0.107 ± 0.002

Since the previous results indicated that positively charged residues in the peptides were responsible for the inhibition of VIM-2, a variety of peptides containing different numbers of core arginine residues were evaluated for their inhibitory potency. As shown in Table 4.1, the successive truncation of the $(Arg)_8$ core of the peptides to an $(Arg)_4$ core led to a dramatic decrease in inhibition with IC_{50} values increasing from 0.174 μM to over 500 μM (see peptides **4** to **8** in Table 4.1). The largest decrease in inhibition occurred following the shortening of the $(Arg)_6$ core to an $(Arg)_5$ core with IC_{50} values increasing from 2.484 μM to 500 μM (see peptides **6** and **7** in Table 4.1). Since these results indicated that the positively charged core residues of the peptides were important for the inhibition of VIM-2, a peptide that contained lysine residues instead of arginine residues was evaluated (peptide **9**). This peptide was found to be a poor

inhibitor of VIM-2 (IC_{50} > 500 μM; see Table 4.1). However, the replacement of the C-terminal proline and the $(Lys)_4$ motif of the peptide with arginine residues caused the inhibition to significantly increase from over 500 μM to 27 μM (see peptides **9** and **10** in Table 4.1). These results demonstrate that incorporation of arginine residues into the peptides leads to more potent inhibition than that observed with lysine residues. Indeed, a peptide containing only arginine residues was shown to be a very potent inhibitor of VIM-2 with an IC_{50} value of 17 nM (see peptide **11** in Table 4.1). Furthermore, when comparing peptides **9** and **10**, which contain the same core motif and C-terminal residues, it was observed that just the slight difference in their N-terminal residues caused a dramatic difference in inhibition with the IC_{50} values decreasing from over 500 μM for peptide **8** (Ac-Gly-Tyr-βAla) to 27 μM for peptide **10** (Ac-Nle). To further confirm that changes in the N-terminus affect inhibition, peptides that contained an N-terminal cysteine residue instead of a glycine residue were evaluated. For the $(Arg)_4$ core peptide, this substitution caused a significant increase in the inhibitory potency (compare peptides **8** and **12** in Table 4.1). In addition, oxidation of peptide **12** to the disulfide led to a further increase in inhibition as shown by its IC_{50} value of 534 nM (see peptide **13** in Table 4.1). For the $(Arg)_8$ core peptide, the substitution of the N-terminal glycine residue with a cysteine residue only minimally increased the inhibitory potency of the peptide (see peptides **4** and **14** in Table 4.1). In addition, a peptide containing an N-terminal and a C-terminal cysteine residue exhibited a slight increase in its inhibitory potency in comparison to its cysteine-devoid equivalent (compare peptides **4** and **16** in Table 4.1). Interestingly, oxidation of the cysteine-containing $(Arg)_8$ core peptide was shown to cause a significant increase in inhibition as shown by its IC_{50} value of 13 nM (see peptide **15** in Table 4.1). Indeed, among the peptides investigated in this study, peptide **15** was found to be the most potent inhibitor of VIM-2.

4.2 β-Lactam Substrates

In order to investigate whether the inhibition of VIM-2 by cationic peptides is substrate-dependent, a variety of β-lactam substrates other than nitrocefin including a variety of cephalosporins, benzylpenicillin and imipenem (a carbapenem) were employed in the assessment of the inhibitory potency of S-*p*NA (peptide **1** in Table 4.1). As shown in Table 4.2, the inhibitory potency of S-*p*NA decreased significantly upon the substitution of nitrocefin with other substrates. Nonetheless, moderate inhibition of VIM-2 by S-*p*NA was observed with all of the β-lactam substrates tested. The degree of inhibition appeared to be mainly dependent on the nature of the R_2 group of the substrates. For instance, in the case of nitrocefin, cephaloridine and cephalothin, which share the same R_1 moiety (but not the same R_2 substituent), the inhibitory potency of S-*p*NA varied significantly with activities ranging from 13% to 84% (see Table 4.2). Similar results were obtained when comparing cefoxitin and cephalothin since these two substrates demonstrated significantly different activities (see Table 4.2). Although cefoxitin and cephalothin share the same R_1 moiety and possess similar R_2 groups, cefoxitin contains a methoxy group at the α-carbon of the β-lactam ring. Another difference between both of these substrates is that the inhibition with cephalothin was assessed using 10 μM S-*p*NA while that of cefoxitin was assessed using only 1 μM S-*p*NA. Therefore, even at a 10-fold decrease in concentration, S-*p*NA demonstrated a higher degree of inhibition with cefoxitin as a substrate. On the other hand, in the case of cephalosporin C and cephalothin, which share the same R_2 moiety, but vary in their R_1 substituent, the degree on inhibition was similar with activities of 67% and 84%, respectively (see Table 4.2). A penicillin and a carbapenem were also used as substrates. The results indicated that S-*p*NA-mediated inhibition with these two substrates gave similar residual activities (see Table 4.2).

Table 4.2: The dependence of the inhibition of VIM-2 by S-*p*NA on the chosen substrate. Inhibition was assessed in HEPES buffer (50 mM, pH 7.0) at room temperature using 6 nM VIM-2 and 10 μM S-*p*NA (except for assays in the presence of nitrocefin and cefoxitin where it was 1 μM). Benzylpenicillin and imipenem were used at final concentrations of 45 and 350 μM, respectively. All other substrates were measured at a final concentration of 100 μM. These substrate concentrations were employed as they were approximately five times larger than the Michaelis constant of the substrates. The values represent the mean (± 1 s.d.) of three independent experiments.

β-Lactam substrate	**Structure**	**Activity (%)**
Nitrocefin (Cephalosporin)	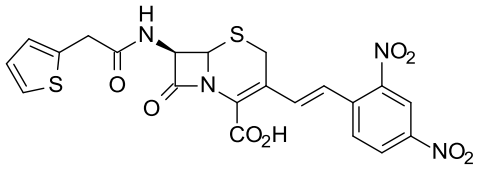	13 ± 1
Cephaloridine (Cephalosporin)	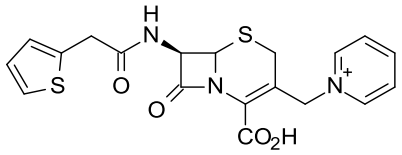	30 ± 2
Cephalothin (Cephalosporin)	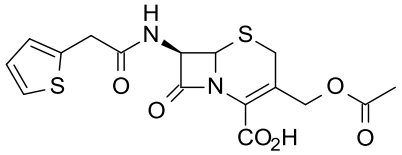	84 ± 5
Cephalosporin C (Cephalosporin)	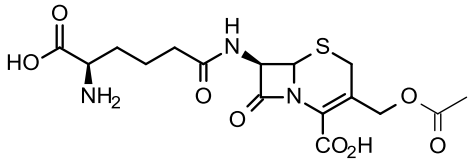	67 ± 9
Cefoxitin (Cephamycin)	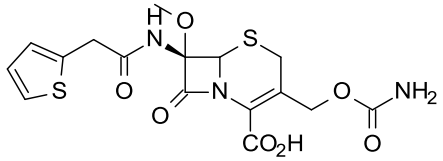	30 ± 3
Benzylpenicillin (Penicillin)	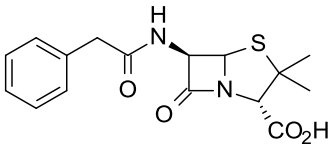	45 ± 1
Imipenem (Carbapenem)	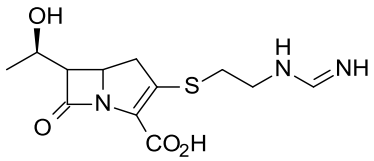	38 ± 3

Since nitrocefin was the substrate with which the lowest activity, and hence highest degree of inhibition by S-*p*NA was observed, two substrates structurally similar to nitrocefin (UW-57 and UW-58) were assayed. When comparing nitrocefin, UW-57 and UW-58, which share the same R_1 moiety, but differ in their R_2 groups, the degree of inhibition was determined to be fairly similar ranging from 13% to 22% (see Table 4.3). In view of these results, the IC_{50} values of all three substrates were measured. As shown in Table 4.3, the IC_{50} values of the UW substrates were found to be five to six times larger than that of nitrocefin.

Table 4.3: Inhibition of VIM-2 by S-*p*NA using nitrocefin and nitrocefin-like substrates. Inhibition was assessed in HEPES buffer (50 mM, pH 7.0) at room temperature using 6 nM VIM-2 and 100 μM substrate. The percentage of activity was determined using 1 μM of S-*p*NA. The concentration of S-*p*NA varied in the activity assays for the determination of the IC_{50} values. The values represent the mean (± 1 s.d.) of three independent experiments.

β-Lactam substrate	Structure	Activity (%)	IC_{50} (nM)
Nitrocefin	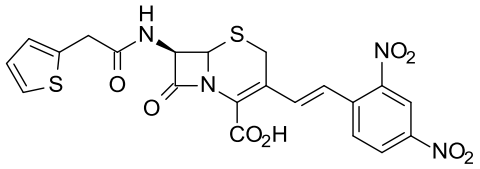	13 ± 1	96 ± 2
UW-57	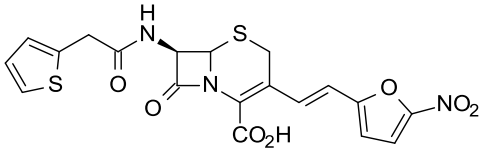	22 ± 4	523 ± 87
UW-58	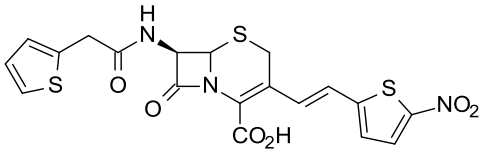	18 ± 1	575 ± 40

4.3 The Effect of Salts on the Inhibition of VIM-2 by the Cationic Peptides

In view of the ionic nature of the peptide inhibitors, the effect of salts on the inhibition of VIM-2 by S-*p*NA was explored. As shown in Table 4.4, all salts had approximately the same ionic strength, and showed similar activities in the absence of inhibitor. The addition of salt to the

inhibition assays greatly increased the level of residual activity (see Table 4.4). Therefore, all salts were capable of reducing S-*p*NA-mediated inhibition. Furthermore, the results illustrate that the relief of inhibition was particularly strong with salts containing divalent anions such as Na_2SO_4 and $MgSO_4$ which demonstrated residual activities of 76% and 78%, respectively. Na_2WO_4 displayed the greatest relief of inhibition with 93% of residual activity being observed.

Table 4.4: Dependence of the inhibition of VIM-2-mediated nitrocefin hydrolysis by S-*p*NA on the chosen salt. Inhibition was assessed in HEPES buffer (50 mM, pH 7.0) at room temperature using 6 nM VIM-2, 100 μM nitrocefin and 1 μM S-*p*NA. The values represent the mean (± 1 s.d.) of three independent experiments.

Salt	Concentration (mM)	Ionic Strength	Activity (%)	
			- S-*p*NA	+ S-*p*NA[1]
None	—	—	100	13 (± 1)
NaBr	100	0.100	77 (± 9)	68 (± 8)
NaCl	100	0.100	115 (± 10)	37 (± 3)
$MgCl_2$	25	0.075	94 (± 13)	46 (± 5)
$CaCl_2$	25	0.075	74 (± 12)	55 (± 2)
Na_2SO_4	25	0.075	98 (± 14)	76 (± 6)
$MgSO_4$	25	0.100	111 (± 8)	78 (± 7)
Na_2WO_4	25	0.075	82 (± 7)	93 (± 5)

[1] Activities are expressed relative to those recorded in the absence of S-pNA.

4.4 Enzyme Kinetics of VIM-2 and the Cationic Peptides

The mode of inhibition of VIM-2 by S-*p*NA was evaluated using nitrocefin as a substrate. The inhibition of VIM-2 by S-*p*NA revealed a complex and unusual mode of inhibition. A Lineweaver-Burk plot was obtained by plotting the reciprocal velocity against the reciprocal nitrocefin concentration demonstrating that the lines crossed in the negative (third) quadrant (see Figure 4.1). For competitive inhibition, the lines intersect on the y axis while for pure non-competitive inhibition, the lines intersect on the x axis.

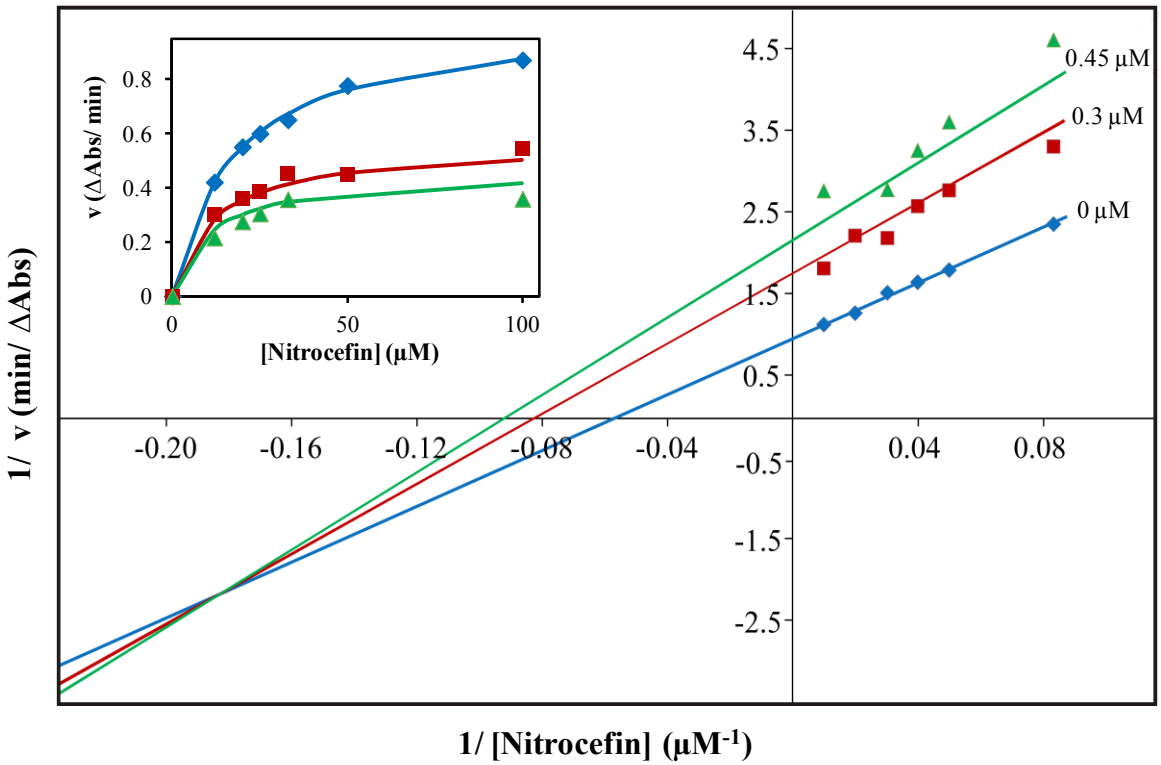

Figure 4.1: Lineweaver-Burk and Michaelis-Menten (inset) plots of VIM-2 inhibition by S-*p*NA. The lines depict the best fit of the data to equation 3.1 describing the formation of an enzyme-product-inhibitor ternary complex as outlined in section 3.3. VIM-2 was used at a final concentration of 6 nM.

Although the data demonstrated an unusual type of inhibition, the data could be fit reasonably well to two equations describing two distinct mechanisms. The first mechanism involved an enzyme-product-inhibitor ternary complex while the second mechanism was hyperbolic (partial) mixed-type inhibition. As shown in Figure 4.2, the enzyme-product-inhibitor ternary complex mechanism describes a type of inhibition where the product and the inhibitor bind the enzyme at two different sites. This produces three different enzyme-containing complexes called EI, EP and EPI. On the other hand, hyperbolic (partial) mixed-type inhibition illustrates a type of mechanism where the substrate and the inhibitor bind the enzyme at two different sites. This also produces three different enzyme-containing complexes (EI, ES and EIS). In the case of hyperbolic (partial) mixed-type inhibition, the value of α is between 0 and 1, while β is < 1, but

the fits where obtained with β equal to 0. An α value between 0 and 1 causes the lines (in the Lineweaver-Burk plot) to intersect in the third quadrant with the inhibitor binding more tightly to the enzyme-substrate complex than to the free enzyme [129]. The main difference between both mechanisms lies in the production of the EPI and EIS complexes.

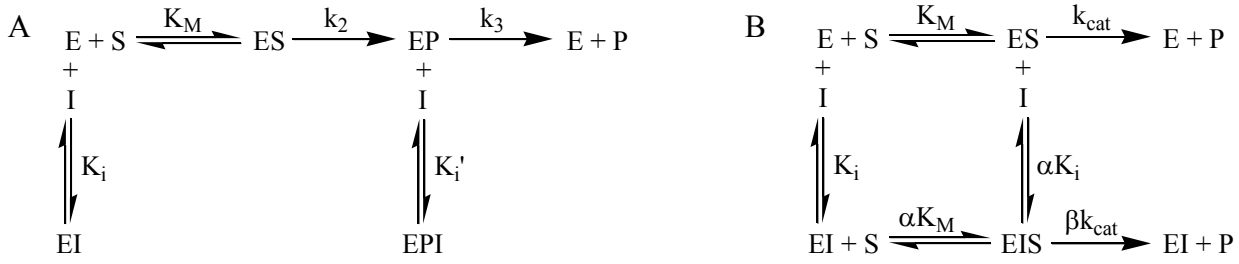

Figure 4.2: Schemes for the enzyme-product-inhibitor ternary complex mechanism (A) and hyperbolic mixed-type inhibition (B). E denotes the free enzyme, S represents the substrate, I is the inhibitor, P is the product, EI symbolizes the enzyme-inhibitor complex, ES is the enzyme-substrate complex, EIS represents the enzyme-substrate-inhibitor complex, EP denotes the enzyme-product complex, and EPI is the enzyme-product-inhibitor complex. Schemes adapted from references [128, 129].

It is important to note that both mechanisms cannot be distinguished on basis of the virtually identical velocity equations and Lineweaver-Burk expressions (see section 3.3). Indeed, the only major difference is that $K_{i\,app}^{'}$ is replaced by αK_i in hyperbolic (partial) mixed-type inhibition (see equations 3.2 and 3.4). Hence, it is not surprising that the V_{max}, K_M, K_i and k_{cat} values obtained by fitting the data to both models were identical, while the $K_{i\,app}^{'}$ value is the product of α and K_i (i.e., $K_{i\,app}^{'} = \alpha \times K_i$) (see Table 4.5). In addition, the K_M and the k_{cat} values for VIM-2 and nitrocefin in the literature are 18 μM and 770 s^{-1}, respectively [126]. Hence, the experimental K_M values that were determined for both mechanisms were identical to the literature value, while the values for k_{cat} were different by a factor of ~ 4.

Table 4.5: Kinetic parameters for both the mechanism involving the formation of an enzyme-product-inhibitor ternary complex as well as the hyperbolic (partial) mixed-type inhibition. V_{max} is the maximum velocity, K_M is the Michaelis constant, K_i is the inhibition constant, $K_{i\,app}^{'}$ is $(k_3/k_2)K_i^{'}$ and k_{cat} is the catalytic constant.

Kinetic parameters	Enzyme-Product-Inhibitor Ternary Complex	Hyperbolic (partial) mixed-type inhibition
V_{max}	1.03 (± 0.04) Δ abs/min	1.03 (± 0.04) Δ abs/min
K_M	17.63 (± 2.15) μM	17.63 (± 2.23) μM
K_i	1.17 (± 0.79) μM	1.17 (± 0.83) μM
$K_{i\,app}^{'}$	0.36 (± 0.05) μM	—
α	—	0.31 (± 0.26)
β	—	0
k_{cat}	178 (± 7) s^{-1}	178 (± 7) s^{-1}

4.5 Stopped-flow Analysis of VIM-2 and the Cationic Peptides

Since the enzyme kinetics of the reaction between VIM-2 and S-*p*NA could be fit to two possible inhibition mechanisms, rapid scanning stopped-flow experiments were performed to determine the type of inhibition [enzyme-product-inhibitor ternary complex vs. hyperbolic (partial) mixed-type inhibition]. The rapid-scanning studies were conducted under double-turnover conditions by rapidly mixing 10 μM VIM-2 with 20 μM nitrocefin. The reaction was monitored over the wavelength range of 350 nm to 575 nm for 1.2 s. The spectra showed two prominent peaks at 390 nm and 490 nm (see Figure 4.3). The peak at 390 nm was due to the absorbance of nitrocefin, and disappeared as the experiment progressed due to substrate turnover. The peak at 490 nm was due to the absorbance of the product (hydrolyzed nitrocefin). The product was completely formed (> 99%) after approximately 400 ms. Furthermore, since previous studies conducted on similar MBLs such as NDM-1 demonstrated a peak at 665 nm, the stopped-flow experiments were repeated from 475 nm to 700 nm. The peak at 665 nm corresponds to a ring-opened anionic intermediate which is thought to be stabilized by the active site zinc ions [132]. As expected, the spectra demonstrated the appearance of the hydrolyzed nitrocefin at 490 nm as

the experiment progressed. However, there was no spectral evidence of the peak of the nitrocefin intermediate at 665 nm (data not shown).

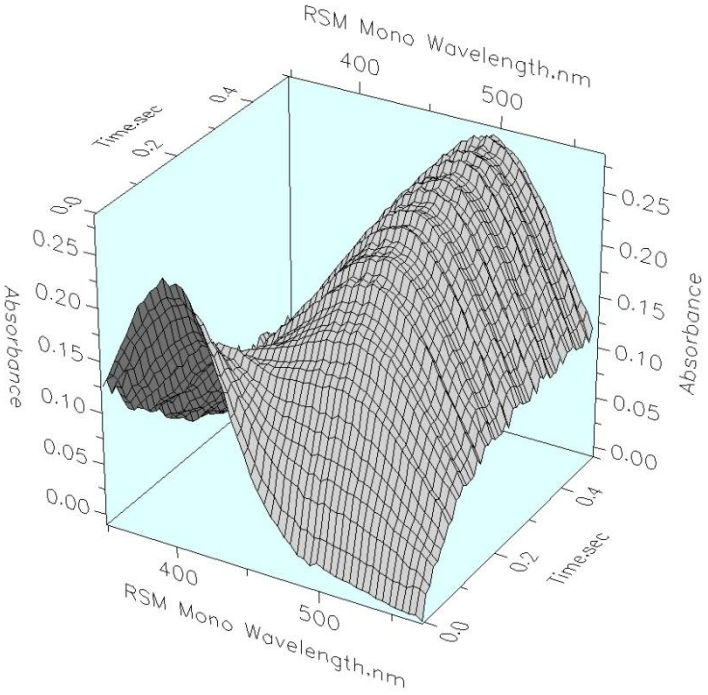

Figure 4.3: Time course for the VIM-2-catalyzed hydrolysis of nitrocefin. Nitrocefin hydrolysis was measured in HEPES buffer (50 mM, pH 7.0) at a temperature of 20 °C. VIM-2 and nitrocefin were rapidly mixed using a U.S.A. stopped-flow device to achieve final concentrations of 10 μM and 20 μM, respectively. The time course demonstrates the depletion of nitrocefin through the disappearance of the peak at 390 nm, and the formation of hydrolyzed nitrocefin through the appearance of the peak at 490 nm. The reaction was complete in ~ 400 ms.

Single-wavelength stopped-flow analyses were conducted for the substrate and the product which absorbed at 390 nm and 490 nm, respectively. The absorbance data obtained at these two wavelengths were converted into concentrations, and plotted as a function of time (see Figure 4.4). Data sets were acquired from the hydrolysis of 20 μM nitrocefin by 10 μM VIM-2 in the absence and in the presence of 10 μM of the $(Arg)_7$ core peptide (peptide **5**). In the case of supplementation with the $(Arg)_7$ core peptide, two data sets were recorded; one where the peptide was pre-exposed to VIM-2 prior to the start of the reaction, and the other where the peptide was pre-exposed to nitrocefin. The results demonstrated that in the presence of the

$(Arg)_7$ core peptide, a decrease in the rate of hydrolysis was observed. As seen in Figure 4.4, the rate reduction was particularly prominent following the first turnover. During the first turnover, the curves demonstrate fairly similar hydrolysis rates. However, once the nitrocefin concentration reached 10 μM (i.e., after the first turnover), the curves started to deviate. The results also illustrate that the rate reduction depended on whether the $(Arg)_7$ core peptide was pre-exposed to nitrocefin or to VIM-2. As shown in Figure 4.4, the rate of nitrocefin hydrolysis by VIM-2 upon the pre-exposure of the $(Arg)_7$ core peptide to nitrocefin was slower than that of the pre-exposure of the $(Arg)_7$ core peptide to VIM-2.

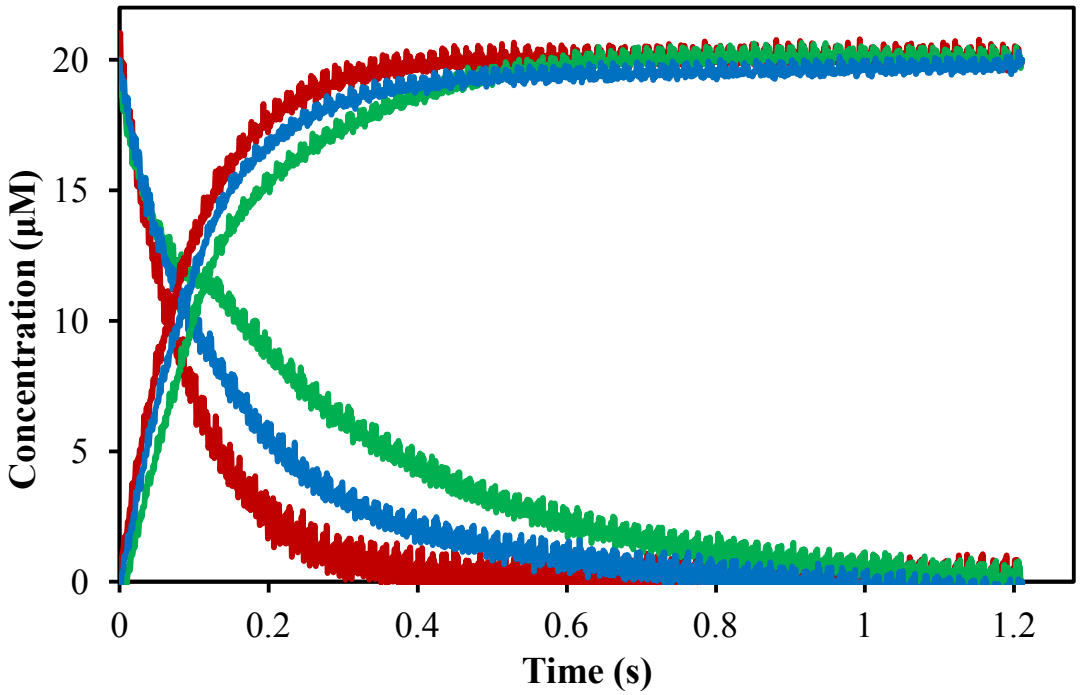

Figure 4.4: Time course of nitrocefin hydrolysis by VIM-2 in the absence and presence of the $(Arg)_7$ core peptide (10 μM; peptide **5**). Nitrocefin hydrolysis was measured at a temperature of 20 °C in HEPES buffer (50 mM, pH 7.0). The time course demonstrates substrate and product concentrations which were measured at 390 nm and 490 nm, respectively. VIM-2 and nitrocefin were rapidly mixed to achieve final concentrations of 10 μM and 20 μM, respectively (red). The blue and green traces represent the progress of nitrocefin hydrolysis following the pre-exposure of the $(Arg)_7$ core peptide to VIM-2 and nitrocefin, respectively.

The rapid-scanning stopped-flow experiments were also performed under single-turnover conditions by rapidly mixing 20 μM VIM-2 with 20 μM nitrocefin. Similar to the previous

stopped-flow studies, the spectra demonstrated prominent peaks including a substrate peak at 390 nm that decreased over time, and a product peak at 490 nm that emerged over time (see Figure 4.5A). When poly-arginine (50 μM; peptide **11**) was used as an inhibitor and pre-exposed to nitrocefin, the substrate peak at 390 nm appeared very similar to that of the reaction between VIM-2 and nitrocefin conducted in the absence of the inhibitor (see t = 0 s trace in Figure 4.5B). However, the emergence of the peak at 490 nm was delayed in comparison to that of the reaction between VIM-2 and nitrocefin in the absence of poly-arginine, a feature indicative of poly-arginine inhibiting nitrocefin turnover. Furthermore, as the reaction progressed both substrate and product peaks became distorted with higher than expected absorption being observed especially at shorter wavelengths (see Figure 4.5B). This result is consistent with the emergence of scattering during the VIM-2-mediated hydrolysis of nitrocefin in the presence of poly-arginine. When poly-arginine was pre-exposed to VIM-2, the substrate peak at 390 nm was considerably different from those of the two previous reactions (see Figure 4.5C). The absorbance of the peak at t = 0 s was considerably higher, presumably due to scattering. However, the product peak at 490 nm was fairly similar to that noted for poly-arginine pre-exposed to nitrocefin (compare Figure 4.5B and Figure 4.5C).

A

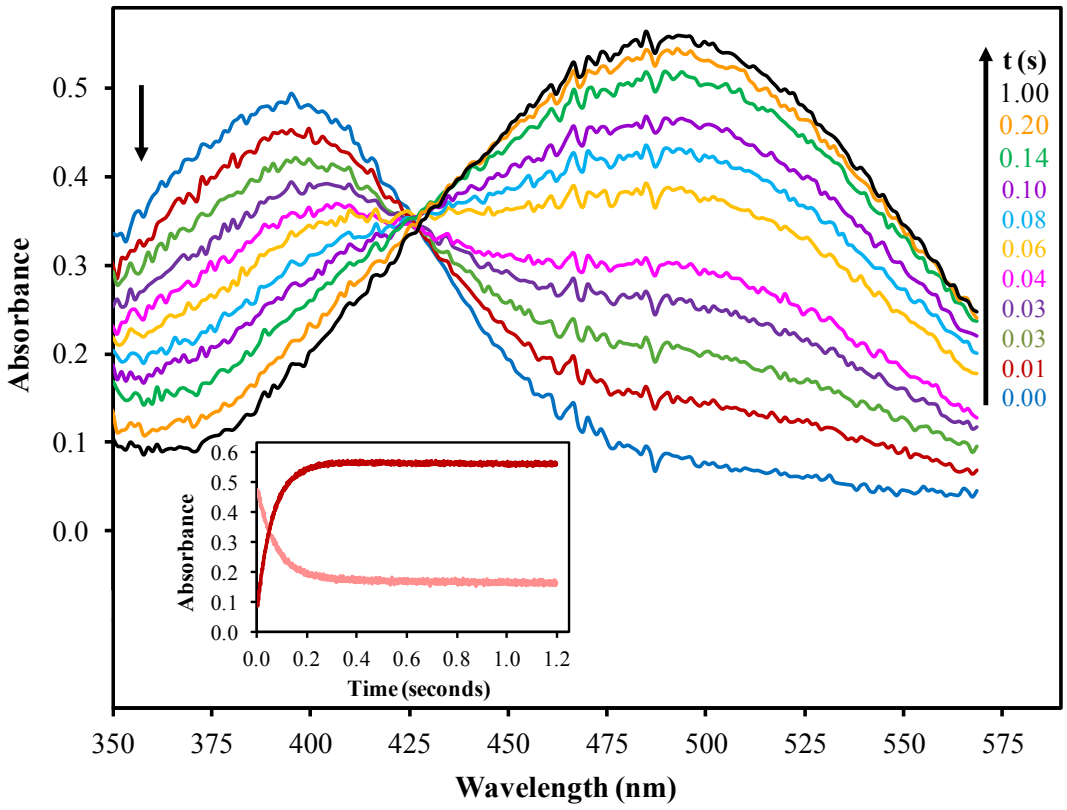
t (s)
1.00
0.20
0.14
0.10
0.08
0.06
0.04
0.03
0.03
0.01
0.00
Absorbance
Wavelength (nm)
Time (seconds)

B

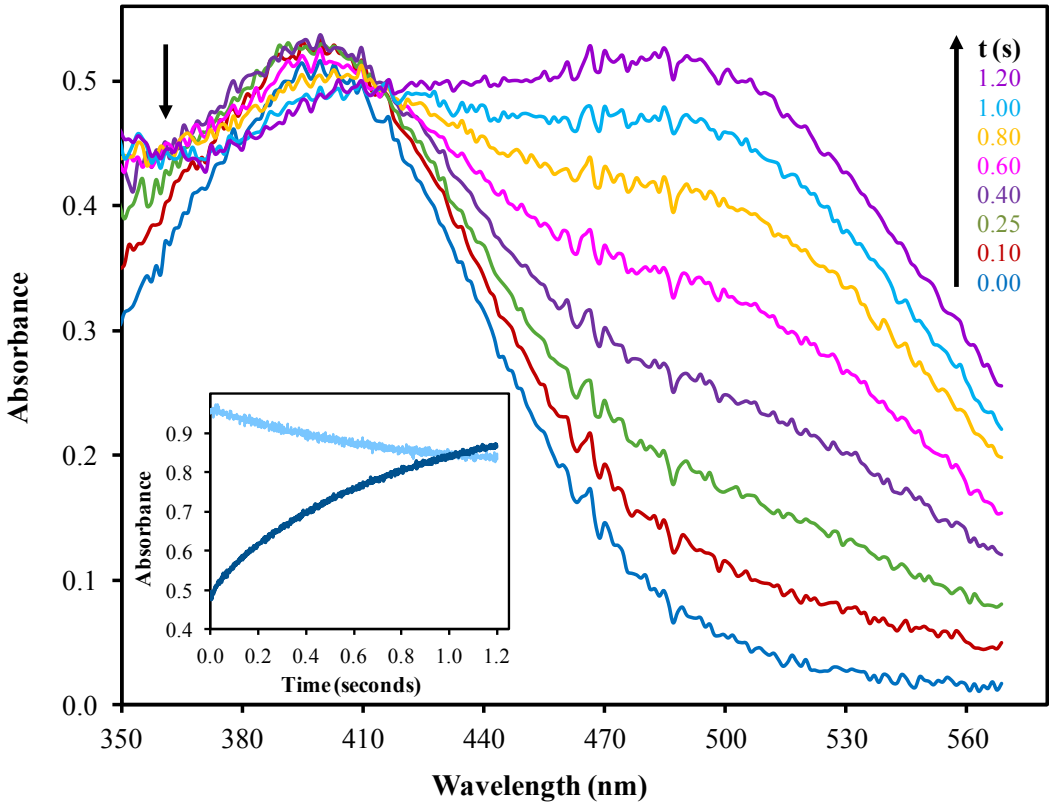
t (s)
1.20
1.00
0.80
0.60
0.40
0.25
0.10
0.00
Absorbance
Wavelength (nm)
Time (seconds)

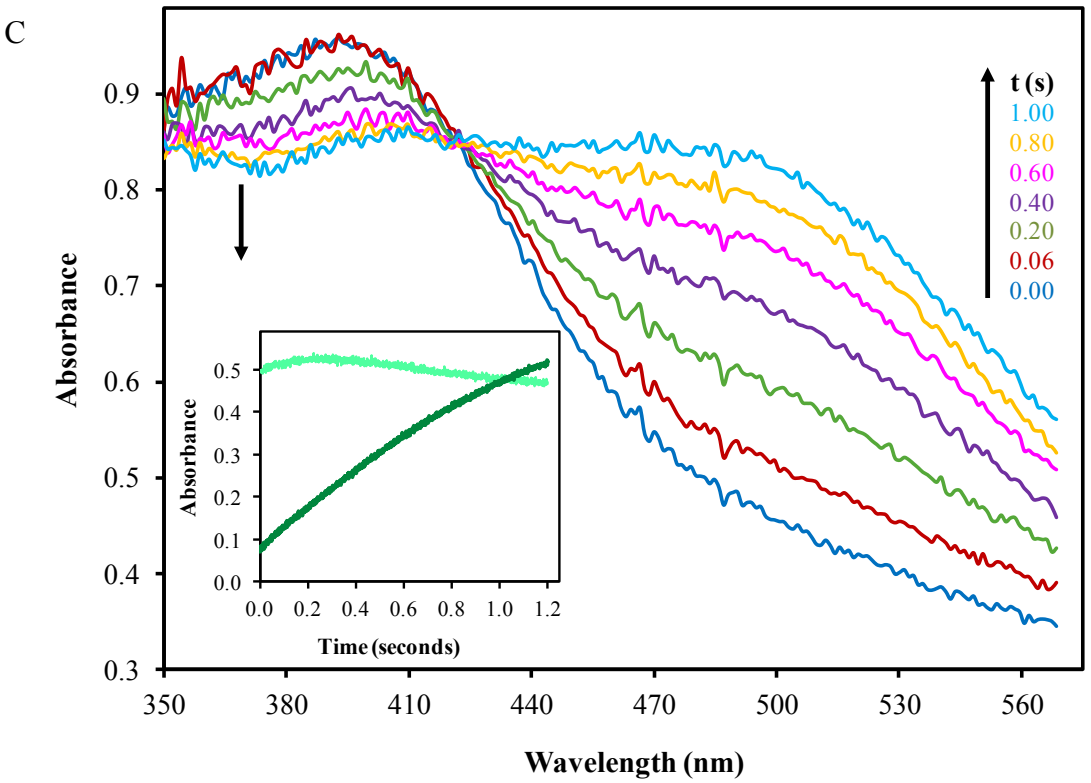

Figure 4.5: Time courses for nitrocefin hydrolysis by VIM-2 in the absence and the presence of poly-arginine. a) Time course for the VIM-2 catalyzed hydrolysis of nitrocefin in the absence of inhibitor. b) Time course for nitrocefin hydrolysis by VIM-2 with poly-arginine pre-exposed to the nitrocefin. c) Time course for the VIM-2 catalyzed hydrolysis of nitrocefin with poly-arginine pre-exposed to VIM-2. For all the experiments, nitrocefin hydrolysis was measured at a temperature of 20 °C in HEPES buffer (50 mM, pH 7.0). VIM-2 and nitrocefin were rapidly mixed to achieve final concentrations of 20 μM in the absence and the presence of 50 μM poly-arginine. The time courses demonstrate the depletion of nitrocefin through the disappearance of the peak at 390 nm and the formation of hydrolyzed nitrocefin through the appearance of the peak at 490 nm. The insets illustrate changes in the absorbance at 390 nm (lighter trace) and 490 nm (darker trace) during the reaction.

In addition, for all three reactions, single-wavelength stopped-flow analyses were performed for the substrate and the product which absorbed at 390 nm and 490 nm, respectively (see insets in Figure 4.5). The results demonstrated that in the presence of poly-arginine, a decrease in the rate of hydrolysis was observed (see insets in Figure 4.5). The results also indicated that the rate reduction was fairly similar regardless of poly-arginine being pre-exposed to nitrocefin or to VIM-2. When the data was fit to an A → B model (i.e., nitrocefin → hydrolyzed nitrocefin), the rate constant for the hydrolysis of nitrocefin by VIM-2 in the absence of inhibitor was 15.1 (±

1.4) s^{-1}. Using the same model, the rate constant for the hydrolysis of nitrocefin by VIM-2 was 1.42 (± 0.14) s^{-1}, and thus one order of magnitude smaller, when poly-arginine was pre-exposed to VIM-2 prior to the reaction. The data from the hydrolysis of nitrocefin by VIM-2 when poly-arginine was pre-exposed to nitrocefin could not be fit to any model in view of the hydrolysis of nitrocefin and protein aggregation occurring at the same time during the stopped-flow reaction.

4.6 Fluorescence Studies on VIM-2 and the Cationic Peptides

In order to study the interaction between VIM-2 and the cationic peptides, intrinsic tryptophan fluorescence studies were conducted. If the interaction between VIM-2 and the cationic peptides were to induce conformational changes within the protein, alterations in the fluorescence emission spectrum of the protein (shift in λ_{max} or change in fluorescence intensity) should be observable. Furthermore, fluorescence spectroscopy is a sensitive technique for identifying light scattering, a phenomenon observed in the previous single-turnover stopped-flow study. The results revealed that the fluorescence emission spectrum of VIM-2 shows one distinct peak at a wavelength of 333 nm whereas that of the $(Arg)_7$ core peptide (peptide **5** in Table 4.1) was essentially featureless (see Figure 4.6). However, the fluorescence spectrum of VIM-2 in the presence of the $(Arg)_7$ core peptide, although displaying a virtually identical λ_{max} value, and similar fluorescence intensities, showed a dramatic increase in fluorescence intensity at 295 nm. This prominent increase in fluorescence intensity (at 295 nm; i.e., the excitation wavelength) is likely to be caused by light scattering due to aggregation.

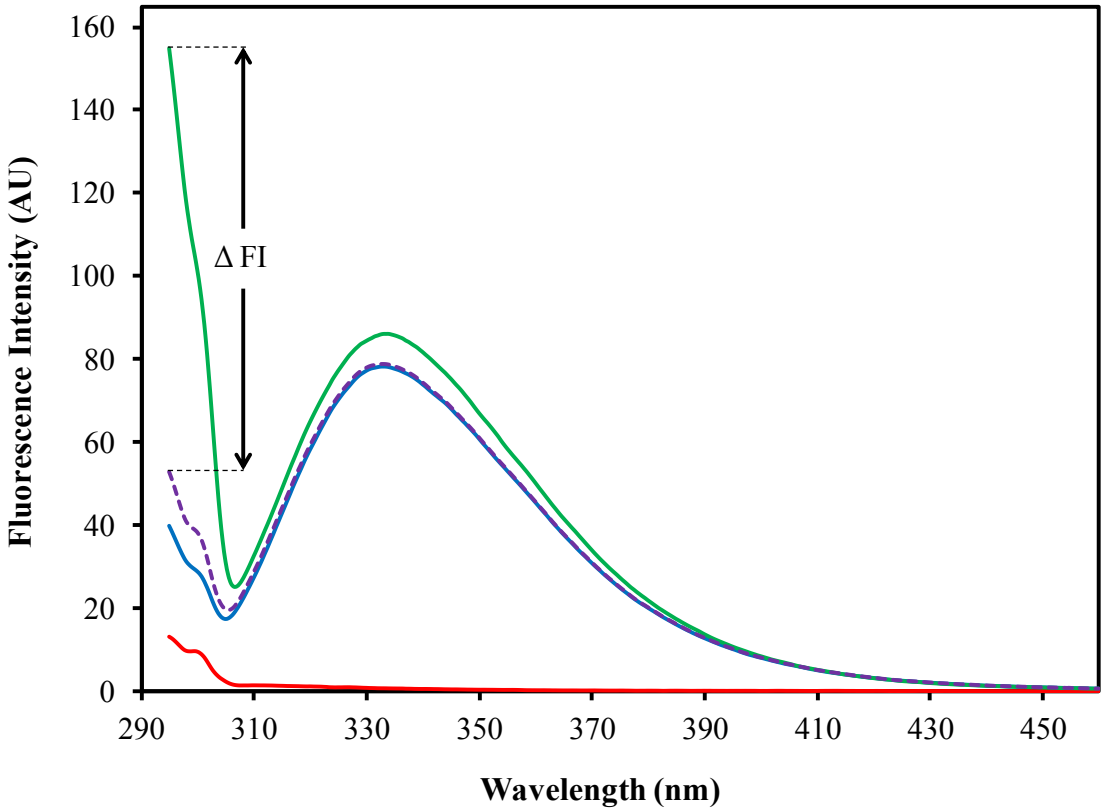

Figure 4.6: Tryptophan fluorescence emission spectra of VIM-2 and the $(Arg)_7$ core peptide (peptide **5**). The spectra were measured in HEPES buffer (50 mM, pH 7.0) at room temperature using an excitation wavelength of 295 nm. VIM-2 and the $(Arg)_7$ core peptide were tested at final concentrations of 1 μM and 5 μM, respectively. Spectrum of VIM-2 (blue), the $(Arg)_7$ core peptide (red), and VIM-2 + $(Arg)_7$ core peptide (green and purple). The solid lines represent experimental data while the dashed line symbolizes the additive spectrum obtained through the addition of the blue and the red traces. ΔFI denotes the difference in the fluorescence intensity at 295 nm between the green and the purple traces. The spectra represent the average of three independent experiments.

To analyze the level of scattering at 295 nm, the fluorescence intensity at 295 nm of the additive spectrum was subtracted from that of the experimental spectrum. Using the $(Arg)_7$ peptide as an example, if there was no interaction between VIM-2 and the peptide, the fluorescence emission spectrum of the mixture should equal the sum of the individual spectra of VIM-2 and the $(Arg)_7$ core peptide (see Figure 4.6). As outlined above, however, the large discrepancy between the additive spectrum and that observed experimentally (ΔFI; Figure 4.6) is

indicative of peptide-induced VIM-2 aggregation. Hence, the propensity of other cationic peptides to cause VIM-2 aggregation was assessed based on the ΔFI value.

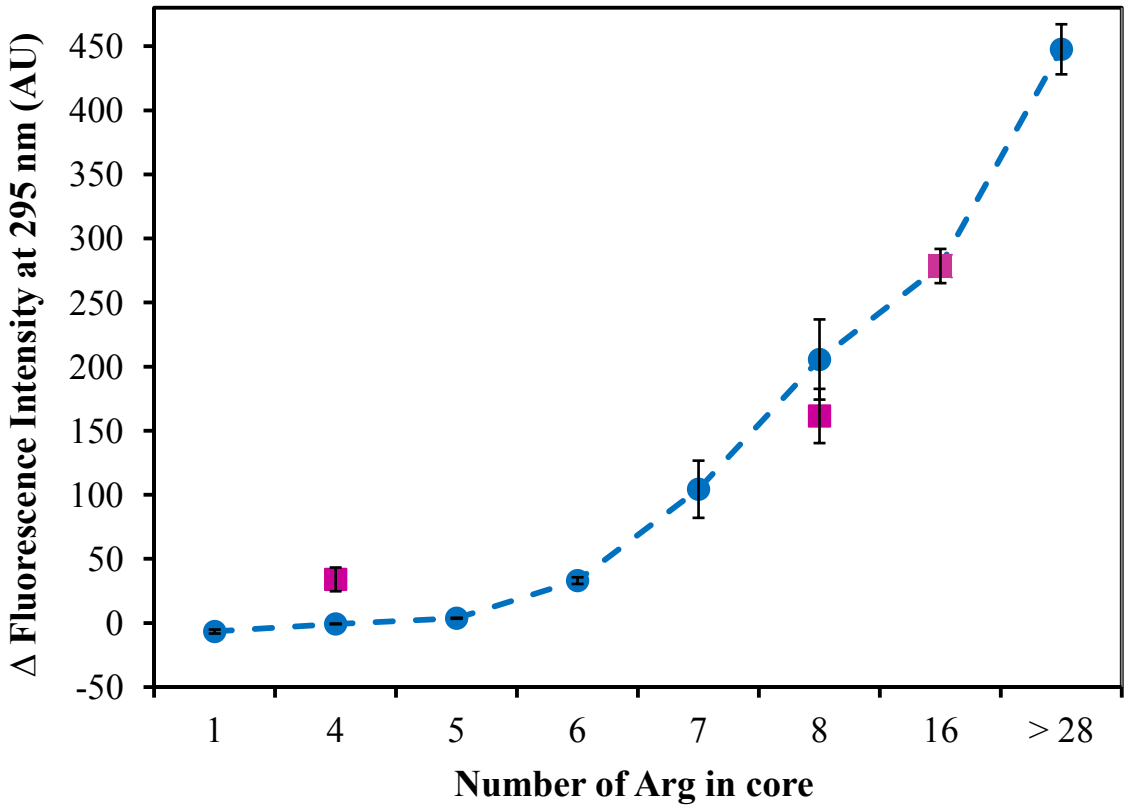

Figure 4.7: Difference of fluorescence intensity at 295 nm for the emission spectra of VIM-2 in the presence of various cationic peptides. The spectra were measured in HEPES buffer (50 mM, pH 7.0) at room temperature using an excitation wavelength of 295 nm. VIM-2 and the cationic peptides were used at final concentrations of 1 μM and 5 μM, respectively. The purple squares correspond to the peptides that contained a cysteine residue in their N-terminus instead of a glycine residue (peptides **12**, **14** and **15**). The 16 arginine peptide denotes the $(Arg_8Cys)_2$ core peptide (peptide **15**) while the >28 core peptide represents poly-arginine (peptide **11**). ΔFluorescence intensity denotes the difference in fluorescence intensity between the experimental and additive spectra. Data shown represent the mean of three independent experiments. The error bars symbolize the mean (± 1 s.d.) of the three independent experiments.

As shown in Figure 4.7, the difference of the fluorescence intensity at 295 nm increased with the number of arginine residues in the peptides. This observation corresponds well with the inhibitory potency of these peptides obtained in previous experiments (see Table 4.1). For instance, the $(Arg)_4$ and the $(Arg)_5$ core peptides (peptides **8** and **7**, respectively) were poor VIM-2 inhibitors, and they did not display an appreciable value for ΔFI. Furthermore, an increase in

the number of core arginine residues to six (peptide **6**) not only resulted in an increase in inhibitory potency, but also in the first observable increase in ΔFI, and hence, scattering. Finally, poly-arginine (peptide **11**) and the disulfide-containing $(Arg)_8$ core peptide [$(Arg_8Cys)_2$; peptide **15**] were not only the most potent inhibitors of VIM-2, but they also demonstrated the highest ΔFI values.

4.7 UV-Vis Wave Scans with VIM-2 and the Cationic Peptides

Since the fluorescence studies suggested aggregation of VIM-2 in the presence of cationic peptides, UV-Vis wave scans were performed to confirm the existence of such aggregates. As in the previous fluorescence studies, aggregation of VIM-2 should be observable through an increase of absorbance in the short wavelength limb of the protein spectrum. As shown in Figure 4.8, the absorption spectrum of VIM-2 revealed a distinct peak at a wavelength of 280 nm. The UV-Vis wave scans were also conducted with inhibitors. The inhibitors used were the $(Arg)_5$ and the $(Arg_8Cys)_2$ core peptides (peptides **7** and **15**, respectively). The results show that the absorption spectra of VIM-2 with these two peptides exhibited one distinct peak at a wavelength of approximately 275 nm (see Figure 4.8).

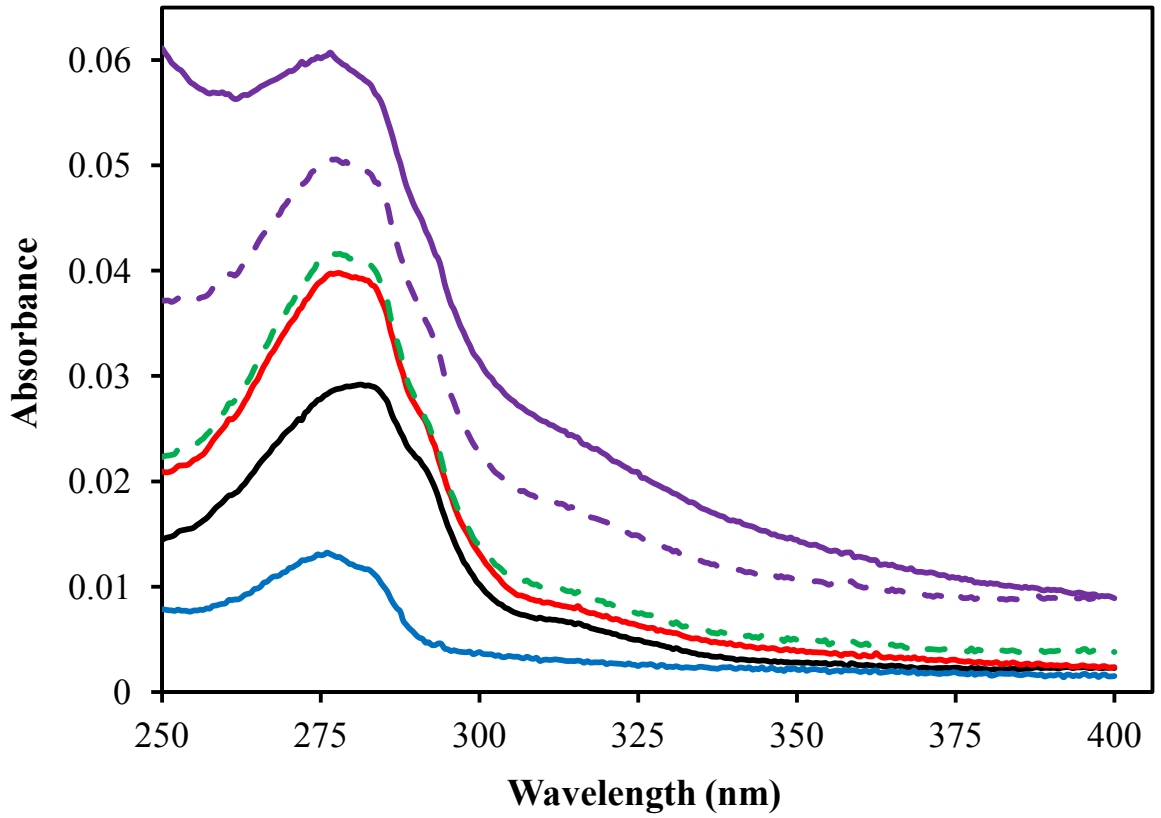

Figure 4.8: Absorption spectra of VIM-2 in the presence and absence of the $(Arg)_5$ and $(Arg_8Cys)_2$ core peptides. The spectra were measured in HEPES buffer (50 mM, pH 7.0) at room temperature. VIM-2 and the cationic peptides were used at final concentrations of 1 μM and 5 μM, respectively. Spectrum of VIM-2 (black); the $(Arg)_5$ core peptide (blue); VIM-2 + $(Arg)_5$ core peptide (red and green), and VIM-2 + $(Arg_8Cys)_2$ core peptide (purple). The solid lines indicate experimental data while the dashed lines denote the additive spectra obtained through the addition of the individual spectra of VIM-2 and the cationic peptides. The spectra represent the average of three independent experiments.

Similar to the fluorescence studies, the scattering at 250 nm in the absorption spectra was evaluated through the comparison of the experimental and additive spectra. Using the $(Arg)_5$ core peptide as an example, if there was no interaction between VIM-2 and the $(Arg)_5$ core peptide, the experimental spectrum should match that of the individual spectra of VIM-2 and the $(Arg)_5$ core peptide added together. Actual experimental data demonstrated that the interaction between VIM-2 and the $(Arg)_5$ core peptide was minimal since the experimental spectrum was nearly identical to the additive spectrum. However, using the $(Arg_8Cys)_2$ core peptide as an

example, there was an interaction between VIM-2 and this peptide since the experimental spectrum did not coincide with that of the additive spectrum for this sample. In comparison to the additive spectrum, the experimental spectrum demonstrated no shift in λ_{max}, but a considerable amount of scattering in the entire spectrum, especially at 250 nm (see Figure 4.8). Therefore, the difference in absorbance at 250 nm was evaluated for a variety of peptides by subtracting the absorbance at 250 nm of the additive spectra from that of the experimental spectra. The results demonstrate that the difference in absorbance at 250 nm, and thus the degree of scattering, increased with the number of arginine residues in the peptides (see Table 4.6). Therefore, these results correlate well with the inhibitory potency of these peptides, and with those observed in the previous fluorescence studies (see Table 4.1 and Figure 4.7).

Table 4.6: Difference in absorbance at 250 nm for the spectra of VIM-2 with various cationic peptides. The spectra were measured in HEPES buffer (50 mM, pH 7.0) at room temperature. VIM-2 and the cationic peptides were used at final concentrations of 1 μM and 5 μM, respectively. ΔAbsorbance denotes the difference in absorbance at 250 nm between the experimental and additive spectra. The values represent the mean (± 1 s.d.) of three independent experiments.

Peptide # in Table 4.1	Number of Arg in core	Δ Absorbance at 250 nm
7	5	-0.005 (± 0.002)
4	8	0.008 (± 0.001)
14	8	0.038 (± 0.001)
15	16	0.028 (± 0.004)
11	> 28	0.126 (± 0.035)

4.8 Native PAGE of VIM-2 in the Presence of Cationic Peptides

Since the fluorescence studies as well as the UV-Vis wave scans indicated the occurence of aggregation between VIM-2 and the cationic peptides, native polyacrylamide gel electrophoresis (PAGE) was performed to initially estimate the size of the aggregates (e.g., dimer, tetramer, etc.) As seen in Figure 4.9, the VIM-2 preparation was found to be homogeneous as evidenced by the appearance of one distinct band in the gel. However, for a sample comprised of 10 μM VIM-2,

and 100 μM of the $(Arg)_5$ core peptide (peptide **7**) or 100 μM of the $(Arg)_8$ core peptide (peptide **4**), the same band was found to be very weak (see Figure 4.9). To confirm that the reduction in the intensity of the bands was truly caused by the interaction of the cationic peptides with VIM-2, a BSA sample in the absence and the presence of the $(Arg)_8$ core peptide was run as a control, revealing two prominent bands. These bands correspond to the monomeric and the dimeric forms of BSA which have molecular masses of 66 kDa and 132 kDa, respectively (see Figure 4.9). More importantly, the bands of the BSA/$(Arg)_8$ peptide sample did not diminish in intensity in comparison to the bands of the sample containing only BSA. Therefore, these results suggest that the diminished intensity of the VIM-2 bands was caused by the interaction between VIM-2 and the cationic peptide.

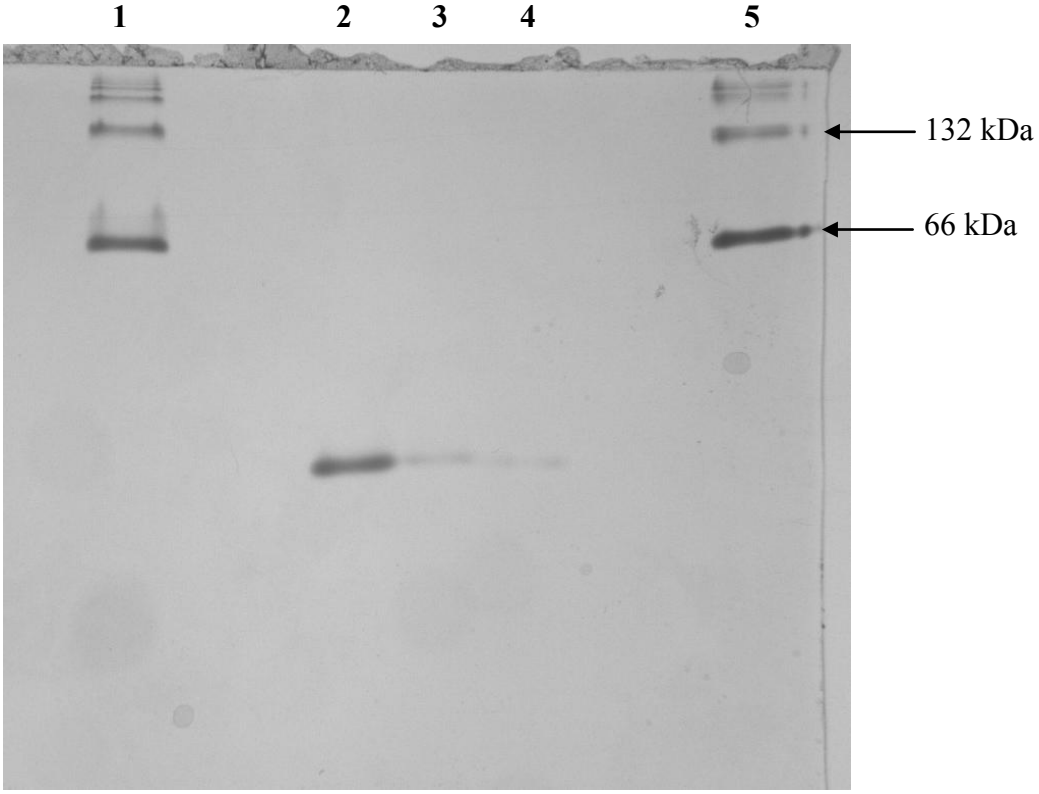

Figure 4.9: Native PAGE of VIM-2 in the absence and the presence of the $(Arg)_5$ and the $(Arg)_8$ core peptides. All experiments were conducted with 1 mg/ mL of BSA, 10 μM of VIM-2 and/or 100 μM of the $(Arg)_5$ or $(Arg)_8$ core peptides. Lane 1, BSA; lane 2, VIM-2; lane 3, VIM-2 + $(Arg)_5$ core peptide; lane 4, VIM-2 + $(Arg)_8$ core peptide; lane 5, BSA + the $(Arg)_8$ core peptide.

Densitometry was employed to quantify the intensity of the bands of the samples containing VIM-2. The densitometry results confirmed that the band for the sample containing only VIM-2 was more intense than the bands of the samples containing VIM-2 and the cationic peptides. The sample consisting of VIM-2 and the $(Arg)_5$ core peptide had a band intensity of 14.3% relative to that of the sample containing only VIM-2, whereas the sample comprised of VIM-2 and the $(Arg)_8$ core peptide had an intensity of 1.7%. Interestingly, no bands of higher molecular mass could be detected in the gel to justify the decreased intensity of the VIM-2 bands or to demonstrate the presence of distinct aggregates in the samples.

4.9 Paper Electrophoresis of VIM-2 in the Presence of Cationic Peptides

Since no distinct aggregates of VIM-2 and the cationic peptides could be detected by native PAGE, paper electrophoresis was conducted to determine if the aggregates traveled in the opposite direction (i.e., towards the cathode) during the experiment (due to the aggregates potentially being highly positively charged). As shown in Figure 4.10, a sample containing 10 μM VIM-2 revealed a circular shape on the TLC paper which migrated towards the anode. A sample consisting of 10 μM VIM-2 and 100 μM of the $(Arg)_8$ core peptide was also measured. The cone-like spot seemed to have been the result of the migration of two different species in the sample. The base of the cone appeared to be migrating towards the anode. This migration pattern was similar to that of VIM-2. However, the tip of the cone-like shape seemed to have remained in the same place where it was originally deposited on the TLC paper. Hence, it appears that a fraction of VIM-2 molecules forms (presumably large) immobile aggregates after being exposed to the $(Arg)_8$ peptide, which are incapable of moving towards neither the anode nor towards the cathode.

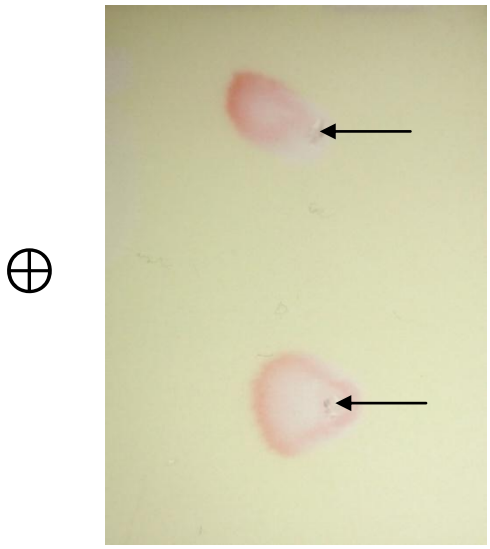

Figure 4.10: Paper electrophoresis of VIM-2 in the absence and presence of the $(Arg)_8$ core peptide. Prior to electrophoresis, a TLC paper was soaked in HEPES buffer (50 mM, pH 7.0), followed by exposure to nitrocefin (20 μM). All experiments were conducted with 10 μM VIM-2 and/or 100 μM of the $(Arg)_8$ core peptide. Top, VIM-2; bottom, VIM-2 + $(Arg)_8$ core peptide; ⊕, anode; ⊖, cathode. The locations where the samples were applied to the TLC paper are indicated by arrows.

4.10 Dynamic Light Scattering with VIM-2 and the Cationic Peptides

Since the previous experiments suggested aggregation between VIM-2 and the cationic peptides, dynamic light scattering was performed to determine the size of the aggregates. HEPES buffer (20 mM, pH 7.4) was run as a control in these experiments since it was used for the dilution of all samples. The spectrum of HEPES buffer showed one peak with a diameter of 358 nm (see Figure 4.11). However, this peak represented only 0.1% of the mass of the buffer sample, hence rendering this peak negligible. Therefore, the data was consistent with the buffer not scattering in solution.

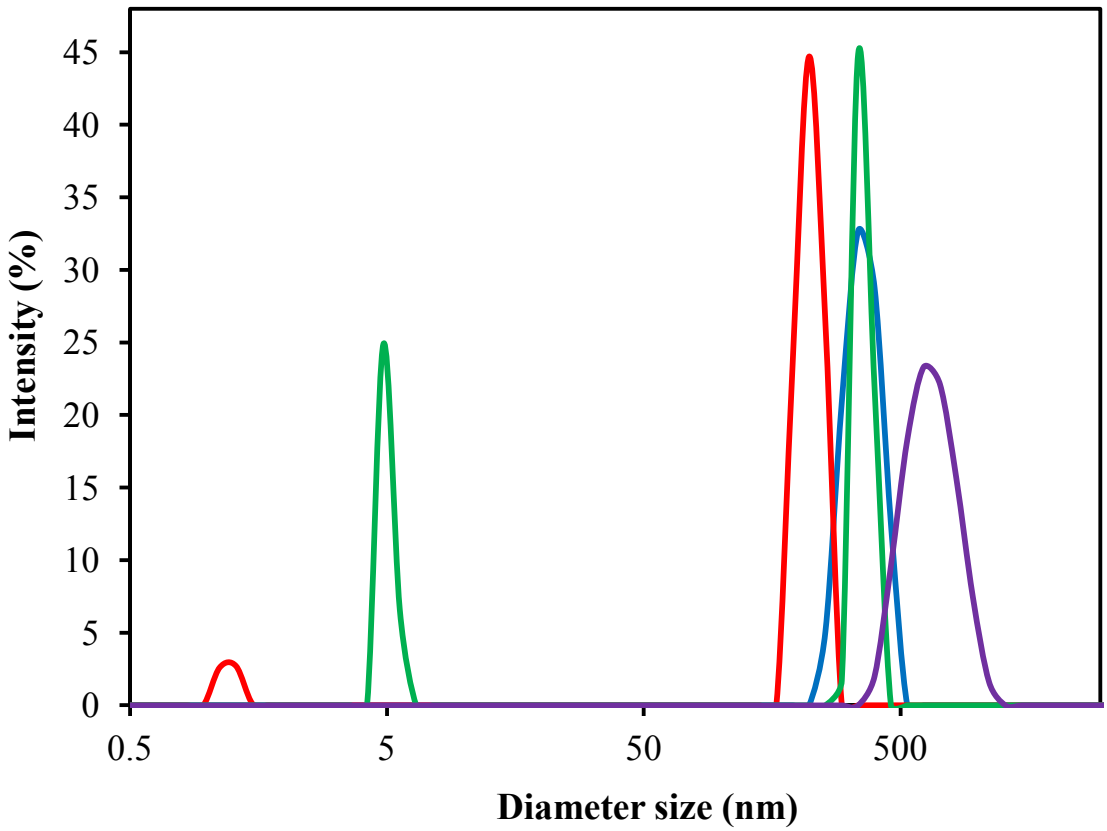

Figure 4.11: Dynamic light scattering following the reaction between VIM-2 and the $(Arg)_8$ core peptide. All experiments were conducted in HEPES buffer (20 mM, pH 7.4) at a temperature of 25 °C. VIM-2 and the $(Arg)_8$ core peptide were measured at final concentrations of 8 µM and 80 µM, respectively. Spectra of HEPES buffer (blue), VIM-2 (green), the $(Arg)_8$ core peptide (red), and VIM-2 + $(Arg)_8$ peptide (purple). The results are presented as particle size distributions.

The spectrum of a sample containing 8 µM VIM-2 demonstrated two peaks: one exhibited a diameter of 5.0 nm while the other peak displayed a diameter of 358 nm (see Figure 4.11). The peak at 358 nm represented only 0.1% of the mass of VIM-2, and was therefore negligible. The peak at 5.0 nm (99.9% of the mass of VIM-2) corresponded to a molecular weight of 28.8 kDa. The diameter size of 5.0 nm for VIM-2 is consistent for other MBLs in the same class as VIM-2 such as NDM-1 (diameter of 4.8 nm; molecular weight of 25 kDa) [133]. Furthermore, similar to the dynamic light scattering experiments conducted with NDM-1, a small amount of VIM-2 (calculated as 0.1% mass by dynamic light scattering instruments) formed non-specific aggregates due to the high concentration of protein used in the experiments. A sample

containing 80 μM of the $(Arg)_8$ core peptide revealed two peaks: one with a diameter of 1.2 nm and the other exhibiting a diameter of 222 nm (see Figure 4.11). The peak at 222 nm was composed 0.1% of the mass of the $(Arg)_8$ core peptide, and was therefore negligible. The peak at 1.2 nm represented 99.9% of the mass of the $(Arg)_8$ core peptide. The sample containing both VIM-2 and the $(Arg)_8$ peptide showed only one peak with a diameter of 668 nm (see Figure 4.11). This data is consistent with the formation of large aggregates between VIM-2 and the $(Arg)_8$ core peptide since the individual peaks of VIM-2 and the $(Arg)_8$ core peptide were no longer visible in the spectrum. Furthermore, the sample containing both VIM-2 and the $(Arg)_8$ core peptide showed visual aggregation at the concentrations employed since the sample became turbid (see Figure 4.12).

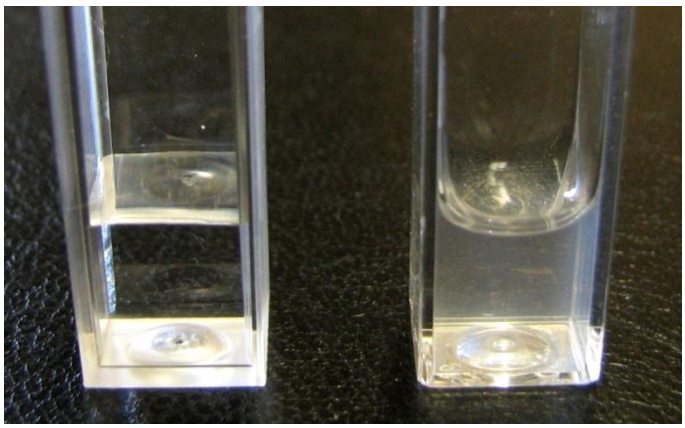

Figure 4.12: Visual aggregation following the reaction of VIM-2 with the $(Arg)_8$ core peptide. The experiment was performed in HEPES buffer (20 mM, pH 7.4) at a temperature of 25 °C. VIM-2 and the $(Arg)_8$ core peptide were employed at final concentrations of 8 μM and 80 μM, respectively. These are the same concentrations employed in the dynamic light scattering studies. Cuvette with VIM-2 (left), and VIM-2 + $(Arg)_8$ core peptide (right).

The dynamic light scattering experiments were repeated with increasing inhibitor concentrations to determine the amount of inhibitor necessary for the formation of the aggregates. As in the previous experiments, the spectrum of 8 μM VIM-2 demonstrated two peaks: one revealing a diameter of 5.0 nm, the other displaying a diameter of 276 nm (see Figure

4.13). Following the addition of the $(Arg)_8$ core peptide to the sample (concentration of 1.6 µM; 0.2 equivalents), the spectrum exhibited only one peak at a diameter of 219 nm (see Figure 4.13). Therefore, these results (surprisingly) suggest that aggregation occurs with only 0.2 molar equivalents of inhibitor. Addition of 0.5, 1, 2, 5 and 10 molar equivalents of inhibitor to the sample resulted in the appearance of only one peak at a diameter of 361, 528, 532, 667 and 692 nm, respectively. Therefore, a steady increase in the size of the aggregates was observed until it reached a plateau at ≥ 5 molar equivalents of inhibitor (see Figure 4.13 inset).

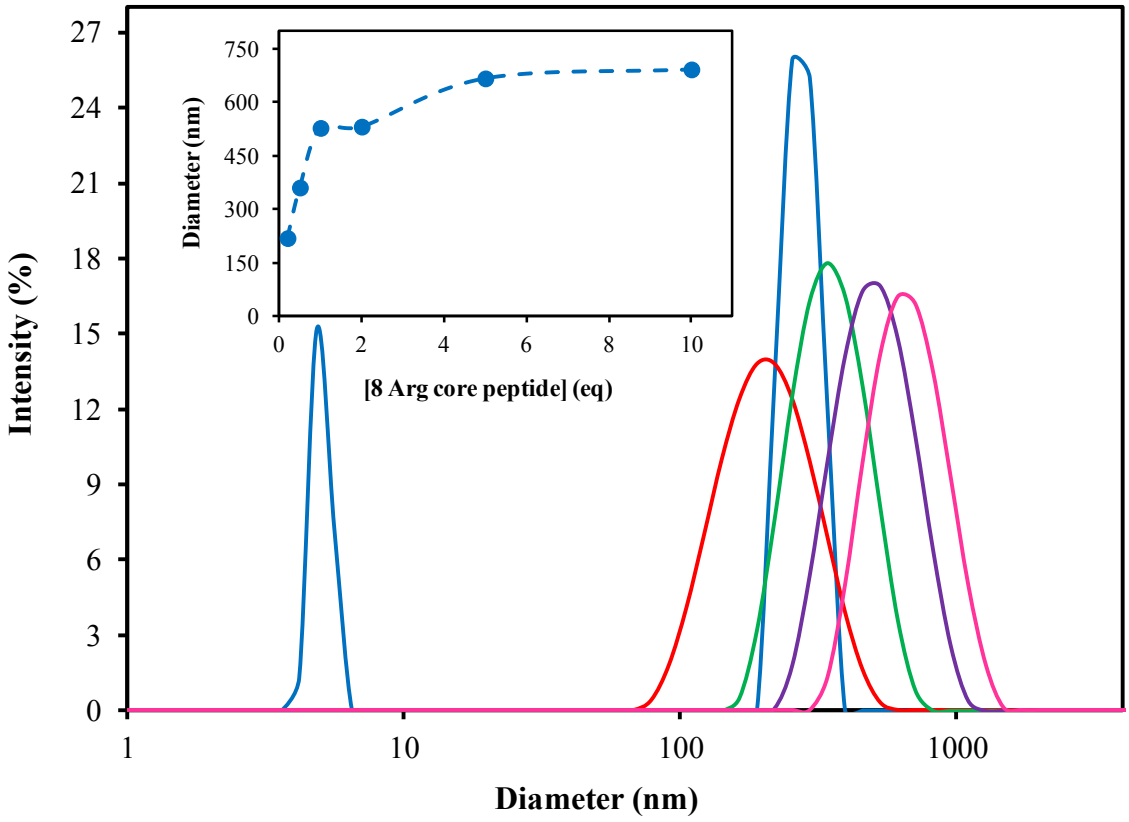

Figure 4.13: Dependence of the aggregate diameter on the concentration of the $(Arg)_8$ core peptide. All experiments were conducted in HEPES buffer (20 mM, pH 7.4) at a temperature of 25 °C. VIM-2 was measured at a final concentration of 8 µM. The $(Arg)_8$ core peptide was employed at final concentrations of 1.6, 4, 8, 16, 40 and 80 µM. Spectra of VIM-2 (blue), VIM-2 + 1.6 µM (0.2 eq) of the $(Arg)_8$ core peptide (red), VIM-2 + 4 µM (0.5 eq) of the $(Arg)_8$ core peptide (green), VIM-2 + 8 µM (1 eq) of the $(Arg)_8$ core peptide (purple), and VIM-2 + 80 µM (10 eq) of the $(Arg)_8$ core peptide (pink). The results are presented as particle size distributions. The inset shows the particle size distribution as a function of inhibitor concentration.

4.11 Reversibility of VIM-2 Aggregation

To assess whether VIM-2 aggregation is reversible, sodium sulfate was added to the sample containing 8 μM VIM-2 and 80 μM of the $(Arg)_8$ core peptide after the dynamic light scattering measurements. A salt was added since previous studies demonstrated that salts had the ability to alleviate inhibition (see Table 4.4). As shown in Figure 4.14, the addition of Na_2SO_4 greatly diminished the scattering intensity in the absorption spectrum of the sample. Indeed, the Na_2SO_4-treated VIM-2/$(Arg)_8$ peptide sample displayed a spectrum similar to that of the spectrum obtained by addition of the individual spectra of VIM-2 and the $(Arg)_8$ core peptide (see Figure 4.14). Therefore, the results indicate that the aggregation of VIM-2 in the presence of the $(Arg)_8$ core peptide is reversible, although a small degree of light scattering could still be observed in the spectrum even after the addition of Na_2SO_4 (see Figure 4.14). Furthermore, the addition of Na_2SO_4 to the visually aggregated sample containing VIM-2 and the $(Arg)_8$ core peptide diminished the turbidity of the sample, resulting in the disappearance of the white precipitate (results not shown). Finally, activity assays were performed on the sample in the absence and presence of Na_2SO_4. The results demonstrated that VIM-2 regained ~ 30% of its original activity upon the addition of Na_2SO_4 to the aggregated sample.

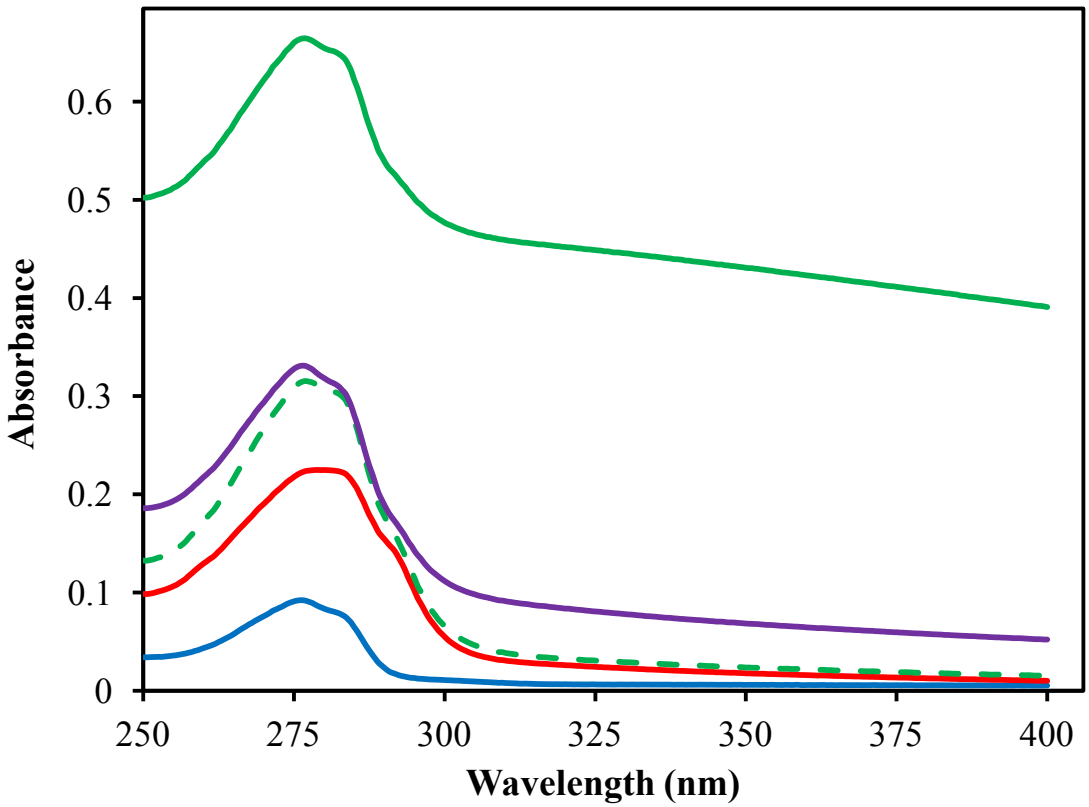

Figure 4.14: Absorption spectra of VIM-2 in the presence of the $(Arg)_8$ core peptide. Spectra were measured in HEPES buffer (50 mM, pH 7.0) at room temperature. VIM-2, the $(Arg)_8$ core peptide and sodium sulfate were employed at final concentrations of 1 µM, 5 µM and 25 mM, respectively. Spectrum of VIM-2 (blue), the $(Arg)_8$ core peptide (red), VIM-2 + $(Arg)_8$ core peptide (green), and VIM-2 + $(Arg)_8$ core peptide + sodium sulfate (purple). The solid lines indicate experimental data while the dashed line denotes the additive spectrum obtained by the addition of the blue and red traces. The spectra represent the average of three independent experiments.

Since the UV-Vis spectra suggested that the aggregation between VIM-2 and the cationic peptides was reversible, fluorescence studies were performed to further confirm the reversibility of this phenomenon. Previous fluorescence studies demonstrated a high level of scattering at 295 nm for samples containing both VIM-2 and cationic peptides (see Figure 4.6 and Figure 4.7). For the fluorescence studies, a sample containing VIM-2 and the $(Arg_8Cys)_2$ core peptide (peptide **15**) was measured, and was shown to have an elevated level of scattering at 295 nm in comparison to that of the additive spectrum (see Figure 4.15). To determine the reversibility of this aggregation, TCEP was added to the sample. The results revealed that the addition of TCEP

significantly reduced the level of scattering at 295 nm. This result is a consequence of TCEP being capable of breaking the disulfide bond of the $(Arg_8Cys)_2$ core peptide to yield the $(Arg)_8Cys$ peptide (peptide **14**), which scatters significantly less than the disulfide (see Figure 4.7). However, the scattering intensity at 295 nm of the sample containing VIM-2, the $(Arg_8Cys)_2$ peptide and TCEP remained higher than that of the sample containing VIM-2, the $(Arg)_8Cys$ peptide and TCEP. This result may be due to the former sample containing twice as many molecules of $(Arg)_8Cys$ peptide. Nevertheless, these results imply that the reaction between VIM-2 and the cationic peptides was (at least partially) reversible akin to the previous results obtained from the UV-Vis experiments.

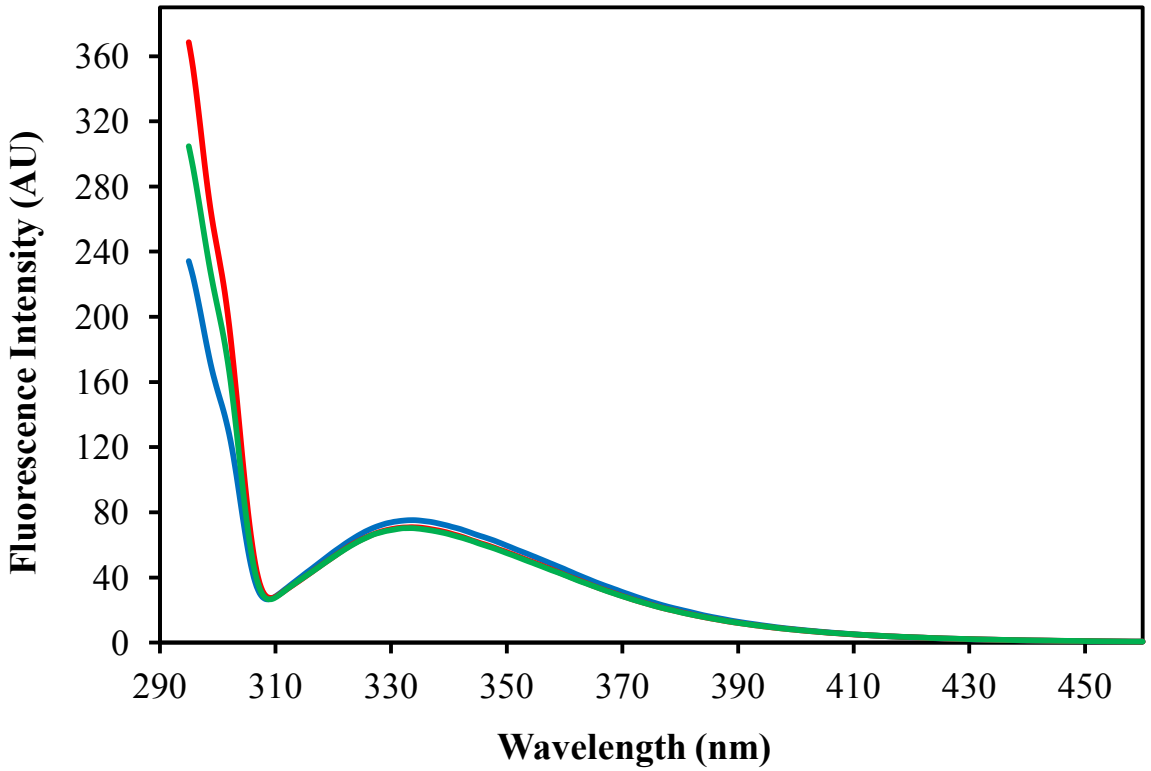

Figure 4.15: Fluorescence emission spectra of VIM-2 in the presence of the $(Arg)_8Cys$ and the $(Arg_8Cys)_2$ core peptides. The spectra were measured in HEPES buffer (50 mM, pH 7.0) at room temperature using an excitation wavelength of 295 nm. VIM-2, the cationic peptides and TCEP were employed at final concentrations of 1 μM, 5 μM and 25 μM, respectively. Spectrum of VIM-2 + $(Arg)_8Cys$ peptide + TCEP (blue), VIM-2 + $(Arg_8Cys)_2$ peptide (red), and VIM-2 + $(Arg_8Cys)_2$ peptide + TCEP (green). The spectra represent the average of three independent experiments.

4.12 FRET Studies

Since previous experiments indicated the occurrence of aggregation between VIM-2 in the presence of the cationic peptides, fluorescence resonance energy transfer (FRET) was employed to confirm the presence of these protein aggregates. VIM-2 was labeled with either Alexa Fluor 488 (donor) or Alexa Fluor 546 (acceptor). The fluorescence emission spectrum of VIM-2 labeled with Alexa Fluor 488 in the presence of the $(Arg)_8Cys$ core peptide (peptide **14**) demonstrated one distinct peak at a wavelength of 514 nm (see Figure 4.16). The fluorescence emission spectrum of VIM-2 labeled with Alexa Fluor 546 in the presence of the $(Arg)_8Cys$ core peptide showed a single peak at a wavelength of 568 nm (see Figure 4.16). The fluorescence emission spectrum for the sample containing both of the labeled portions of VIM-2 exhibited two distinct peaks; one at a wavelength of 514 nm and another at a wavelength of 568 nm (see Figure 4.16). If there was no interaction between the donor- and acceptor-labeled VIM-2, the experimental spectrum should be equal to that of the added spectra of VIM-2 labeled with Alexa Fluor 488 and VIM-2 labeled with Alexa Fluor 546. However, the experimental data revealed that there was an interaction between the labeled proteins since the experimental fluorescence spectrum demonstrated quenching of the peak at 514 nm, but no change in the peak at 568 nm (compare green and purple traces in Figure 4.16). Therefore, the results indicate that there was no FRET between the samples as there was no increase in the λ_{max} of the peak at 568 nm to accompany the quenching of the peak at 514 nm. Furthermore, the distance between the donor and acceptor moieties of the labeled proteins was calculated to be ~ 90 Å. Such a large distance between the labeled proteins is indicative of very weak FRET, and, hence, of the absence of protein-protein interactions.

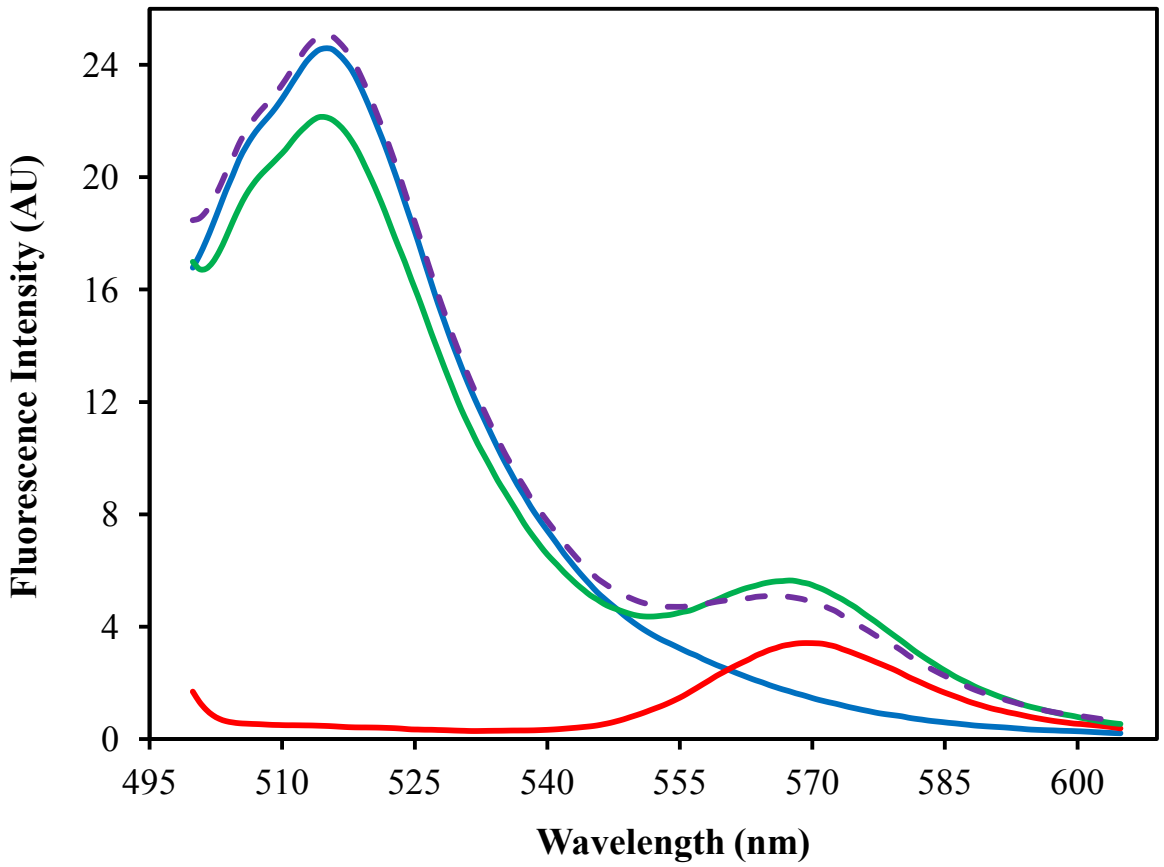

Figure 4.16: Fluorescence emission spectra of labeled VIM-2. The spectra were measured in HEPES buffer (50 mM, pH 7.2) at room temperature using an excitation wavelength of 492 nm. A portion of VIM-2 was labeled with Alexa Fluor 488 (donor) while another portion of VIM-2 was labeled with Alexa Fluor 546 (acceptor). Both labeled portions of VIM-2 were both employed at a concentration of 100 nM while the $(Arg)_8Cys$ core peptide was used at a final concentration of 400 nM. Spectrum of VIM-2 labeled with Alexa Fluor 488 + $(Arg)_8Cys$ peptide (blue), VIM-2 labeled with Alexa Fluor 546 + $(Arg)_8Cys$ peptide (red), VIM-2 labeled with Alexa Fluor 488 + VIM-2 labeled with Alexa Fluor 546 + $(Arg)_8Cys$ peptide (green and purple). The solid lines denote experimental data while the dashed line indicates the additive spectrum obtained by the addition of the blue and red traces. The curves represent the average of three independent experiments.

In light of the absence of protein-protein FRET, it was of interest to gain insight into the location of the peptide binding site by FRET. The fluorescence emission spectrum of the sample containing (donor-) labeled VIM-2 demonstrated one distinct peak at a wavelength of 515 nm (see Figure 4.17). Furthermore, the fluorescence emission spectrum of the acceptor-labeled $(Arg)_8Cys$ core peptide showed one distinct peak at a wavelength of 567 nm (see Figure 4.17).

The fluorescence emission spectrum of the sample containing both labeled VIM-2 and the labeled $(Arg)_8Cys$ peptide demonstrated distinct peaks at 514 nm and 566 nm (see Figure 4.17).

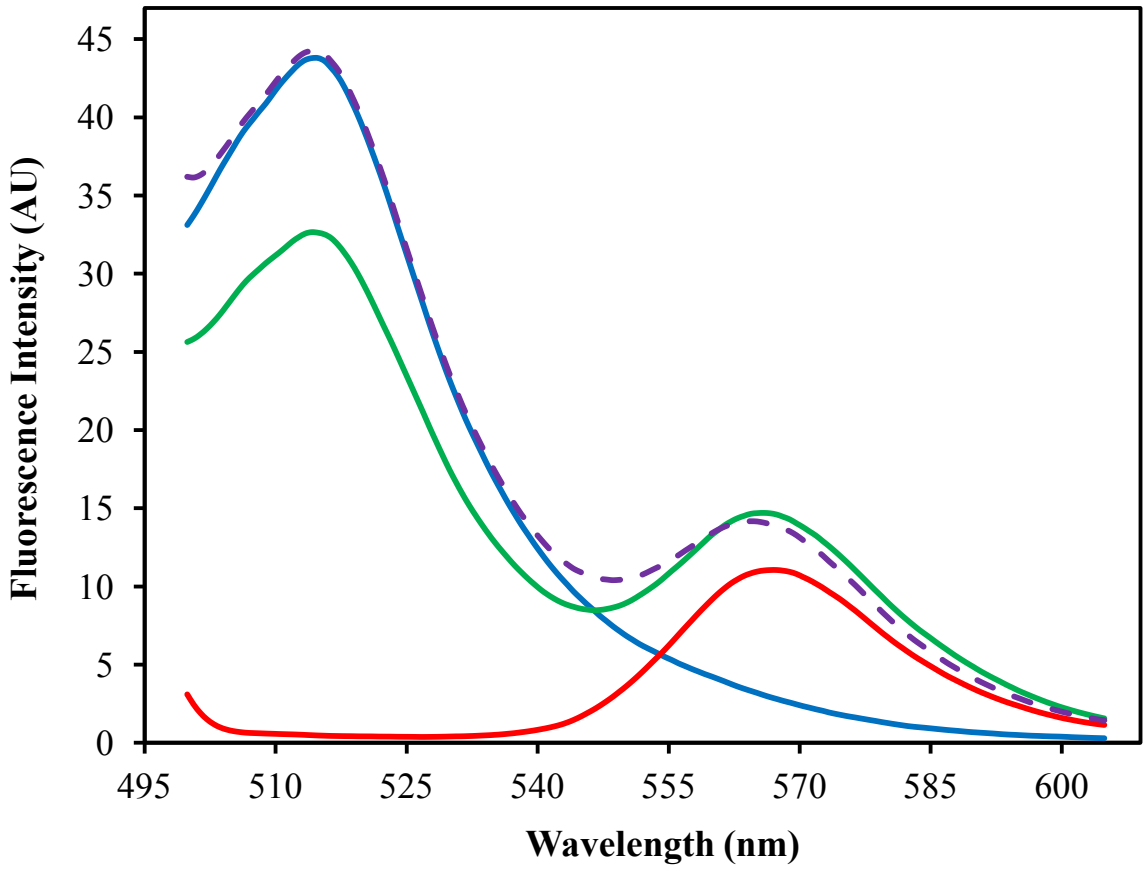

Figure 4.17: Fluorescence emission spectra of labeled VIM-2 and the labeled $(Arg)_8Cys$ core peptide. The spectra were measured in HEPES buffer (50 mM, pH 7.2) at room temperature using an excitation wavelength of 492 nm. VIM-2 was labeled with Alexa Fluor 488 while the $(Arg)_8Cys$ core peptide was labeled with Alexa Fluor 546. Labeled VIM-2 and the labeled $(Arg)_8Cys$ core peptide were measured at final concentrations of 200 nM and 800 nM, respectively. Spectra of labeled VIM-2 (blue), the labeled $(Arg)_8Cys$ core peptide (red), and labeled VIM-2 + labeled $(Arg)_8Cys$ peptide (green and purple). The solid lines indicate experimental data while the dashed line denotes the additive spectrum obtained by the addition of the blue and red traces. The curves represent the average of three independent experiments.

If there was no interaction between the labeled protein and the labeled peptide, the experimental spectrum should correspond to the sum of labeled VIM-2 and labeled $(Arg)_8Cys$ peptide. However, actual experimental data demonstrated that there was an interaction between the labeled protein and the labeled peptide since the experimental emission spectrum

demonstrated significant quenching of the peak at 514 nm, but no change in peak in intensity at 568 nm in comparison to the additive spectrum (see Figure 4.17). When the distance between the labeled protein and labeled peptide was calculated, a very large distance of ~ 70 Å was obtained.

Since significant FRET was not observed between labeled VIM-2 and the labeled $(Arg)_8Cys$ core peptide, additional studies were conducted to reveal the underlying cause of this phenomenon. Hence, activity assays were performed to determine the inhibitory potency of the labeled peptides. The results revealed that the labeled peptides were essentially non-inhibitory. For instance, exposure of VIM-2 to 5 μM donor- or acceptor-labeled $(Arg)_8Cys$ resulted in only 5% inhibition, an observation very different from that noted with the unlabeled peptide for which an IC_{50} value of 118 nM was noted (see Table 4.1). Furthermore, fluorescence studies were conducted to determine if, in the presence of VIM-2, the labeled peptides demonstrated high levels of scattering at 295 nm. The results revealed that the levels of scattering at 295 nm for the labeled peptides in the presence of VIM-2 were much lower than those obtained with their unlabeled equivalents, and essentially identical to those of the additive spectra (see Figure 4.18). This observation suggests that no aggregation occurred between VIM-2 and the $(Arg)_8$ peptide due to the label on the peptide. Therefore, it is also likely that the dye molecule prevented the peptide from binding VIM-2, which could explain the absence of FRET in the previous experiments.

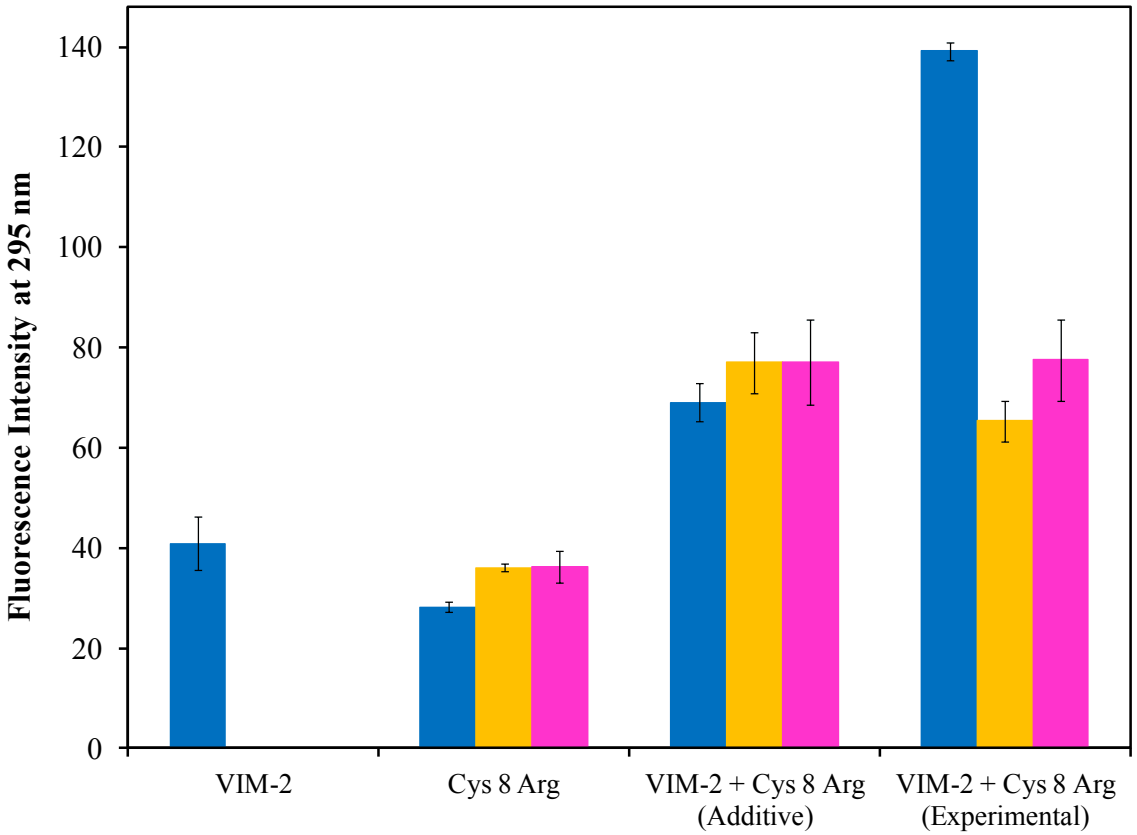

Figure 4.18: Fluorescence emission at 295 nm of VIM-2 and the $(Arg)_8Cys$ core peptide in the absence and the presence of fluorescent labels. The fluorescence emission spectra were measured in HEPES buffer (50 mM, pH 7.2) at room temperature using an excitation wavelength of 492 nm. Columns of unlabeled species (VIM-2 or peptide) (blue), the $(Arg)_8Cys$ core peptide labeled with Alexa Fluor 488 (orange), and the $(Arg)_8Cys$ core peptide labeled with Alexa Fluor 546 (pink). The VIM-2 + $(Arg)_8Cys$ peptide (additive) data was obtained by the addition of the individual VIM-2 and $(Arg)_8Cys$ peptide data. The columns represent the average (± 1 s.d.) of three independent experiments.

4.13 Interaction of Cationic Peptides with IMP-1

Since cationic peptides were shown to be potent inhibitors of VIM-2, it was of interest to observe whether these peptides proved to be effective inhibitors against other metallo-β-lactamases such as IMP-1. The interaction between IMP-1 and the cationic peptides was investigated by recording the catalytic activity of IMP-1 in the presence of these peptide inhibitors. Since previous results obtained with VIM-2 suggested that inhibition was dependent on the number of arginine residues, peptides containing a varying numbers of core arginine residues were

employed as inhibitors of IMP-1. The results demonstrated that the elongation of the $(Arg)_5$ core to an $(Arg)_8$ core peptide had a minimal effect on the inhibitory potency of the peptides with IC_{50} values located in the high micromolar range (see peptides **7** and **4** in Table 4.7). Replacement of the N-terminal glycine residue of peptide **4** with a cysteine residue (peptide **14**) led to a considerable increase in the inhibitory potency with the IC_{50} value decreasing from over 200 μM to 46 μM (compare peptides **4** and **14** in Table 4.7).

Table 4.7: Inhibition of IMP-1 by various cationic peptides. Inhibition was assessed at room temperature by pre-incubating 2 nM IMP-1 with the desired peptide for 1 min prior to the determination of the protein's catalytic activity following the introduction of 100 μM of nitrocefin. The values represent the mean (± 1 s.d.) of three independent experiments. The IC_{50} values for VIM-2 were taken from Table 4.1.

Peptide		IC_{50} (μM)	
		IMP-1	**VIM-2**
7	Ac-Gly-Tyr-βAla-$(Arg)_5$-Val-Leu-Arg-OH	> 500	> 500
4	Ac-Gly-Tyr-βAla-$(Arg)_8$-Val-Leu-Arg-OH	> 200	0.18 ± 0.01
14	Ac-Cys-Tyr-βAla-$(Arg)_8$-Val-Leu-Arg-OH	46 ± 4	0.118 ± 0.021
15	Ac-Cys-Tyr-βAla-$(Arg)_8$-Val-Leu-Arg-OH | Ac-Cys-Tyr-βAla-$(Arg)_8$-Val-Leu-Arg-OH	122 ± 13	0.013 ± 0.001
11	Poly-arginine (5 to 15 kDa)	0.72 ± 0.06	0.017 ± 0.004

The cysteine-containing $(Arg)_8$ core peptide was dimerized to give the disulfide-containing analogue (peptide **15**). This peptide was shown to be a less potent inhibitor of IMP-1 with an IC_{50} value of 122 ± 13 μM, a finding quite distinct from that documented for VIM-2 (see Table 4.1). Furthermore, the results revealed that poly-arginine was the only potent inhibitor of IMP-1 with an IC_{50} value of 720 ± 60 nM (see peptide **11** in Table 4.7). This data suggested that the cationic peptides are generally less potent inhibitors of IMP-1 in comparison to VIM-2.

Since previous studies with VIM-2 suggested aggregation of the protein in the presence of the cationic peptides, fluorescence studies were conducted with IMP-1 to determine whether this aggregation was also occurring between IMP-1 and the cationic peptides. In the previous

studies, a high fluorescence intensity at 295 nm was indicative of aggregation in the samples. As shown in Figure 4.19, the fluorescence emission spectrum of IMP-1 demonstrated one distinct peak at a wavelength of 334 nm. In the presence of poly-arginine, the fluorescence spectrum of IMP-1 exhibited significant quenching, but no shift of λ_{max}. Furthermore, similar to the results obtained with VIM-2, a considerable increase in fluorescence intensity at 295 nm was detected for the sample containing IMP-1 and poly-arginine. Although such increase in fluorescence intensity was lower than that of the VIM-2 samples, these results suggest aggregation of the protein in the presence of poly-arginine.

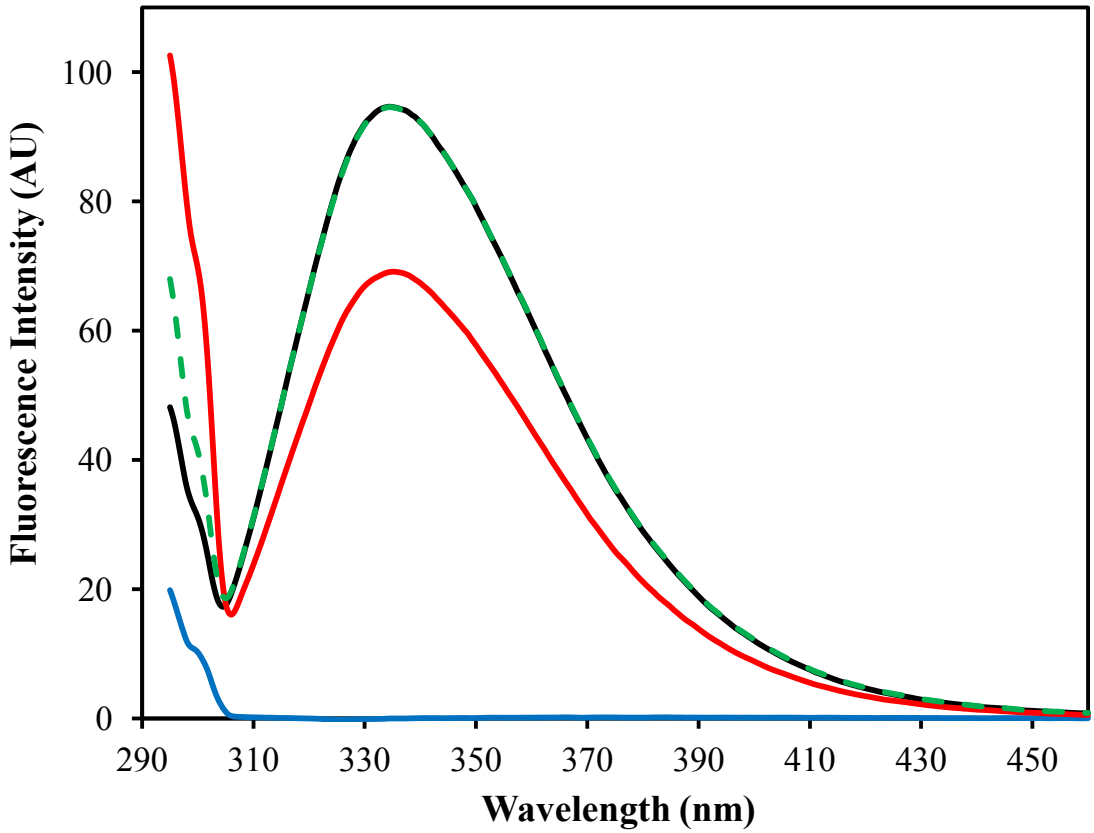

Figure 4.19: Fluorescence emission spectra of IMP-1 with poly-arginine. The spectra were measured in HEPES buffer (50 mM, pH 7.2) at room temperature using an excitation wavelength of 295 nm. IMP-1 and poly-arginine were employed at final concentrations of 1 µM and 5 µM, respectively. Spectrum of IMP-1 (black), poly-arginine (blue) and IMP-1 + poly-arginine (red and green). The solid lines represent experimental data while the dashed line indicates the additive spectrum obtained by the addition of the black and blue curves. The spectra represent the average of three independent experiments.

As in the case of VIM-2, the difference in fluorescence intensity of IMP-1 at 295 nm between the experimental spectrum and the additive spectrum was evaluated for a variety of cationic peptides. The results revealed that the difference in fluorescence intensity at 295 nm (and hence the degree of scattering) increased with the number of (core) arginine residues (see Figure 4.20), a finding identical to those obtained with VIM-2 (see Figure 4.7). Furthermore, the ΔFI values obtained with IMP-1 correlate with the inhibitory potency of the peptides (just as it did for VIM-2), except for the $(Arg_8Cys)_2$ peptide which shows a higher ΔFI value, but lower inhibitory potency than its reduced $(Arg)_8Cys$ analogue (see Table 4.7). Therefore, IMP-1 and VIM-2 exhibited a similar dependence on the number of core arginine residues for inhibition and fluorescence intensity. However, in comparison to VIM-2, the cationic peptides appear to be less inhibitory against IMP-1.

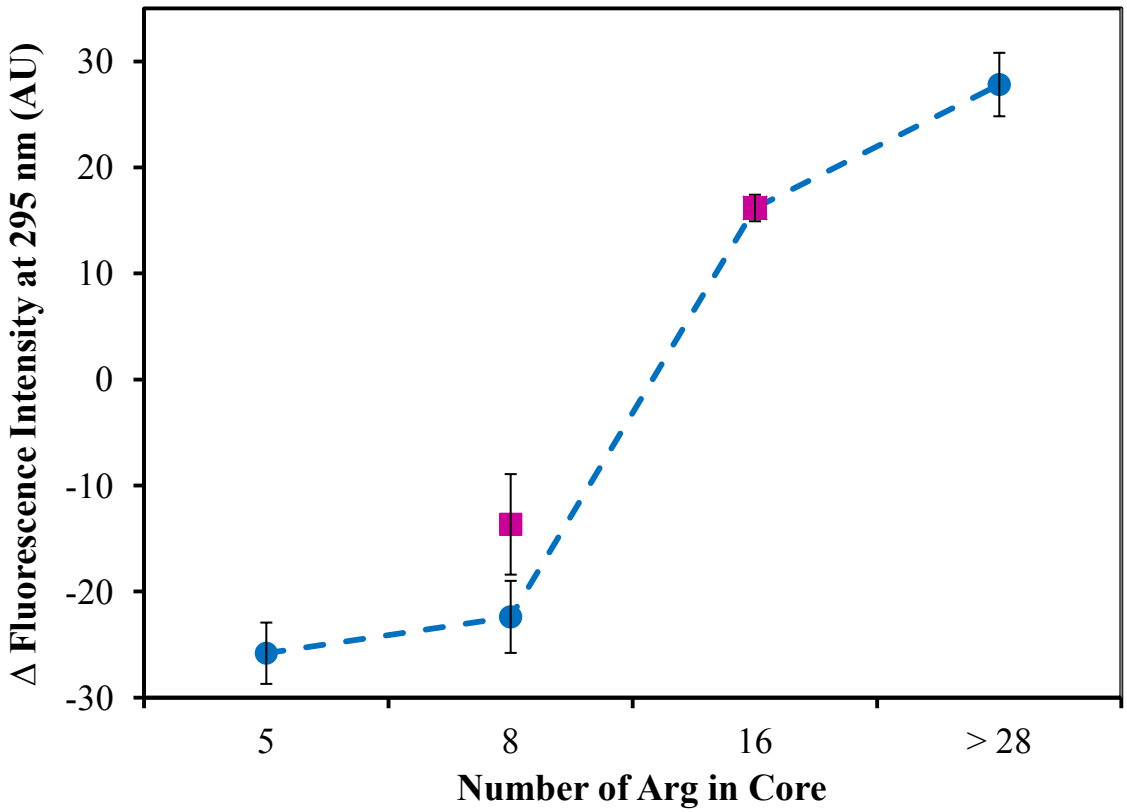

Figure 4.20: Difference in fluorescence intensity at 295 nm for the emission spectra of IMP-1 with various cationic peptides. The spectra were measured in HEPES buffer (50 mM, pH 7.2) at room temperature using an excitation wavelength of 295 nm. IMP-1 and the cationic peptides were employed at final concentrations of 1 μM and 5 μM, respectively. The purple squares correspond to the peptides that contained a cysteine residue in their N-terminus instead of a glycine residue (peptides **14** and **15**). The 16 arginine core peptide denotes the $(Arg_8Cys)_2$ peptide (peptide **15**) while the >28 core peptide represents poly-arginine (peptide **11**). ΔFluorescence intensity denotes the difference in fluorescence intensity between the experimental and additive spectra. Data shown represent the average of three independent experiments. The error bars symbolize the mean (± 1 s.d.) of the three independent experiments.

Chapter 5: Discussion

The discovery of antibiotics over 70 years ago was expected to bring about an end to infectious diseases [134]. However, despite the progress in the design of antibiotics, their golden age is rapidly coming to an end in the midst of an increasing emergence of infectious diseases, more specifically bacterial infections [4, 135]. While β-lactam antibiotics (i.e., penicillins, cephalosporins and carbapenems) remain the most widely used antibacterial agents, their effectiveness against bacterial infections is quickly decreasing due to the growing number of bacteria possessing antibiotic resistance mechanisms [90, 135]. The most prevalent manner by which bacteria become resistant to β-lactams is through the production of enzymes termed β-lactamases which are capable of hydrolyzing these antibiotics [90, 91, 135]. Among the different classes of β-lactamases, class B enzymes (termed metallo-β-lactamases, MBLs) rely on the presence of zinc ions for their catalytic function [92]. MBLs are rapidly becoming a global concern since they not only possess the capacity to cleave most classes of β-lactam antibiotics, but they are also able to hydrolyze class A β-lactamase inhibitors (i.e., clavulanic acid) as well as carbapenems, antibiotics with the broadest spectrum of activity rendering them the last resort antibiotics for many serious bacterial infections [92, 93, 96, 98, 116]. Even with the decreasing number of treatment options presently available, there are no clinically approved inhibitors for MBLs [136]. Therefore, new options must be pursued in order to find inhibitors for these increasingly problematic enzymes.

5.1 Cationic Peptide Inhibitors

Cationic peptides have received considerable attention as potential inhibitors of MBLs since preliminary studies (unpublished) demonstrated that S-*p*NA, a lethal factor (LF) substrate containing an octa-arginine motif, had the ability to inhibit MBLs. However, the structure-

activity relationship between the MBLs and S-*p*NA still remains unknown. Henceforth, the majority of the cationic peptides used in this study originated around modifications of the amino acid sequence of S-*p*NA to allow for a more thorough study of the structure-activity relationship between MBLs and cationic peptides. Initially, in the case of alterations to the C-terminal region of S-*p*NA, whether it was a substitution of the C-terminal moiety or of C-terminal amino acid residues, only minor changes in the inhibitory potency of the peptides were observed (see Table 4.1). Even incorporation of a zinc-binding C-terminal hydroxamate moiety into the peptide was found to have a negligible effect on the inhibition of VIM-2. This feature is quite different from that noted with the zinc endopeptidase LF, where the hydroxamate moiety was found to be a strong zinc-binding group [137]. Thus, these observations are most likely a consequence of the C-terminal end of the peptide not having the ability to interact with VIM-2's active site. Therefore, it appears that the C-terminal end of the cationic peptides plays a minimal role in the inhibition of the MBLs.

The structure of S-*p*NA was modified to create cationic peptides varying in their number of core arginine residues. As a result of this modification, a significant decrease in the inhibitory potency of the peptides was detected upon the shortening of the octa-arginine core to a tetra-arginine core. Hence, the most potent inhibitors of VIM-2 were poly-arginine and the $(Arg_8Cys)_2$ core peptide (peptides **11** and **15** in Table 4.1, respectively). This observation may be a consequence of the increasing number of arginine residues having the capacity to bind additional negatively charged regions on the surface of VIM-2. Furthermore, the results revealed that the $(Arg)_6$ core peptide was a considerably more potent inhibitor of VIM-2 than the $(Arg)_5$ core peptide (by a factor of 200). Thus, the additional (sixth) core arginine residue may have the ability to bind an additional negatively charged site on the surface of VIM-2. These observations

gained further support through the comparison of the inhibitory potency of the reduced and oxidized forms of the $(Arg)_8Cys$ peptide. The oxidized form of this peptide was the most potent inhibitor of VIM-2, although its two octa-arginine motifs are separated by six other non-positively charged amino acid residues. These observations support the notion that the positively charged arginine residues of the cationic peptides may bind negatively charged regions on the surface of VIM-2. Therefore, it appears that the number of arginine residues in the peptidic chain is important for the inhibition of VIM-2 by the cationic peptides.

The importance of arginine residues for the inhibition of VIM-2 was also evaluated through the incorporation of a tetra-lysine core peptide, which was found to be a poor inhibitor of VIM-2. However, upon the replacement of the C-terminal proline and the $(Lys)_4$ motif of this peptide with arginine residues, a significant increase in inhibitory potency was observed, underlining the importance of arginine residues for the effective inhibition of VIM-2. Although arginine and lysine residues are both positively charged at neutral pH, the difference in their inhibitory potencies may be a consequence of the nitrogen atoms of the guanidinium group allowing for interactions in three possible directions (whereas the functional group of lysine only allows for one such direction) [138]. Furthermore, the Ac-Nle-$(Arg)_4$-Val-Leu-Arg-OH peptide was found to be a significantly more potent inhibitor than Ac-Gly-Tyr-βAla-$(Arg)_4$-Val-Leu-Arg-OH (see Table 4.1). Hence, minor differences in the N-terminal residues of both of these peptides (Ac-Nle vs. Ac-Gly-Tyr-βAla) caused a significant alteration in their inhibitory potencies. These observations may be a consequence of the N-terminal end of the cationic peptide having the ability to (strongly) bind to VIM-2. This notion gained further support upon the substitution of the N-terminal glycine residue in the amino acid sequence of S-*p*NA with an N-terminal cysteine residue, revealing that the $(Arg)_4Cys$ and the $(Arg)_8Cys$ core peptides were more potent

inhibitors of VIM-2 than their glycine-containing equivalents (see Table 4.1). These observations may be a consequence of the cysteine residue's sulfhydryl group interacting with the protein (possibly interacting with a zinc ion in the active site of VIM-2) [139]. Interestingly, these peptides remain potent inhibitors of VIM-2 in their oxidized state, although their sulfhydryl groups are forming disulfide bridges. The increased inhibitory potency of the oxidized peptides might be a consequence of having twice as many core arginine residues. Therefore, it is most likely a combination of the number of core arginine residues in conjunction with the N-terminal region (Ac-Nle vs. Ac-Gly-Tyr-βAla) of the cationic peptides which are important for their inhibitory effect on VIM-2.

To further investigate the structure-activity relationship between MBLs and cationic peptides, various β-lactam substrates other than nitrocefin including a variety of cephalosporins, benzylpenicillin and imipenem were employed in the assessment of the inhibitory potency of S-*p*NA. The results demonstrated that nitrocefin and the nitrocefin-like substrates (UW-57 and UW-58) were the substrates with which the highest degree of inhibition by S-*p*NA was observed, and that the inhibitory potency of S-*p*NA decreased significantly upon the substitution of nitrocefin with other substrates. In particular, inhibition was found to be susceptible to changes in the R_2 moiety of cephalosporins. Furthermore, in view of the ionic nature of the cationic peptides, the effect of salts on VIM-2 inhibition was studied, revealing that all salts, especially those containing divalent anions, were capable of relieving S-*p*NA-mediated inhibition of VIM-2. It is not unlikely that the anions of the salts bind to the positively charged arginine residues of the peptides, thus decreasing their inhibitory potency against VIM-2.

5.2 Mechanism of Inhibition

The mode of inhibition of VIM-2 by S-*p*NA was found to be complex. The data obtained during the study of the inhibition of VIM-2 by S-*p*NA was fit to two mechanisms involving (a) an enzyme-product-inhibitor ternary complex, and (b) hyperbolic (partial) mixed-type inhibition which cannot be distinguished experimentally by steady-state kinetic assays.

Since the enzyme kinetics of the reaction between VIM-2 and S-*p*NA could be fit to two indistinguishable mechanisms, stopped-flow spectrophotometry was used to differentiate between both mechanisms. Single-turnover experiments were conducted using poly-arginine as an inhibitor. As expected, the results demonstrated the presence of the nitrocefin peak at 390 nm and a peak at 490 nm indicative of the presence of hydrolyzed nitrocefin. However, there was no evidence of a peak at 665 nm. Previous experiments focusing on CcrA and NDM-1 demonstrated a peak at 665 nm [132, 140], which corresponds to a ring-opened anionic nitrogen intermediate of nitrocefin [132]. Although, there was no evidence of this peak in the studies performed on VIM-2, the intermediate was also absent in experiments conducted on MBLs such as BcII, Bla2 and IMP-1 [141–143]. Therefore, it is not unusual that the stopped-flow experiments performed with VIM-2 did not demonstrate any evidence of the nitrocefin intermediate since the occurrence of this species seems to depend on the MBL employed. Two possible scenarios could account for the absence of the intermediate in the mechanism of VIM-2-mediated nitrocefin hydrolysis: (i) the intermediate is not formed, and (ii) the intermediate forms, but decays so rapidly (within less than 1 ms) that stopped-flow instruments are unable to detect it. Regardless of the presence or absence of this intermediate, the stopped-flow studies could still help distinguish between the two mechanisms that could be used to describe the interaction between VIM-2 and cationic peptides. Following the addition of nitrocefin (pre-exposed to poly-

arginine) to VIM-2, the emergence of the peak at 490 nm (hydrolyzed nitrocefin) was significantly delayed. Furthermore, evidence of light scattering in the spectrum became more apparent as the reaction progressed. These observations demonstrate that the hydrolysis of nitrocefin is strongly inhibited, a finding to be expected in view of poly-arginine's high inhibitory potency. This strong inhibition also persisted when poly-arginine was pre-exposed to VIM-2 prior to the addition of nitrocefin. However, the absorbance of both nitrocefin and hydrolyzed nitrocefin were considerably higher than those revealed with nitrocefin pre-exposed to poly-arginine due to light scattering. Nonetheless, it was observed that, regardless of whether poly-arginine was pre-exposed to VIM-2 or to nitrocefin, the A_{390} and A_{490} curves demonstrated similar rates of nitrocefin hydrolysis suggesting that inhibition precedes protein aggregation. Furthermore, the inhibition of VIM-2 by poly-arginine appears to follow the hyperbolic (partial) mixed-type inhibition. This is apparent since the first turnover of nitrocefin in this mechanism would be slow (i.e., inhibited) due to the pre-product stage inhibition through the production of the EIS complex [129]. If the mechanism involving the enzyme-product-inhibitor ternary complex was followed, the first turnover of nitrocefin would have been more rapid since the inhibitor has a higher affinity for the EP complex than for the free enzyme [128], a feature not observed in the experiments. Therefore, the inhibition of VIM-2 by poly-arginine most likely follows the hyperbolic (partial) mixed-type inhibition.

Double-turnover stopped-flow experiments were also performed to distinguish the two mechanisms of inhibition [hyperbolic (partial) mixed-type inhibition vs. enzyme-product-inhibitor ternary complex]. Single-wavelength stopped-flow analyses for the substrate peak at 390 nm and product peak at 490 nm demonstrated that in the presence of the $(Arg)_7$ core peptide, the rate of nitrocefin hydrolysis only slightly decreased during the first turnover. However, the

rate reduction became increasingly prominent during the second turnover. The data appears to suggest that the mechanism producing the enzyme-product-inhibitor ternary complex (since the first turnover was rapid). Therefore, when the results from both the single and double-turnover experiments are taken into consideration, it seems not unlikely that the inhibition of VIM-2 by the cationic peptides follows a combination of both of the mechanisms of inhibition. Such combination would still allow for the production of the EIS complex. However, the EIS complex would still be active allowing the turnover of substrate for the formation of product resulting in the formation of an EPI complex as per the mechanism involving the enzyme-product-inhibitor ternary complex (see Figure 5.1). It is important to note that the possibility of the mechanism of VIM-2 inhibition being slightly different for poly-arginine and the $(Arg)_7$ peptide cannot be ruled out at the present time.

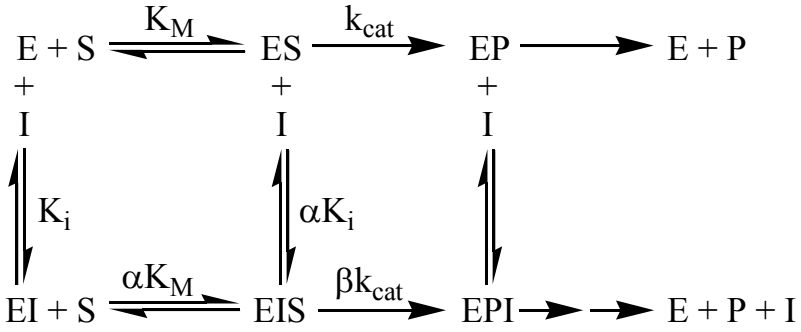

Figure 5.1: Proposed scheme for the inhibition of VIM-2 by cationic peptides.

5.3 Protein Aggregation

Intrinsic tryptophan fluorescence studies were conducted to further investigate the structure-activity relationship between the MBLs and the cationic peptides. These studies demonstrated that the interaction between VIM-2 and the cationic peptides only induced minimal conformational changes within the protein since only slight alterations of the fluorescence emission spectra of VIM-2 (shift in λ_{max} or change in fluorescence intensity) were observable

upon the addition of a cationic peptide. However, the fluorescence emission spectra of VIM-2 displayed a dramatic increase in fluorescence intensity at 295 nm upon the addition of cationic peptides with greater than six arginine core residues. This prominent increase in fluorescence intensity is indicative of light scattering caused by protein aggregation. Furthermore, the degree of scattering increased with the number of arginine residues in the peptides, an observation corresponding well with the increase in their inhibitory potency. In addition, UV-Vis spectroscopy revealed an increase in absorbance in the short wavelength limb (especially prominent at 250 nm) of the VIM-2 spectrum upon the addition of the cationic peptides, suggesting protein aggregation.

To estimate the size of the aggregates, native PAGE was performed. This study demonstrated the presence of an interaction between VIM-2 and the cationic peptides since the VIM-2 band on the gel diminished in intensity upon the addition of the cationic peptides. However, no aggregates of higher molecular weight could be detected to justify the decreased intensity of the VIM-2 bands, or to confirm the presence of distinct aggregates in the samples. Paper electrophoresis confirmed the absence of a charge reversal (from negative to positive) upon the addition of a cationic peptide to VIM-2. Indeed, two distinct migration patterns were observed on the TLC paper with one remaining stationary, and the other migrating, as expected, towards the anode. The sample that remained stationary during the paper electrophoresis is most likely due to the aggregates being too large to migrate within the electric field, a hypothesis gaining support from the inability to detect aggregates of higher molecular weights during native PAGE. Therefore, it appears that large aggregates are formed during the interaction between VIM-2 and the more potent cationic peptide inhibitors.

Since the size of aggregates formed between VIM-2 and the cationic peptides could not be determined by native PAGE, dynamic light scattering experiments were performed to estimate the size of the aggregates. As a control, VIM-2 was analyzed, demonstrating an average diameter of 5.0 nm. This diameter is similar to that obtained for NDM-1, which is in the same subclass as VIM-2, and was found to have a diameter of 4.8 nm [133]. Upon the addition of the $(Arg)_8$ core peptide to VIM-2, an aggregate formed with a diameter of ~ 670 nm. These observations confirm the results from the native PAGE studies that only one large aggregate is formed during the interaction between VIM-2 and the cationic peptides. Indeed, the sample demonstrated visible aggregation (precipitate; increased turbidity), which may be a consequence of the high concentrations employed for VIM-2 and the cationic peptide. Furthermore, the dynamic light scattering experiments were also conducted with increasing concentrations of the cationic peptide to determine the equivalent amount of inhibitor necessary for the formation of aggregates. Even at only 0.2 molar equivalents of inhibitor, aggregation was detected in the sample. In addition, the size of the aggregates increased with the concentration of inhibitor. These observations suggest that only a small quantity of peptide is required to induce the formation of VIM-2 aggregates, and that the aggregates grow in size at higher concentrations of inhibitor.

UV-Vis spectroscopy was performed to determine the reversibility of the interaction between VIM-2 and the cationic peptides. A salt shown to relieve cationic peptide-mediated inhibition was added to the $(Arg)_8$ core peptide-supplemented VIM-2 sample to determine if the aggregation was reversible. The results showed that the addition of Na_2SO_4 led to a decrease in absorbance in the spectrum of the aggregated sample, and a reduction of turbidity. However, the absorbance spectrum of the sample still showed evidence of light scattering following the

addition of Na_2SO_4, suggesting that aggregation is only partially reversible. This notion was further supported through activity assays following the addition of Na_2SO_4 to the aggregated sample. The results demonstrated that only ~ 30% of VIM-2 activity is recovered following the supplementation with Na_2SO_4. These observations may be a consequence of VIM-2 misfolding during aggregation. The partial relief of protein aggregation was also confirmed through intrinsic tryptophan fluorescence studies. These investigations demonstrated that TCEP was capable of relieving the $(Arg_8Cys)_2$ core peptide (peptide **15** in Table 4.1)-mediated aggregation of VIM-2 as evidenced by a decrease in the fluorescence intensity at 295 nm. However, the fluorescence intensity of this sample was still considerably higher than that of VIM-2 supplemented with the reduced $(Arg)_8Cys$ peptide (peptide **14** in Table 4.1) suggesting that the interaction between VIM-2 and the cationic peptides is only partially reversible.

5.4 FRET

FRET studies were conducted to further support the presence of aggregation, and to gain insight into the molecular nature of the aggregates. These studies demonstrated that no FRET was observable between donor- and acceptor-labeled VIM-2. Although FRET was not observable between the labeled proteins, these studies showed that there was a quenching of the fluorescence intensity of the donor. These observations may be a consequence of the unlabeled peptide interacting with the dye molecule bound to VIM-2, and changing the polarity of the micro-environment of the dye. Furthermore, it is highly unlikely that the absence of FRET was caused by improperly labeled reagents since additional tests (e.g., by UV-Vis, PAR assays and calculations of the degree of labeling) were conducted to ensure that both of the proteins were properly labeled. Therefore, it is most likely that protein aggregation did not occur with labeled VIM-2, and could hence not be detected by FRET.

FRET was employed to investigate the binding site of the cationic peptides to VIM-2 since activity assays, tryptophan fluorescence and UV-Vis studies, native PAGE, and dynamic light scattering investigations all confirmed the presence of an interaction between the MBLs and the cationic peptides. These studies demonstrated that FRET was not observable between the donor-labeled VIM-2 and the acceptor-labeled $(Arg)_8Cys$ peptide, although a quenching of the fluorescence intensity of the donor was noticeable. Additional studies demonstrated that the covalent binding of the dye to the $(Arg)_8Cys$ peptide caused the peptide to become a considerably less potent inhibitor of VIM-2, and prevented aggregation between the unlabeled protein and the labeled peptide. Therefore, it is likely that the labeled peptide is incapable of binding to VIM-2, which may account for the absence of FRET during the studies.

5.5 Inhibition of IMP-1 by Cationic Peptides

Previous studies revealed that cationic peptides were potent inhibitors of VIM-2. To investigate this further, additional activity assays and tryptophan fluorescence studies were employed to determine whether the cationic peptides showed the same inhibitory potency against IMP-1, another B1 metallo-β-lactamase. The cationic peptides proved to be significantly less potent against IMP-1 than VIM-2, although the inhibition of both MBLs by the cationic peptides appeared to demonstrate the same dependence on the nature of the N-terminal amino acids (Cys vs. Gly), and the number of core arginine residues in the peptides. These observations may be a consequence of differences in the electrostatic potentials of VIM-2 and IMP-1 in the regions surrounding the active site of both of these MBLs since this is a plausible binding site of the cationic peptides.

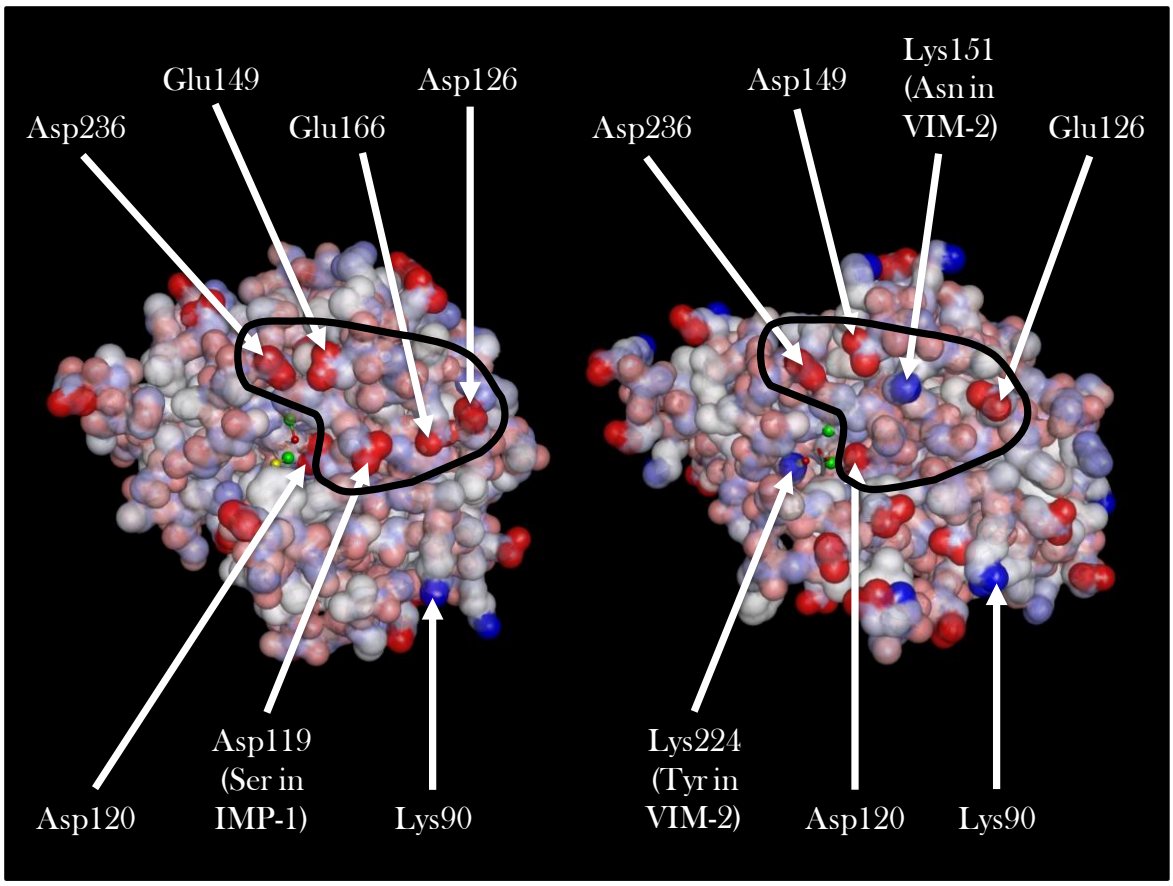

Figure 5.2: Surface of VIM-2 and IMP-1 in terms of their electrostatic potentials. The amino acid residues of interest surrounding the potential cationic peptide binding site are labeled according to the BBL numbering scheme. A plausible cationic peptide binding site is encircled in black. Surfaces of VIM-2 (left) and IMP-1 (right).

A comparison of the surfaces of VIM-2 and IMP-1 shows that a considerable portion of the electrostatic potentials of these two proteins remained similar regardless of some aspartate and glutamate substitutions since these regions still possess an overall negative charge (see Figure 5.2). However, IMP-1 contains some additional positively charged regions near its active site in comparison to that of VIM-2. These additional positively charged regions stem from Lys224 and Lys151 which are substituted with an asparagine residue and a tyrosine residue, respectively, in the amino acid sequence of VIM-2 (see Figure 5.2). Furthermore, these lysine residues reside in the plausible binding site of the cationic peptides (see Figure 5.2). If the additional positively charged regions in IMP-1 are located in the binding site of the cationic peptides, they may lead to

a repulsion of the positively charged arginine core of the cationic peptides. Therefore, this repulsion would render the cationic peptides less inhibitory against IMP-1 since they can no longer properly bind to the MBL. As a consequence, additional core arginine residues may be required to span the binding pocket of IMP-1, while avoiding the repulsion of the additional lysine residues. This hypothesis gains support from the observation that poly-arginine and the $(Arg_8Cys)_2$ peptide remain the most potent inhibitors of IMP-1. This notion is further supported by the observation that the scattering at 295 nm in intrinsic tryptophan fluorescence studies performed on IMP-1 was also dependent on the number of arginine residues in the peptides. Hence, it appears that the inhibitory potency of the cationic peptides depends on the surface characteristics of the MBL under investigation.

A plausible mechanism for the inhibition of the MBLs by the cationic peptides begins with the docking of the cationic peptide to the MBL, resulting in inhibition. The peptide (by virtue of its high positive charge) can then attract other MBL molecules, or change the surface of the MBL to promote the formation of aggregates. Salts are able to relieve MBL inhibition (and aggregation) by the cationic peptides since they most likely interact with the peptides rendering them incapable of remaining bound to the protein.

Chapter 6: Conclusions and Future Studies

Louis Pasteur once said that microbes always have the last word [144]. With the ever growing number of bacteria equipped with antibiotic resistance mechanisms such as target site alterations, multidrug efflux pumps and antibiotic-degrading enzymes, bacteria have become highly resilient to antibiotics. It is therefore important that alternatives to antibiotics be developed to help treat infectious diseases caused by bacteria which are resistant to almost all known antibiotics.

This research project explored the possibility of inhibiting MBLs with cationic peptides. The results obtained from this research confirmed that cationic peptides have the ability to inhibit VIM-2 and IMP-1. Furthermore, the inhibitory potency of the cationic peptides was dependent on the MBL employed, and the number of core arginine residues in these peptides (IC_{50} of ~ 10 nM for the best inhibitor). In addition, inhibition also depended on the nature of the N-terminal residues of the peptides. Therefore, the peptides containing either an N-terminal cysteine or greater than seven core arginine residues demonstrated the highest degree of MBL inhibition. The inhibitory potency of the peptides also varied depending on the substrate employed and whether or not salt was present in the samples. Hence, the cationic peptides were more potent inhibitors upon the employment of nitrocefin and nitrocefin-like substrates while salts, especially those with divalent anions, were shown to relieve this inhibition. The reaction between the MBLs and the cationic peptides also suggested the formation of protein aggregates. This protein aggregation can only occur once the peptide binds and inhibits the MBL. Furthermore, protein aggregation increases with the number of arginine residues in the cationic peptides, and can be relieved upon the addition of salt.

The mode of inhibition of the MBLs by the cationic peptides is complex, and appears to involve the production of an enzyme-product-inhibitor complex and enzyme-substrate-inhibitor complex.

Future studies could include using different enzymes, other than VIM-2 and IMP-1, to investigate whether these MBLs are also inhibited by cationic peptides. Furthermore, different peptides varying in their N-terminal residues should be used to further explore the effect of the N-terminal moiety on MBL inhibition. In addition, core arginine residues could be substituted with non-positively charged amino acids to see which arginine residues are important for the inhibition of the MBLs. The appropriate rate equation for the observed mechanism of inhibition, based on a combination of the mechanism producing an enzyme-product-inhibitor ternary complex and hyperbolic (partial) mixed-type inhibition, could to be developed using the King-Altman method to obtain reliable estimates of the kinetic constants. Molecular modeling could also be used to determine the binding site of the cationic peptides to the MBLs. Ultimately, if the cationic peptides prove to be potent inhibitors of a variety of MBLs, peptidomimetics could be used to create novel inhibitors of MBLs. However, until such time as inhibitors of MBLs are developed and clinically approved, education and restraint on the proper use of antibiotics is the key to controlling the spread of bacterial antibiotic resistance.

References

1. Thirumala, S., Nathu, M. P., and Aravind, H. B. (2014) Air borne microbial hazards in dairy and poultry farm workers of Davangere, Karnataka. *Curr. Res. Microbiol. Biotechnol.* **2**, 325–328.

2. Klaenhammer, T. R. (2000) Probiotic Bacteria: Today and Tomorrow. *J. Nutr.* **130**, 415–416.

3. Saarela, M., Mogensen, G., Fondén, R., Mättö, J., and Mattila-Sandholm, T. (2000) Probiotic bacteria: safety, functional and technological properties. *J. Biotechnol.* **84**, 197–215.

4. Rasko, D., and Sperandio, V. (2010) Anti-virulence strategies to combat bacteria-mediated disease. *Nat. Rev. Drug Discov.* **9**, 117–128.

5. Lederberg, J. (2000) Infectious history. *Science.* **288**, 287–293.

6. Haensch, S., Bianucci, R., Signoli, M., Rajerison, M., Schultz, M., Kacki, S., Vermunt, M., Weston, D., Hurst, D., Achtman, M., Carniel, E., and Bramanti, B. (2010) Distinct clones of *Yersinia pestis* caused the black death. *PLoS Pathog.* **6**, e1001134.

7. Porter, J. R. (1976) Antony van Leeuwenhoek: Tercentenary of His Discovery of Bacteria. *Bacteriol. Rev.* **40**, 260–269.

8. Behbehani, A. M. (1983) The Smallpox Story: Life and Death of an Old Disease. *Microbiol. Rev.* **47**, 455–509.

9. Riedel, S. (2005) Edward Jenner and the history of smallpox and vaccination. *Proc. (Bayl. Univ. Med. Center)* **18**, 21–25.

10. Stewart, A. J., and Devlin, P. M. (2006) The history of the smallpox vaccine. *J. Infect.* **52**, 329–334.

11. Henderson, D. (1997) Edward Jenner's vaccine. *Public Health Rep.* **112**, 116–121.

12. Barquet, N., and Domingo, P. (1997) Smallpox: the triumph over the most terrible of the ministers of death. *Ann. Intern. Med.* **127**, 635–642.

13. Blevins, S. M., and Bronze, M. S. (2010) Robert Koch and the "golden age" of bacteriology. *Int. J. Infect. Dis.* **14**, e744–e751.

14. Sternbach, G. (2003) The history of anthrax. *J. Emerg. Med.* **24**, 463–467.

15. Schwartz, M. (2009) Dr. Jekyll and Mr. Hyde: a short history of anthrax. *Mol. Aspects Med.* **30**, 347–355.

16. Flynn, J., and Chan, J. (2001) Tuberculosis: latency and reactivation. *Infect. Immun.* **69**, 4195–4201.

17. Daniel, T. M. (2006) The history of tuberculosis. *Respir. Med.* **100**, 1862–1870.

18. Kaufmann, S. H. E., and Schaible, U. E. (2005) 100th anniversary of Robert Koch's Nobel Prize for the discovery of the tubercle bacillus. *Trends Microbiol.* **13**, 469–475.

19. Smith, I. (2003) *Mycobacterium tuberculosis* pathogenesis and molecular determinants of virulence. *Clin. Microbiol. Rev.* **16**, 463–496.

20. Gradmann, C. (2011) Robert Koch and the Pressures of Scientific Research: Tuberculosis and Tuberculin. *Med. Hist.* **45**, 1–32.

21. Vanden Broeck, D., Horvath, C., and De Wolf, M. J. S. (2007) *Vibrio cholerae*: cholera toxin. *Int. J. Biochem. Cell Biol.* **39**, 1771–1775.

22. Matson, J. S., Withey, J. H., and DiRita, V. J. (2007) Regulatory networks controlling *Vibrio cholerae* virulence gene expression. *Infect. Immun.* **75**, 5542–5549.

23. Reidl, J., and Klose, K. E. (2002) *Vibrio cholerae* and cholera: out of the water and into the host. *FEMS Microbiol. Rev.* **26**, 125–139.

24. Lipp, E., Huq, A., and Colwell, R. (2002) Effects of global climate on infectious disease: the cholera model. *Clin. Microbiol. Rev.* **15**, 757–770.

25. Gradmann, C. (2006) Robert Koch and the white death: from tuberculosis to tuberculin. *Microbes Infect.* **8**, 294–301.

26. Bordenave, G. (2003) Louis Pasteur (1822-1895). *Microbes Infect.* **5**, 553–560.

27. Berche, P. (2012) Louis Pasteur, from crystals of life to vaccination. *Clin. Microbiol. Infect.* **18**, 1–6.

28. Plotkin, S. A. (2005) Vaccines: past, present and future. *Nat. Med.* **11**, S5–S11.

29. Blancou, J., Kieny, M., Lathe, R., and Lecocq, J. (1986) Oral vaccination of the fox against rabies using a live recombinant vaccinia virus. *Nature* **332**, 373–375.

30. Haider, S. (2008) Rabies: old disease, new challenges. *Can. Med. Assoc. J.* **178**, 6–7.

31. Rupprecht, C. E., Hanlon, C. A., and Hemachudha, T. (2002) Rabies re-examined. *Lancet Infect. Dis.* **2**, 327–343.

32. Clardy, J., Fischbach, M., and Currie, C. (2009) The natural history of antibiotics. *Curr. Biol.* **19**, 1–8.

33. Zaffiri, L., Gardner, J., and Toledo-Pereyra, L. H. (2012) History of antibiotics. From salvarsan to cephalosporins. *J. Invest. Surg.* **25**, 67–77.

34. Bentley, R. (2009) Different roads to discovery; Prontosil (hence sulfa drugs) and penicillin (hence β-lactams). *J. Ind. Microbiol. Biotechnol.* **36**, 775–786.

35. Larson, E. (2007) Community factors in the development of antibiotic resistance. *Annu. Rev. Public Health* **28**, 435–447.

36. Duckett, S. (1999) Ernest Duchesne and the concept of fungal antibiotic therapy. *Lancet* **354**, 2068–2071.

37. Ligon, B. L. (2004) Penicillin: its discovery and early development. *Semin. Pediatr. Infect. Dis.* **15**, 52–57.

38. McNulty, C., Boyle, P., Nichols, T., Clappison, P., and Davey, P. (2007) The public's attitudes to and compliance with antibiotics. *J. Antimicrob. Chemother.* **60**, i63–i68.

39. Pankey, G. A., and Sabath, L. D. (2004) Clinical relevance of bacteriostatic versus bactericidal mechanisms of action in the treatment of Gram-positive bacterial infections. *Clin. Infect. Dis.* **38**, 864–870.

40. Kohanski, M., Dwyer, D., and Collins, J. (2010) How antibiotics kill bacteria: from targets to networks. *Nat. Rev. Microbiol.* **8**, 423–435.

41. Saene, R., Fairclough, S., and Petros, A. (1998) Broad- and narrow-spectrum antibiotics: a different approach. *Clin. Microbiol. Infect.* **4**, 56–57.

42. Willing, B. P., Russell, S. L., and Finlay, B. B. (2011) Shifting the balance: antibiotic effects on host-microbiota mutualism. *Nat. Rev. Microbiol.* **9**, 233–243.

43. Von Nussbaum, F., Brands, M., Hinzen, B., Weigand, S., and Häbich, D. (2006) Antibacterial natural products in medicinal chemistry–Exodus or revival? *Angew. Chem. Int. Ed.* **45**, 5072–5129.

44. Lewis, K. (2013) Platforms for antibiotic discovery. *Nat. Rev. Drug Discov.* **12**, 371–387.

45. Emmerson, A. M., and Jones, A. M. (2003) The quinolones: decades of development and use. *J. Antimicrob. Chemother.* **51**, 13–20.

46. Aristoff, P. A., Garcia, G. A., Kirchhoff, P. D., and Showalter, H. D. (2010) Rifamycins – Obstacles and opportunities. *Tuberculosis* **90**, 94–118.

47. Yonath, A. (2005) Antibiotics targeting ribosomes: resistance, selectivity, synergism and cellular regulation. *Annu. Rev. Biochem.* **74**, 649–679.

48. Mingeot-Leclercq, M. P., Glupczynski, Y., and Tulkens, P. M. (1999) Aminoglycosides: activity and resistance. *Antimicrob. Agents Chemother.* **43**, 727–737.

49. Yim, G., Thaker, M. N., Koteva, K., and Wright, G. (2014) Glycopeptide antibiotic biosynthesis. *J. Antibiot.* **67**, 31–41.

50. Fisher, J. F., Meroueh, S. O., and Mobashery, S. (2005) Bacterial resistance to β-lactam antibiotics: compelling opportunism, compelling opportunity. *Chem. Rev.* **105**, 395–424.

51. Kim, Y., Tesar, C., Mire, J., Jedrzejczak, R., Binkowski, A., Babnigg, G., Sacchettini, J., and Joachimiak, A. (2011) Structure of apo- and monometalated forms of NDM-1– A highly potent carbapenem-hydrolyzing metallo-β-lactamase. *PLoS One* **6**, e24621.

52. Barends, T. R. M., Yoshida, H., and Dijkstra, B. W. (2004) Three-dimensional structures of enzymes useful for β-lactam antibiotic production. *Curr. Opin. Biotechnol.* **15**, 356–363.

53. Karsisiotis, A. I., Damblon, C. F., and Roberts, G. C. K. (2014) A variety of roles for versatile zinc in metallo-β-lactamases. *Metallomics* **6**, 1181–1197.

54. Dalhoff, A., Janjic, N., and Echols, R. (2006) Redefining penems. *Biochem. Pharmacol.* **71**, 1085–1095.

55. Cooper, R. (1992) The carbacephems: A new β-lactam antibiotic class. *Am. J. Med.* **92**, 2S–6S.

56. Baggaley, K., Brown, A., and Schofield, C. (1997) Chemistry and biosynthesis of clavulanic acid and other clavams. *Nat. Prod. Rep.* **14**, 309–333.

57. Zhanel, G. G., Wiebe, R., Dilay, L., Thomson, K., Rubinstein, E., Hoban, D. J., Noreddin, A. M., and Karlowsky, J. a (2007) Comparative review of the carbapenems. *Drugs* **67**, 1027–1052.

58. Singh, G. S. (2004) Beta-lactams in the new millennium. Part-I: monobactams and carbapenems. *Mini Rev. Med. Chem.* **4**, 69–92.

59. Antúnez, C., Martín, E., Cornejo-García, J. A., Blanca-Lopez, N., R-Pena, R., Mayorga, C., Torres, M. J., and Blanca, M. (2006) Immediate hypersensitivity reactions to penicillins and other β-lactams. *Curr. Pharm. Des.* **4**, 3327–3333.

60. Scheffers, D., and Pinho, M. (2005) Bacterial cell wall synthesis: new insights from localization studies. *Microbiol. Mol. Biol. Rev.* **69**, 585–607.

61. Meroueh, S. O., Bencze, K. Z., Hesek, D., Lee, M., Fisher, J. F., Stemmler, T. L., and Mobashery, S. (2006) Three-dimensional structure of the bacterial cell wall peptidoglycan. *Proc. Natl. Acad. Sci. U. S. A.* **103**, 4404–4409.

62. Schwartz, B., Markwalder, J. A., and Wang, Y. (2001) Lipid II: total synthesis of the bacterial cell wall precursor and utilization as a substrate for glycosyltransfer and transpeptidation by penicillin binding protein (PBP) 1b of *Escherichia coli*. *J. Am. Chem. Soc.* **123**, 11638–11643.

63. Sauvage, E., Kerff, F., Terrak, M., Ayala, J., and Charlier, P. (2008) The penicillin-binding proteins: structure and role in peptidoglycan biosynthesis. *FEMS Microbiol. Rev.* **32**, 234–258.

64. Roujeinikova, A. (2008) Crystal structure of the cell wall anchor domain of MotB, a stator component of the bacterial flagellar motor: implications for peptidoglycan recognition. *Proc. Natl. Acad. Sci. U. S. A.* **105**, 10348–10353.

65. Alanis, A. J. (2005) Resistance to antibiotics: Are we in the post-antibiotic era? *Arch. Med. Res.* **36**, 697–705.

66. Wassmer, G. T., Kipe-nolt, J. A., and Chayko, C. A. (2006) Why Finish Your Antibiotics? *Am. Biol. Teach.* **68**, 476–480.

67. Girou, E., Chai, S. H. T., Oppein, F., Legrand, P., Ducellier, D., Cizeau, F., and Brun-Buisson, C. (2004) Misuse of gloves: the foundation for poor compliance with hand hygiene and potential for microbial transmission? *J. Hosp. Infect.* **57**, 162–169.

68. Muniesa, M., Colomer-Lluch, M., and Jofre, J. (2013) Could bacteriophages transfer antibiotic resistance genes from environmental bacteria to human-body associated bacterial populations? *Mob. Genet. Elements* **3**, e25847.

69. Levy, S. B., and Marshall, B. (2004) Antibacterial resistance worldwide: causes, challenges and responses. *Nat. Med.* **10**, S122–S129.

70. De la Cruz, F., and Davies, J. (2000) Horizontal gene transfer and the origin of species: lessons from bacteria. *Trends Microbiol.* **8**, 128–133.

71. Recchia, G. D., and Hall, R. M. (1997) Origins of the mobile gene cassettes found in integrons. *Trends Microbiol.* **5**, 389–394.

72. Clewell, D. B. (2014) Antibiotic Resistance Plasmids in Bacteria. In: *eLS*, John Wiley & Sons, Ltd: Chichester.

73. Lanka, E., and Wilkins, B. (1995) DNA processing reactions in bacterial conjugation. *Annu. Rev. Biochem.* **64**, 141–169.

74. Andersson, D. I., and Hughes, D. (2010) Antibiotic resistance and its cost: is it possible to reverse resistance? *Nat. Rev. Microbiol.* **8**, 260–271.

75. Chen, I., and Dubnau, D. (2004) DNA uptake during bacterial transformation. *Nat. Rev. Microbiol.* **2**, 241–249.

76. Pitout, J. D., Sanders, C. C., and Sanders, W. E. (1997) Antimicrobial resistance with focus on β-lactam resistance in gram-negative bacilli. *Am. J. Med.* **103**, 51–59.

77. Georgopapadakou, N. H. (1993) Penicillin-Binding Proteins and Bacterial Resistance to β-Lactams. *Antimicrob. Agents Chemother.* **37**, 2045–2053.

78. Chambers, H. F. (1999) Penicillin-binding protein-mediated resistance in pneumococci and staphylococci. *J. Infect. Dis.* **179**, S353–S359.

79. Wilke, M. S., Lovering, A. L., and Strynadka, N. C. J. (2005) β-lactam antibiotic resistance: a current structural perspective. *Curr. Opin. Microbiol.* **8**, 525–533.

80. Hakenbeck, R., Grebe, T., Zähner, D., and Stock, J. B. (1999) β-lactam resistance in *Streptococcus pneumoniae*: penicillin-binding proteins and non-penicillin-binding proteins. *Mol. Microbiol.* **33**, 673–678.

81. Zapun, A., Contreras-Martel, C., and Vernet, T. (2008) Penicillin-binding proteins and beta-lactam resistance. *FEMS Microbiol. Rev.* **32**, 361–385.

82. Nikaido, H. (1998) Antibiotic resistance caused by gram-negative multidrug efflux pumps. *Clin. Infect. Dis.* **27**, S32–S41.

83. Delcour, A. (2009) Outer membrane permeability and antibiotic resistance. *Biochim. Biophys. Acta* **1794**, 808–816.

84. Piddock, L. J. V (2006) Multidrug-resistance efflux pumps - not just for resistance. *Nat. Rev. Microbiol.* **4**, 629–636.

85. Paulsen, I. T. (2003) Multidrug efflux pumps and resistance: regulation and evolution. *Curr. Opin. Microbiol.* **6**, 446–451.

86. Ernst, R., Kueppers, P., Stindt, J., Kuchler, K., and Schmitt, L. (2010) Multidrug efflux pumps: substrate selection in ATP-binding cassette multidrug efflux pumps–first come, first served? *FEBS J.* **277**, 540–549.

87. Omote, H., Hiasa, M., Matsumoto, T., Otsuka, M., and Moriyama, Y. (2006) The MATE proteins as fundamental transporters of metabolic and xenobiotic organic cations. *Trends Pharmacol. Sci.* **27**, 587–593.

88. Saier, M. H., Paulsen, I. T., Sliwinski, M. K., Pao, S. S., Skurray, R. a, and Nikaido, H. (1998) Evolutionary origins of multidrug and drug-specific efflux pumps in bacteria. *FASEB J.* **12**, 265–274.

89. Kievit, T. De, Parkins, M., Gillis, R., Srikumar, R., Ceri, H., Poole, K., Iglewski, B., and Storey, D. (2001) Multidrug efflux pumps: expression patterns and contribution to antibiotic resistance in *Pseudomonas aeruginosa* biofilms. *Antimicrob. Agents Chemother.* **45**, 1761–1770.

90. Yamaguchi, Y., Kuroki, T., Yasuzawa, H., Higashi, T., Jin, W., Kawanami, A., Yamagata, Y., Arakawa, Y., Goto, M., and Kurosaki, H. (2005) Probing the role of Asp-120(81) of metallo-β-lactamase (IMP-1) by site-directed mutagenesis, kinetic studies, and X-ray crystallography. *J. Biol. Chem.* **280**, 20824–20832.

91. Zhang, H., and Hao, Q. (2011) Crystal structure of NDM-1 reveals a common β-lactam hydrolysis mechanism. *FASEB J.* **25**, 2574–2582.

92. Bebrone, C., Lassaux, P., Vercheval, L., Sohier, J.-S., Jehaes, A., Sauvage, E., and Galleni, M. (2010) Current challenges in antimicrobial chemotherapy: focus on β-lactamase inhibition. *Drugs* **70**, 651–679.

93. Concha, N. O., Janson, C. A., and Rowling, P. (2000) Crystal Structure of the IMP-1 Metallo β-lactamase from *Pseudomonas aeruginosa* and Its Complex with a Mercaptocarboxylate Inhibitor: Binding Determinants of a Potent, Broad-spectrum Inhibitor. *Biochemistry* **39**, 4288–4298.

94. Rawat, D., and Nair, D. (2010) Extended-spectrum β-lactamases in Gram Negative Bacteria. *J. Glob. Infect. Dis.* **2**, 263–274.

95. Wright, G. D. (2005) Bacterial resistance to antibiotics: enzymatic degradation and modification. *Adv. Drug Deliv. Rev.* **57**, 1451–1470.

96. Bebrone, C. (2007) Metallo-β-lactamases (classification, activity, genetic organization, structure, zinc coordination) and their superfamily. *Biochem. Pharmacol.* **74**, 1686–1701.

97. Borgianni, L., Vandenameele, J., Matagne, A., Bini, L., Bonomo, R. A., Frère, J.-M., Rossolini, G. M., and Docquier, J.-D. (2010) Mutational analysis of VIM-2 reveals an essential determinant for metallo-β-lactamase stability and folding. *Antimicrob. Agents Chemother.* **54**, 3197–3204.

98. Thomson, J. M., and Bonomo, R. A. (2005) The threat of antibiotic resistance in Gram-negative pathogenic bacteria: β-lactams in peril! *Curr. Opin. Microbiol.* **8**, 518–524.

99. Garau, G., García-Sáez, I., Bebrone, C., Anne, C., Mercuri, P., Galleni, M., Frère, J.-M., and Dideberg, O. (2004) Update of the standard numbering scheme for class B β-lactamases. *Antimicrob. Agents Chemother.* **48**, 2347–2349.

100. Cameron, A. D., Ridderström, M., Olin, B., and Mannervik, B. (1999) Crystal structure of human glyoxalase II and its complex with a glutathione thiolester substrate analogue. *Structure* **7**, 1067–1078.

101. Kim, M. H., Choi, W.-C., Kang, H. O., Lee, J. S., Kang, B. S., Kim, K.-J., Derewenda, Z. S., Oh, T.-K., Lee, C. H., and Lee, J.-K. (2005) The molecular structure and catalytic mechanism of a quorum-quenching N-acyl-L-homoserine lactone hydrolase. *Proc. Natl. Acad. Sci. U. S. A.* **102**, 17606–17611.

102. Silaghi-Dumitrescu, R., Kurtz, D. M., Ljungdahl, L. G., and Lanzilotta, W. N. (2005) X-ray crystal structures of *Moorella thermoacetica* FprA. Novel diiron site structure and mechanistic insights into a scavenging nitric oxide reductase. *Biochemistry* **44**, 6492–6501.

103. Makris, T. M., Knoot, C. J., Wilmot, C. M., and Lipscomb, J. D. (2013) Structure of a dinuclear iron cluster-containing β-hydroxylase active in antibiotic biosynthesis. *Biochemistry* **52**, 6662–6671.

104. Page, M. I., and Badarau, A. (2008) The mechanisms of catalysis by metallo-β-lactamases. *Bioinorg. Chem. Appl.* **2008**, 1–14.

105. Fabiane, S. M., Sohi, M. K., Wan, T., Payne, D. J., Bateson, J. H., Mitchell, T., and Sutton, B. J. (1998) Crystal structure of the zinc-dependent β-lactamase from *Bacillus cereus* at 1.9 Å resolution: binuclear active site with features of a mononuclear enzyme. *Biochemistry* **37**, 12404–12411.

106. Carfi, A., Pares, S., Duée, E., Galleni, M., Duez, C., Frère, J.-M., and Dideberg, O. (1995) The 3-D structure of a zinc metallo-β-lactamase from *Bacillus cereus* reveals a new type of protein fold. *EMBO J.* **14**, 4914–4921.

107. Concha, N. O., Rasmussen, B. A., Bush, K., and Herzberg, O. (1996) Crystal structure of the wide-spectrum binuclear zinc β-lactamase from *Bacteroides fragilis*. *Structure* **4**, 823–836.

108. Guo, Y., Wang, J., Niu, G., Shui, W., Sun, Y., Zhou, H., Zhang, Y., Yang, C., Lou, Z., and Rao, Z. (2011) A structural view of the antibiotic degradation enzyme NDM-1 from a superbug. *Protein Cell* **2**, 384–394.

109. Murphy, T. A., Catto, L. E., Halford, S. E., Hadfield, A. T., Minor, W., Walsh, T. R., and Spencer, J. (2006) Crystal structure of *Pseudomonas aeruginosa* SPM-1 provides insights into variable zinc affinity of metallo-β-lactamases. *J. Mol. Biol.* **357**, 890–903.

110. García-Sáez, I., Docquier, J.-D., Rossolini, G. M., and Dideberg, O. (2008) The three-dimensional structure of VIM-2, a Zn-β-lactamase from *Pseudomonas aeruginosa* in its reduced and oxidised form. *J. Mol. Biol.* **375**, 604–611.

111. Walsh, T. R., Neville, W. A., Haran, M. H., Tolson, D., Payne, D. J., Bateson, J. H., MacGowan, A. P., and Bennett, P. M. (1998) Nucleotide and amino acid sequences of the metallo-β-lactamase, ImiS, from *Aeromonas veronii* bv. sobria. *Antimicrob. Agents Chemother.* **42**, 436–439.

112. Garau, G., Bebrone, C., Anne, C., Galleni, M., Frère, J.-M., and Dideberg, O. (2005) A metallo-β-lactamase enzyme in action: crystal structures of the monozinc carbapenemase CphA and its complex with biapenem. *J. Mol. Biol.* **345**, 785–795.

113. Ullah, J. H., Walsh, T. R., Taylor, I. A., Emery, D. C., Verma, C. S., Gamblin, S. J., and Spencer, J. (1998) The crystal structure of the L1 metallo-β-lactamase from *Stenotrophomonas maltophilia* at 1.7 Å resolution. *J. Mol. Biol.* **284**, 125–136.

114. García-Sáez, I., Mercuri, P., Papamicael, C., Kahn, R., Frère, J.-M., Galleni, M., Rossolini, G., and Dideberg, O. (2003) Three-dimensional Structure of FEZ-1, a Monomeric Subclass B3 Metallo-β-lactamase from *Fluoribacter gormanii*, in Native Form and in Complex with D-Captopril. *J. Mol. Biol.* **325**, 651–660.

115. Mercuri, P., Bouillenne, F., Boschi, L., Lamothe-Brasseur, J., Amicosante, G., Devreese, B., van Neeumen, J., Frère, J.-M., Rossolini, G., and Galleni, M. (2001) Biochemical characterization of the FEZ-1 metallo-β-lactamase of *Legionella gormanii* ATCC 33297^T produced in *Escherichia coli*. *Antimicrob. Agents Chemother.* **45**, 1254–1262.

116. Rolain, J. M., Parola, P., and Cornaglia, G. (2010) New Delhi metallo-β-lactamase (NDM-1): towards a new pandemia? *Clin. Microbiol. Infect.* **16**, 1699–1701.

117. Struelens, M. J., Monnet, D. L., Magiorakos, A. P., Santos O'Connor, F., and Giesecke, J. (2010) New Delhi metallo-β-lactamase 1-producing Enterobacteriaceae: emergence and response in Europe. *Euro Surveill.* **15**, 1–10.

118. Yong, D., Toleman, M. A., Giske, C. G., Cho, H. S., Sundman, K., Lee, K., and Walsh, T. R. (2009) Characterization of a new metallo-β-lactamase gene, *bla*(NDM-1), and a novel erythromycin esterase gene carried on a unique genetic structure in *Klebsiella pneumoniae* sequence type 14 from India. *Antimicrob. Agents Chemother.* **53**, 5046–5054.

119. Liang, Z., Li, L., Wang, Y., Chen, L., Kong, X., Hong, Y., Lan, L., Zheng, M., Guang-Yang, C., Liu, H., Shen, X., Luo, C., Li, K. K., Chen, K., and Jiang, H. (2011) Molecular basis of NDM-1, a new antibiotic resistance determinant. *PLoS One* **6**, e23606.

120. Walsh, T., and Toleman, M. (2005) Metallo-β-lactamases: the quiet before the storm? *Clin. Microbiol. Rev.* **18**, 306–325.

121. Poirel, L., Naas, T., Nicolas, D., Collet, L., Bellais, S., Cavallo, J. D., and Nordmann, P. (2000) Characterization of VIM-2, a carbapenem-hydrolyzing metallo-β-lactamase and its plasmid- and integron-borne gene from a *Pseudomonas aeruginosa* clinical isolate in France. *Antimicrob. Agents Chemother.* **44**, 891–897.

122. Zhao, W. H., and Hu, Z. Q. (2011) Epidemiology and genetics of VIM-type metallo-β-lactamases in Gram-negative bacilli. *Future Microbiol.* **6**, 317–333.

123. Hall, B. (2004) *In vitro* evolution predicts that the IMP-1 metallo-β-lactamase does not have the potential to evolve increased activity against imipenem. *Antimicrob. Agents Chemother.* **48**, 1032–1033.

124. Pannifer, A., Wong, T., Scwarzenbacher, R., Renatus, M., Petosa, C., Bienkowska, J., Lacy, D., Collier, R., Park, S., Leppla, S., Hanna, P., and Liddington, R. (2001) Crystal structure of the anthrax lethal factor. *Nature* **414**, 229–233.

125. Tonello, F., Ascenzi, P., and Montecucco, C. (2003) The metalloproteolytic activity of the anthrax lethal factor is substrate-inhibited. *J. Biol. Chem.* **278**, 40075–40078.

126. Docquier, J.-D. (2003) On functional and structural heterogeneity of VIM-type metallo-β-lactamases. *J. Antimicrob. Chemother.* **51**, 257–266.

127. Siemann, S., Evanoff, D. P., Marrone, L., Clarke, A. J., Viswanatha, T., and Dmitrienko, G. I. (2002) N-Arylsulfonyl Hydrazones as Inhibitors of IMP-1 Metallo-β-Lactamase. *Antimicrob. Agents Chemother.* **46**, 2450–2457.

128. Lanthier, C. M., Parniak, M. A., and Dmitrienko, G. I. (1997) Inhibition of carboxypeptidase a by N-(4-*t*-Butylbenzoyl)-2-hydroxy-1-naphthaldehyde hydrazone. *Bioorg. Med. Chem. Lett.* **7**, 1557–1562.

129. Segel, I. H. (1993) *Enzyme Kinetics: Behavior and Analysis of Rapid Equilibrium and Steady-State Enzyme Systems*, Wiley, New York.

130. Gardonio, D., and Siemann, S. (2009) Chelator-facilitated chemical modification of IMP-1 metallo-β-lactamase and its consequences on metal binding. *Biochem. Biophys. Res. Commun.* **381**, 107–111.

131. Säbel, C. E., Shepherd, J. L., and Siemann, S. (2009) A direct spectrophotometric method for the simultaneous determination of zinc and cobalt in metalloproteins using 4-(2-pyridylazo)resorcinol. *Anal. Biochem.* **391**, 74–76.

132. Yang, H., Aitha, M., Hetrick, A. M., Richmond, T. K., Tierney, D. L., and Crowder, M. W. (2012) Mechanistic and spectroscopic studies of metallo-β-lactamase NDM-1. *Biochemistry* **51**, 3839–3847.

133. Zheng, B., Tan, S., Gao, J., Han, H., Liu, J., Lu, G., Liu, D., Yi, Y., Zhu, B., and Gao, G. F. (2011) An unexpected similarity between antibiotic-resistant NDM-1 and β-lactamase II from *Erythrobacter litoralis*. *Protein Cell* **2**, 250–258.

134. Davies, J. (2006) Where have all the antibiotics gone? *Can. J. Infect. Dis. Med. Microbiol.* **17**, 287–290.

135. Crowder, M. W., Spencer, J., and Vila, A. J. (2006) Metallo-β-lactamases: novel weaponry for antibiotic resistance in bacteria. *Acc. Chem. Res.* **39**, 721–728.

136. Livermore, D. M. (2009) Has the era of untreatable infections arrived? *J. Antimicrob. Chemother.* **64**, i29–i36.

137. Tonello, F., Seveso, M., Marin, O., Mock, M., and Montecucco, C. (2002) Screening inhibitors of anthrax lethal factor. *Nature* **418**, 386.

138. Sokalingam, S., Raghunathan, G., Soundrarajan, N., and Lee, S.-G. (2012) A study on the effect of surface lysine to arginine mutagenesis on protein stability and structure using green fluorescent protein. *PLoS One* **7**, e40410.

139. Maret, W. (2004) Zinc and Sulfur : A Critical Biological Partnership. *Biochemistry* **43**, 3301–3309.

140. Wang, Z., Fast, W., and Benkovic, S. J. (1999) On the mechanism of the metallo-β-lactamase from *Bacteroides fragilis*. *Biochemistry* **38**, 10013–10023.

141. Rasia, R., and Vila, A. (2003) Mechanistic study of the hydrolysis of nitrocefin mediated by *B. cereus* metallo-β-lactamase. *ARKIVOC* **2003**, 507–516.

142. Hawk, M. J., Breece, R. M., Hajdin, C. E., Bender, K. M., Hu, Z., Costello, A. L., Bennett, B., Tierney, D. L., and Crowder, M. W. (2009) Differential binding of Co(II) and Zn(II) to metallo-β-lactamase Bla2 from *Bacillus anthracis*. *J. Am. Chem. Soc.* **131**, 10753–10762.

143. Griffin, D. H., Richmond, T. K., Sanchez, C., Moller, A. J., Breece, R. M., Tierney, D. L., Bennett, B., and Crowder, M. W. (2011) Structural and kinetic studies on metallo-β-lactamase IMP-1. *Biochemistry* **50**, 9125–9134.

144. Spížek, J., Novotná, J., Řezanka, T., and Demain, A. L. (2010) Do we need new antibiotics? The search for new targets and new compounds. *J. Ind. Microbiol. Biotechnol.* **37**, 1241–1248.